

Comparison of ocean heat content from two eddy-resolving hindcast simulations with OFES1 and OFES2

Fanglou Liao^{1,2}, Xiao Hua Wang^{2,3*} and Zhiqiang Liu^{1,4,3*}

¹Department of Ocean Science and Engineering, Southern University of Science and Technology, Shenzhen, 518055, China

²The Sino-Australian Research Consortium for Coastal Management, School of Science, The University of New South Wales, Canberra, 2610, Australia

³~~College of Oceanic and Atmospheric Sciences, Ocean University of China, Qingdao, 266100, China~~

⁴Southern Marine Science and Engineering Guangdong Laboratory (Guangzhou), Guangzhou, 511458, China

Correspondence to: Zhiqiang Liu (liuzq@sustech.edu.cn) or Xiao Hua Wang (x.h.wang@unsw.edu.au)

Abstract. The ocean heat content (OHC) estimates from ~~eddy-resolving high-resolution~~ hindcast simulations from the Ocean General Circulation Model for the Earth Simulator Version 1 (OFES1) and Version 2 (OFES2), and a global objective analysis of subsurface temperature observations (EN4.2.1) were compared. ~~There was an~~ OHC increased in most of the global ocean above 2000 m in the EN4 and OFES1 over ~~a 57-year period 1960–2016~~, mainly a result of ~~vertical displacements deepening~~ of neutral density surfaces, ~~with variations along the neutral density surfaces of regional importance~~. However, we found substantial differences in the temporal and ~~meridional-spatial~~ distributions of the OHC between the two OFES hindcasts, ~~especially in the Atlantic Ocean~~. ~~The spatial distributions of potential-temperature change also differed significantly, especially in the Atlantic Ocean. The spatial distributions of the time-averaged surface heat flux and heat transport from the OFES1 and OFES2 were highly correlated are geographically similar, but regional differences could can be seen. However, these differences, more specifically in the heat transport, were only partially responsible for the OHC differences. It was found~~ A basin-wide budget analysis shows ~~that there i~~was less surface heating for the major basins in the OFES2. The horizontal heat advection ~~i~~was largely similar but ~~the OFES2 had~~ a much stronger meridional heat advection associated with the Indonesian Throughflow (ITF) above 300 m. ~~It was found that the~~ Also, large discrepancies in the vertical heat advection based on the two OFES data ~~differs greatly at the depth of 500 m in both the Atlantic Ocean and Indian Ocean~~ were also identified, especially at the 300 m depth. Therefore, we ~~infer~~ concluded that there exist large discrepancies in the inferred vertical heat diffusion (cannot be directly diagnosed in this paper due to data availability), which, along with the different sea surface heat flux and vertical heat advection, ~~awere~~ ~~claimed to be~~ major factors responsible for the examined OHC differences. ~~The marked OHC differences may arise from the different vertical mixing schemes and may impact the large-scale pressure field, and thus the geostrophic current. The~~ This work ~~here should~~ ~~is~~ ~~excepted to~~ may be a useful reference for future OFES users.

1 Introduction

The global ocean has stored over 90% of the extra heat added to the Earth system since 1955, causing a significant increase in the ocean heat content (OHC) (Levitus et al., 2012; IPCC 2013). The ~~change in the~~ OHC is therefore an

35 important indicator of climate change, and provides useful bounds in estimating the Earth's energy imbalance (Palmer
36 et al., 2011; Von Schuckmann et al., 2016). Although natural factors such as the El Niño–Southern Oscillation
37 (ENSO) and volcanic eruptions can affect the OHC (Balmaseda et al., 2013; Church et al., 2005), the recent warming
38 has mostly resulted from greenhouse gases accumulating in the atmosphere (Abraham et al., 2013; Gleckler et al.,
39 2012; Pierce et al., 2006).

40 ~~As a~~ major concern in both the oceanography and climate communities, ~~the~~ OHC has ~~absorbed~~ attracted a great
41 ~~deal of attention. Although direct observational records are the most trustworthy data to examine in determining the~~
42 ~~oceanic thermal state, the fact is that measurements are far from dense enough in both the temporal and spatial~~
43 ~~domains, especially for the deep and abyssal oceans. This sparseness situation is~~ has greatly improved since the launch
44 of a global array of profiling floats, the Argo, in 2000s. However, the spatial resolution of ~~the Argo program of~~
45 ~~approximately 300 km of the Argo program is not able to capture the~~ mesoscale structures (Sasaki et al., 2020,
46 ~~hereafter S2020~~). Several approaches exist to fill the temporal and spatial gaps in global temperature measurements,
47 and can be used to produce gridded temperature fields to estimate the OHC. ~~These Typical examples of t~~ These
48 approaches include the objective analysis of observational data, ~~and~~ ocean reanalysis ~~by~~ combining physical ocean
49 models ~~constrained by observations with observations~~. In addition, ocean general circulation models (OGCMs) ~~also~~
50 provide ~~the~~ temperature fields by solving the primitive equations of fluid motions and states. Although OGCMs are
51 dynamically consistent ~~(the resulting fields satisfy the underlying fluid dynamics and thermodynamics equations)~~,
52 some are not constrained by observations. How multi-scale dynamical processes are represented in these
53 unconstrained models and their implementation of external forcing ~~will~~ significantly impacts their OHC estimates.

54 The Ocean General Circulation Model for the Earth Simulator (OFES; Masumoto et al., 2004; Sasaki et al., 2004),
55 developed by the Japan Agency for Marine–Earth Science and Technology (JAMSTEC) and other institutes, is a
56 well-known eddy-resolving ocean model, and the hindcast simulation of the OFES Version 1 (OFES1) has been
57 widely used (Chen et al., 2013; Dong et al., 2011; Du et al., 2005; Sasaki et al., 2020; Wang et al., 2013). The hindcast
58 simulation based on the OFES Version 2 (OFES2) ~~is~~ has now publicly available ~~been released~~, and certain
59 improvements have been ~~made~~ demonstrated over the OFES1 (Sasaki et al., 2020). ~~For example, the authors found~~
60 ~~smaller bias in the global sea surface temperature (SST), sea surface salinity (SSS) and the water mass properties in~~
61 ~~the Indonesian and Arabian Seas~~. To our knowledge, however, ~~a~~ comparisons of the multi-decadal OHC ~~at a global~~
62 ~~scale~~ from the OFES1 and OFES2 ~~are~~ is lacking. As this high-resolution quasi-global model is expected to be
63 widely used in the oceanography and climate communities for examining the ocean state in the near future, ~~there is a~~
64 ~~need~~ it is ~~incentive~~ necessary to compare the OHC estimates from these two OFES versions as an indicator of the
65 potential improvements in the OFES2 over the OFES1, ~~and also of their adaptability into the OHC-related studies~~.

66 The aim of this paper is twofold: (1) to estimate the OHC in the global ocean and each major basin using the OFES1
67 and OFES2, with primary focus on their differences; (2) to understand the causes of ~~the~~ differences between these two
68 simulations. To this end, we used the potential temperature θ to calculate the OHC from 1960 to 2016 for both the
69 global ocean and the major basins, the Pacific Ocean, the Atlantic Ocean and the Indian Ocean, between 64°S and
70 64°N.

In Section 2, we give a brief description to the data and methods used here. In Section 3, we describe and discuss the OHC differences between the datasets in both the temporal and spatial domains. A tentative analysis of the possible causes of the differences is also conducted. Section 4 summarises the principal points and possible extensions involving factors that were not examined here due to data availability but could be important. Future work is therefore expected to improve on our work here.

In addition, we decomposed the changes in the potential temperature $\Delta\theta$ into heaving (HV) and spiciness (SP) components following Bindoff and McDougall (1994). The heave-related warming or cooling is a result of vertical displacement of the neutral density surfaces (a continuous analog of discretely referenced potential density surfaces (Jackett and McDougall, 1997)). In general, both the dynamical changes and the change of the renewal rates of water masses can induce the vertical displacement and thus the heave-related warming or cooling as a consequence (Bindoff and McDougall (1994)). The S represents warming or cooling in a way of density compensation in the potential temperature and salinity along the neutral density surfaces. The time-averaged surface heat flux and heat transport advection from the OFES1 and OFES2 were compared to understand the OHC budget. We used the results from an observation-based objective analysis product EN4.2.1 (EN4) as a reference.

In the following section, we give a brief description to the data and methods used in this paper (section 2). In section 3, we describe and discuss the differences between the datasets in both temporal and spatial domains; a tentative analysis of the possible causes responsible for the examined discrepancies is conducted. Section 4 summarises the principal points and makes an extension about other factors that are not examined here due to data availability but could be important, and therefore some future work is expected for improvements on our work here.

2 Data and Methods

2.1 Data

Potential-temperature θ data from both the OFES1 and OFES2 were used to calculate the global and basin OHCs for comparison with each other and with the OHC calculated from the observation-based EN4 potential temperature of the EN4. Although results from the EN4 cannot be taken as the actual oceanic state, it has been widely used in OHC-related studies (Allison et al., 2019; Carton et al., 2019; Häkkinen et al., 2016; Trenberth et al., 2016; Wang et al., 2018). A brief description of the three datasets is given below; readers are referred to Sasaki et al. (2004), Sasaki et al. (2020) and Good et al. (2013) for more details.

The OFES1 has a horizontal spatial resolution of 0.1° and 54 vertical levels from 5 m to with a maximum depth of 6065 m (Sasaki et al., 2004); this high spatial-lateral resolution enables it to include-resolve mesoscale processes. The multi-decadal integration period makes it possible to perform an analysis of oceanic fields at decadal to multidecadal scales. Following a 50-year climatological simulation, the hindcast simulation of the OFES1 is-was integrated from 1950 to two years ago (the publically available data is till 2017). The multi-decadal integration period makes it possible to perform an analysis of oceanic fields at temporal scales from intraseasonal to multi-decadal. Unlike most other datasets used for OHC estimates, the OFES1 is an ocean modelling with no observation-data-involvedal constraints. Therefore, it can be used to demonstrate the potential benefits of high resolution and the adaptability of pure-numerical modelling without data assimilation.

The OFES2 also has ~~a the same~~ horizontal spatial resolution of 0.1° . Vertically, there are 105 ~~layers~~ levels, with a maximum depth of 7500 m. The OFES1 uses daily National Centers for Environmental Prediction (NCEP) reanalysis ($2.5^\circ \times 2.5^\circ$; Kalnay et al., 1996) for the ~~atmospheric surface momentum and heat fluxes forcing~~, whereas the OFES2 is forced by the 3-hourly atmospheric surface dataset JRA55-do Version 08 ($55\text{km} \times 55\text{km}$; Tsujino et al., 2018). ~~Therefore, both~~ the temporal and spatial resolutions of the ~~atmospheric surface~~ forcing have increased ~~significantly greatly~~ in the OFES2. ~~In addition, the~~ The OFES2 also incorporates river runoff and sea-ice models, ~~although no inclusion of polar areas.~~

In the horizontal direction, both the OFES1 and OFES2 use a biharmonic mixing scheme ~~to suppress computational noise~~ (Sasaki et al., 2020). The horizontal diffusivity coefficient ~~is equal to $-9 \times 10^9 \text{ m}^4/\text{s}$ at the Equator~~ (Sasaki et al., 2020), ~~and~~ varies proportional to the cube of the cosine of the latitude ~~(personal communication with Hide Sasaki)~~ and ~~equals $-9 \times 10^9 \text{ m}^4/\text{s}$ at the Equator~~ (Smith et al., 2000; Sasaki et al., 2020). The OFES2 uses a mixed-layer vertical mixing scheme (Noh and Jin Kim 1999) with parametrization of tidal-energy dissipation (Jayne and St. Laurent 2001; St. Laurent et al., 2002), whereas the OFES1 uses the K-profile parameterization ~~scheme (the KPP) mixing scheme~~, (Large et al., 1994). With the ~~oceanic field~~ temperature and salinity on 1st January 1958 from the OFES1 as the initial conditions, the OFES2 used here has been integrated from 1958 to 2016. To ~~limit-reduce~~ the computation ~~and archive~~ cost, we subsampled the OFES1 and OFES2 ~~simulations data~~ every 5 grid points in the horizontal direction.

To ~~validate objectively evaluate~~ the OHC ~~objectively~~ from the two ~~sets of~~ OFES data, we used the EN4 from the UK ~~Meteorological~~ Met Office Hadley Centre as a reference. The ~~monthly~~ EN4 data can be considered as an objective analysis that is primarily based on observations (Good et al., 2013), with a horizontal resolution of 1° and 42 vertical levels ~~down from 5 m~~ to 5350 m. The EN4 assimilates data mainly from the World Ocean Database (WOD) and the Coriolis dataset for ReAnalysis (CORA). Pre-processing and quality checks are conducted before the observational data are used to construct this objective analysis product.

Although we use the EN4 results as a reference for evaluating the OFES performance in simulating the 57-year ocean thermal state, ~~it is also worthy to note should be noted that~~ the EN4 cannot be taken as the actual ocean state. The main reason is that the measurements used to construct the EN4 datasets are sparse and inhomogeneous in both the temporal and spatial domains, and far from sufficient to resolve mesoscale or even sub-mesoscale motions. There ~~were are~~ more observations in the ~~northern Northern hemisphere Hemisphere~~ than in the ~~southern Southern hemisphere Hemisphere~~, and ~~there is also a seasonal bias of in the observational data density-~~ (Abraham et al. 2013; Smith et al. 2015) ~~exists~~. ~~a~~ A higher density of records became available only after the World Ocean Circulation Experiment (WOCE) in the 1990s and ~~installation launch~~ of the Argo profiling floats in the 2000s. Table 1 summarizes these three ocean datasets.

Table 1. Description of the OFES1, OFES2 and EN4 datasets. / means not applicable.

	OFES1	OFES2	EN4
Model	MOM3	MOM3	/
Horizontal coverage	$75^\circ\text{S} - 75^\circ\text{N}$	$76^\circ\text{S} - 76^\circ\text{N}$	$83^\circ\text{S} - 89^\circ\text{N}$
Grids	3600×1500	3600×1520	360×173
Maximum depth	6065 m	7500 m	5350 m

Vertical levels	54	105	42
Atmospheric forcing	Daily NCEP/ NCAR reanalysis	3-hourly JRA55-do ver Ver.08	-/
Data assimilated	-/	-/	WOD, CORA
Time span	since 1950 1950 – 2017	since 1958 1958 – 2016	since 1900 1900 – 2021

We considered water from the sea surface to around 2000 m and divided it into three layers: upper (0–300 m); middle (300–700 m); and lower (700–2000 m). The ocean above 2000 m has often been divided into two layers, 0–700 m and 700–2000 (or even one: 0–2000 m) (Allison et al., 2019; Hakkinen et al., 2016; Häkkinen et al., 2015; Levitus et al., 2012; Zanna et al., 2019); our analysis here will show that it is in fact necessary to divide it into three layers for our purpose, as did Liang et al. (2021). (Allison et al. 2019; Hakkinen et al. 2016; Häkkinen et al. 2015; Levitus et al. 2012; Zanna et al. 2019)(Liang et al. 2021) The temperature and salinity characteristics of the upper ocean, above 300 m, were also analysed in (Carton et al. (2018, 2019).; Carton et al. 2019)

The reasons for ignoring ~~The ocean beneath is ignored~~ water below 2000 m are mainly fourfold. Firstly, the simulated behaviour of the deep ocean depends sensitively on the spin-up of the numerical simulation ~~the deep ocean highly depends on the spin-up of the numerical simulation, which is almost surely always incomplete (Wunsch 2011), at least in the first decade.~~ Secondly, the observational data ~~ingested by~~ used in the EN4 ~~is~~ are largely confined to the ocean above 2000 m (many available measurements do not even go down this deep), with a much lower density of data in the deep and abyssal oceans. ~~Furthermore~~ Thirdly, the ~~ingested~~ data in the EN4 version that we used here ~~is~~ are bias-corrected, following Levitus et al. (2009), in which the ~~upper~~ ocean above 700 m ~~is~~ was considered. Therefore, for instance, the Expendable Bathythermograph (XBT) profiles below 700m are corrected using the correction values provided for 700 m (personal communication from the Meteorology Office Hadley Centre). Lastly, ~~as~~ can be seen, the maximum depth differs ~~by more than 2000 m between the OFES2 and EN4. It was felt that a full-depth OHC is not highly comparable between the three datasets. This, however, does not imply that the deep ocean can be ignored; it can play an essential role in regulating the global-ocean thermal state (Desbruyeres et al. 2016; Desbruyères et al. 2017; Palmer et al. 2011). It is expected that a much better understanding of the deep and abyssal ocean state will be gained with the implementation of the Deep Argo program.~~

2.2 Methods

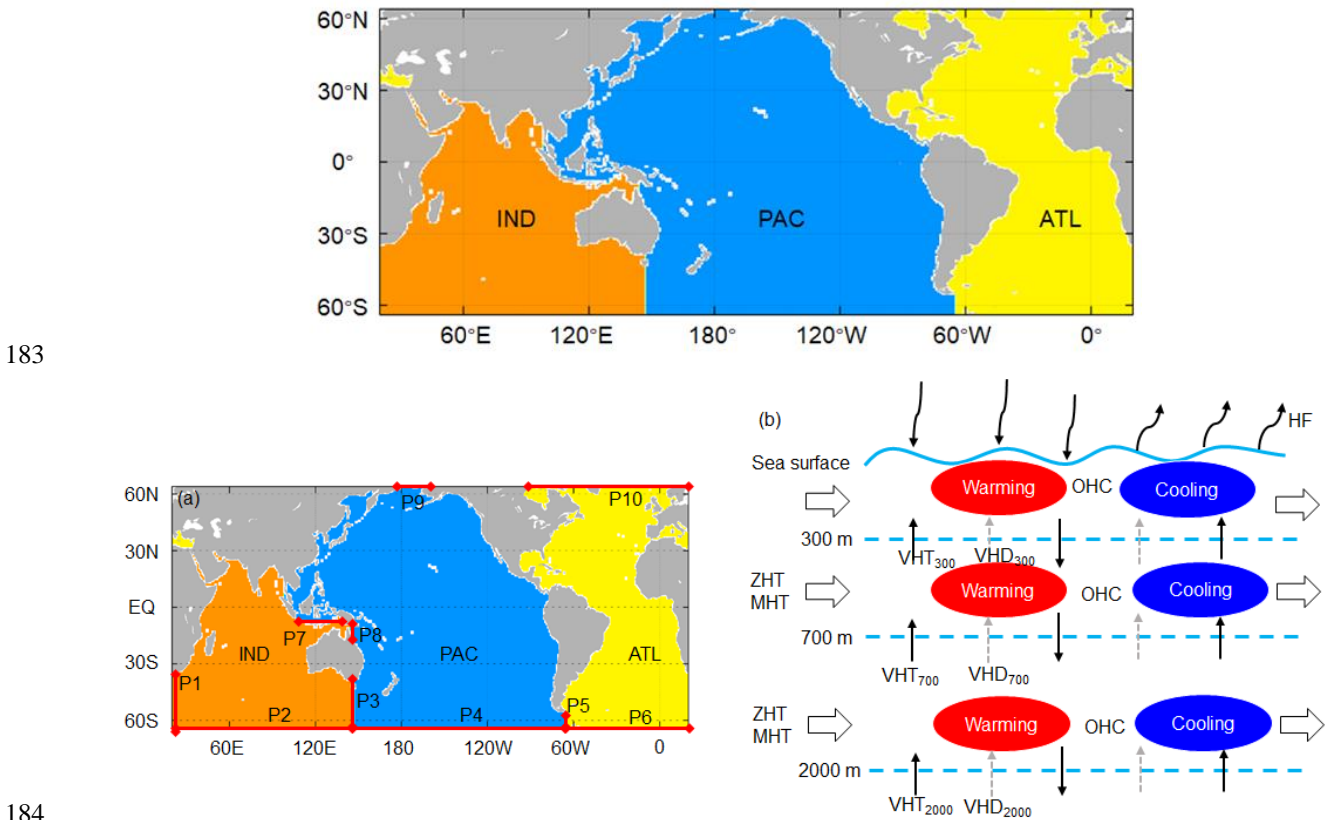
We compared the three datasets ~~during over~~ the period ~~between~~ 1960–2016. ~~Although the two OFES datasets may not be well fully spun up in the beginning, especially the OFES2, the upper ocean is expected to be less impacted and also we focus on their differences on a multi-decadal scale. Moreover, the hot start from the calculated field of the OFES1 may render the OFES2 less sensitive to the spin-up issue compared to a cold start.~~ Following convention, the OHC values here are the OHC anomalies relative to ~~estimates in~~ 1960. At each grid point, the OHC ~~was calculated as is~~ given by

$$\text{OHC} = \rho \delta v C_p (\theta - \theta_{1960}) = \rho \delta v C_p \Delta \theta, \quad (1)$$

where ρ is the seawater density (kg m^{-3}), δv the grid volume (m^3), C_p the specific heat of seawater at constant pressure ($\text{J kg}^{-1} \text{K}^{-1}$), θ the yearly potential temperature ($^{\circ}\text{C}$) and θ_{1960} the averaged potential temperature in

174 1960. The total OHC in the upper ocean layer (above 300 m) is the integral of Eq. (1) from 0 to 300 m. Similar
 175 procedures apply to the other two layers. A value of $4.1 \times 10^6 \text{ kg} \cdot \text{J} \cdot \text{m}^{-3} \cdot \text{K}^{-1}$ was used for the product of ρ and
 176 specific heat of seawater C_p (Palmer et al., 2011).

177 Both the global and individual basin OHCs were calculated for comparison. Figure Fig. 1 shows the domains of
 178 the Pacific, Atlantic and Indian Oceans between 64° S and 64° N, with their respective marginal seas included. The
 179 definition of the marginal seas of the Pacific and Indian Oceans may be inconsistent with some other studies. The
 180 major water passages connecting the different basins are also labelled in Fig. 1a. Also, we label the major water
 181 passages connecting the different basins by red thick lines with diamond arrows on both sides (Fig. 1a). A schematic
 182 diagram showing the primary processes determining the OHC of an ocean basin is presented (Fig. 1b).



184

185 **Figure 1.** Domains of the major basins between 64° S and 64° N and a schematic diagram of the primary processes controlling
 186 the thermal state of an ocean. (a) The Pacific Ocean (PAC), PAC stands for the Pacific Ocean, the ATL for the Atlantic Ocean
 187 and the IND for the Indian Ocean, the Atlantic Ocean (ATL) and Indian Ocean (IND), between 64°S and 64°N. The basin domain
 188 is extracted using the gcmfaces package (Forget et al., 2015) and then interpolated to the corresponding grid of each product. Grey
 189 indicates the land. The red solid lines with diamond arrow stand for the water passage connecting different basins. We label it with
 190 the capital letter P (abbreviation for passage) and a serial number. (b) We use a light blue curve to represent the wave-shaped sea
 191 surface and three dashed lines to indicate the 300 m, 700 m and 2000 m depth. The curve arrow represents the net heat
 192 flux (HF) through the ocean surface. The black hollow arrows show the zonal (ZHT) or meridional (MHT) heat
 193 transport advection. The black thin arrow represents the vertical heat transport advection (VHT) and the grey dash arrow
 194 stands for the vertical heat diffusion (VHD). The red ellipse illustrates warming water and the blue ellipse cooling water. P1: (20°
 195 E, 64° S – 34.5° S – 146.5° E, 64° S); P3: (147° E, 64° S – 36.5° S); P4: (147° E – 65.5° W, 64° S); P5: (67° W, 64° S – 55° S);
 196 P6: (65° W – 19.5° E, 64° S); P7: (118.5° E – 138.5° E, 8.5° S); P8: (142° E, 12.5° S – 8° S); P9: (172.5° W – 166.5° W, 64.5° N);
 197 P10: (88° W – 24.5° E, 64.5° N).

198 =

In addition, the $\Delta\theta$ at a fixed depth are decomposed into a heave (HV component (second term in Eq. (2) below) and a spice (SP) component (third term in Eq. (2)) (Bindoff and McDougall 1994). The HV-related warming or cooling is a result of vertical displacement of the neutral density surfaces (a continuous analogue of discretely referenced potential density surfaces; Jackett and McDougall (1997)). In general, both the dynamical changes and the change in the renewal rates of water masses can induce vertical displacement and thus the HV-related warming or cooling as a consequence (Bindoff and McDougall (1994)). The SP represents warming or cooling as a result of density compensation in the θ and salinity (S) along the neutral density surfaces. This decomposition of $\Delta\theta$ helps to better understand the contributions and ways of different water masses in accounting for the OHC. The changes in the potential temperature $\Delta\theta$ were decomposed into an HV component (second term in Eq. (2) below) and an SP component (third term in Eq. (2)) (Bindoff and McDougall 1994). HV is the Eulerian measure of $\Delta\theta$ at fixed depths, resulting from the vertical displacement of neutral surfaces (Häkkinen et al., 2016). SP represents changes along the neutral surfaces. This decomposition helps to identify the dominant mechanisms ways changing how the potential temperature varies. The formula decomposing the potential temperature is

$$d\theta/dt|_z = - \overbrace{dz/dt|_n}^{\text{HV}} d\theta/dz + \overbrace{d\theta/dt|_n}^{\text{SP}} \quad (2)$$

where t means is the time (year), z means the depth (m) and $|_n$ means along the neutral density surface.

We used the Δ program by Jackett and McDougall (1997) was used to calculate the neutral densities, HV and SP, recognizing that this publically available this code is based on the UNESCO (The United Nations Educational, Scientific and Cultural Organization) 1983 for the computation of fundamental properties of seawater. The code is available from ([http://www.teos-10.org/preteos10 software/neutral_density.html](http://www.teos-10.org/preteos10/software/neutral_density.html)) and; we used its Matlab version. The main inputs for this program are the potential temperature θ and salinity S . As the code limits the latitude domain to between 80°_S and 64°_N , we set further confine our investigation domain to be between 64° from the equator; S and 64°_N equatorward to this also avoids comparisons in sea-ice impacted areas, knowing that (only the OFES2 includes a sea-ice model).

To analyze the causes of OHC differences from thermodynamics and dynamics perspectives, we calculated the surface heat flux (HF), zonal heat transport advection (ZHTZHA), meridional heat transport advection (MHTMHA) and vertical heat transport advection (VHTVHAVHA). Subject Owing to a temporary suspension of the OFES2 data by the JAMSTEC, we cannot could not access to the vertical diffusivity data of the OFES2 (and OFES1 itself does not provide these vertical diffusivity data) when preparing this manuscript. This hampers prevents us to directly compareing the vertical diffusion of heat betweenfrom the OFES1 and OFES2. Alternatively, we calculated the residual of the total OHC and all the other heat inputs (HF, ZHTZHA, MHTMHA and VHTVHAVHA), and taketook itthis as a proxy for the vertical diffusion. As the horizontal heat diffusion was found to be much weaker than the ZHTZHA and MHTMHA (not shown), we therefore neglectdid not include it in the analysis. A diagram of the primary processes is shown in Fig. 1b.

3 Results

The principal aim here is to compare the results from the OFES1 and OFES2, with the EN4 acting as an observation-based reference. If there is a significant difference between the OFES2 result and that of one or both of the other two

235 datasets, does this represent a real phenomenon not present in the other two widely used datasets or is it an unwanted
236 property of the newly released OFES2 simulation? In this section, we compare the three sets of results for the global
237 ocean, and for each of the Pacific, Atlantic and Indian Oceans individually. The first task is to identify significant
238 differences.

239 **3.1 Time evolution of the OHC, HV and SP from 1960 to 2016**

240 ~~In this section, we compare the OHC time series from the three datasets and with some important findings in the~~
241 ~~literature.~~

242 ~~**3.1.1 The upper ocean (0–500 m) time series of OHC, HV and SP**~~

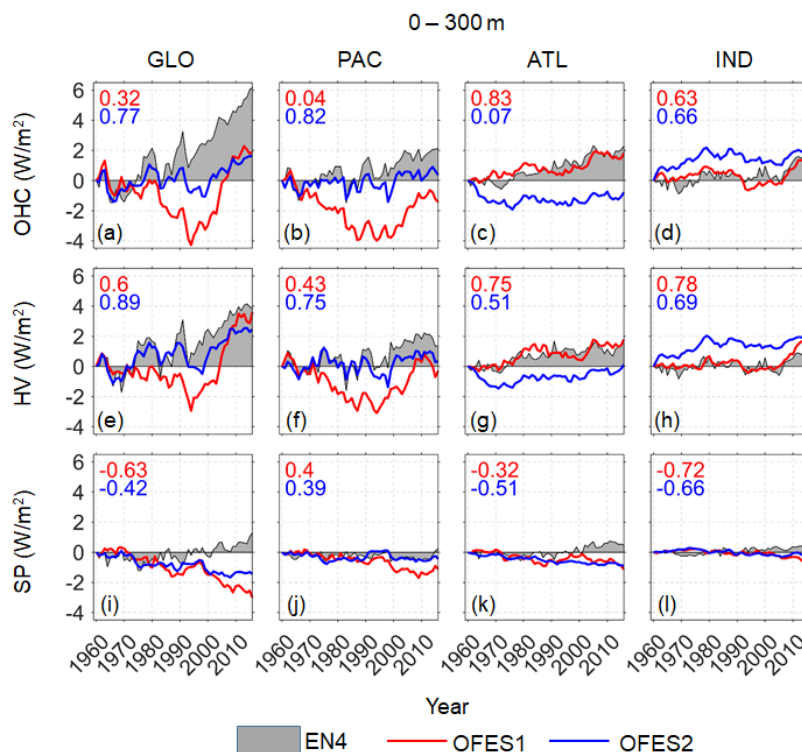
243 ~~Figs. 2–4 present the time series of the total OHC, and its HV and SP components for the upper (0–300 m), middle~~
244 ~~(300–700 m) and lower (700–2000 m) ocean layer, respectively. Note that OHC, HV and SP were calculated as the~~
245 ~~anomaly relative to the estimates in 1960, and converted to an equivalent heat flux applying over the entire surface~~
246 ~~area of the Earth, as suggested by one reviewer.~~

247 *Upper layer*

248 ~~For the global ocean between 0–300 m, all three data indicate cooling from around 1963 to 1966 (Fig. 2a), explained~~
249 ~~as the result of the volcanic eruption of Mount Agung (Balmaseda et al. 2013). A similar cooling over this period can~~
250 ~~also be seen in Domingues et al. (2008) and Allison et al. (2019) for the upper 700 m (their Fig. 1) and (Achutarao et~~
251 ~~al. (2007) for both the 0–700 m and 0–3000 m (their Fig. 1). This short but sharp cooling was found to mainly impact~~
252 ~~the Pacific Ocean (Fig. 2b). Marked OHC reductions associated with the strong volcanic eruptions of El Chichón in~~
253 ~~1982 (a strong ENSO also emerged in 1982–83) and Pinatubo in 1991 were also consistently captured by all the three~~
254 ~~data.~~

255 ~~Both the EN4 and OFES2, but not the OFES1, showed a slowdown in warming and even cooling in the Pacific~~
256 ~~Ocean during the 2000s. This slowdown in Pacific warming corresponded to a sharp warming in the upper layer of~~
257 ~~the Indian Ocean. This relevance between the Pacific and Indian Ocean was found to be a consequence of an~~
258 ~~intensifying Indonesian Throughflow, leading to an increased heat transport from the Pacific to the Indian Oceans~~
259 ~~(Lee et al. 2015; Zhang et al. 2018); however, these two references considered the top 700 m. As will be shown,~~
260 ~~however, this sudden warming of the Indian Ocean was largely confined to the above 300 m, especially as indicated~~
261 ~~by the OFES1 and OFES2 (Fig. 3d). The EN4 showed a clear warming acceleration around 2003 in the global ocean~~
262 ~~above 300 m, which was probably an artefact of the transition of the ocean observation network from a ship-based~~
263 ~~system to Argo floats (Cheng and Zhu, 2014), although these authors mainly used subsurface temperature data from~~
264 ~~the World Ocean Database 2009 (WOD09). Interestingly, a dramatic shift can also be seen in the OFES1 (Fig. 2a),~~
265 ~~remembering that the OFES1 is not directly constrained by observations. A major difference in this jump between the~~
266 ~~EN4 and OFES1 is that it was found to be more closely associated with the SP in the EN4 (Fig. 2i) but with the HV~~
267 ~~in the OFES1 (Fig. 2e). This spiciness warming around 2003, derived from objective analysis of observational data~~
268 ~~can serve as a complement of the work by Cheng and Zhu (2014).~~

270 However, many significant differences can be found between the three datasets. The EN4 indicated an
 271 approximately linear warming since 1970 (Fig. 2a), modulated by the abovementioned climate signals. The OFES1,
 272 however, showed that the cooling persisted almost until the beginning of the 1990s, when a similar linear but stronger
 273 warming appeared afterwards (Fig. 2a); this is more than 20 years later than that indicated by the EN4. The
 274 approximately linear warming appeared even later in the OFES2 from around 2000, and was the weakest among the
 275 three datasets.



276 **Figure 2.** Time series of the global and basin-wide OHC (top), HV (middle) and SP (bottom) between 0–300 m based on the three
 277 temperature products. The OHC, HV and SP here are converted to the accumulative heating in $W \cdot m^{-2}$ applied over the entire
 278 surface of Earth. Grey shadow: EN4; red solid line: OFES1; blue solid line: OFES2. Numbers on the left top corners are the
 279 correlation coefficients between the OFES1 (red) or OFES2 (blue) and EN4. The OHC hereafter is directly calculated from the
 280 potential temperature, rather than the sum of the HV and SP.
 281

282 Compared to the OFES1, the OFES2 agreed better with the EN4 in the temporal profile of the global ocean (Fig.
 283 2a), which, to some extent, is consistent with the smaller sea surface temperature (SST) bias from the OFES2 than
 284 that from the OFES1 when comparing to the World Ocean Atlas 2013 (WOA13) (Sasaki et al. 2020). However, there
 285 was a large magnitude difference after 1980. This came mainly from the spiciness component (Fig. 2i), with both the
 286 OFES1 and OFES2 indicating clear SP cooling. This may imply some discrepancies in the salinity characteristics
 287 from these three data. In contrast, there was quite good agreement in the HV from the EN4 and OFES2 (Fig. 2e).

288 Clear differences can also be easily discerned for each individual basin. The OFES1 differed significantly from the
 289 other two in the Pacific Ocean between around 1970–1990, with the other two similar to each other in both the HV
 290 and SP. In the Atlantic Ocean, however, the OFES1 agreed with the EN4 quite well in the HV. Although the two
 291 OFES datasets had similar spiciness in the Atlantic Ocean, they both disagreed with the spiciness from the EN4. The
 292 OFES2 agreed better with the EN4 in the temporal profile of the global ocean (Fig. 2a), which, to some extent, is consistent with the smaller sea surface temperature (SST) bias from the OFES2 than that from the OFES1 when comparing to the World Ocean Atlas 2013 (WOA13) (Sasaki et al. 2020). However, there was a large magnitude difference after 1980. This came mainly from the spiciness component (Fig. 2i), with both the OFES1 and OFES2 indicating clear SP cooling. This may imply some discrepancies in the salinity characteristics from these three data. In contrast, there was quite good agreement in the HV from the EN4 and OFES2 (Fig. 2e).

293 HV indicated by the OFES2 showed poor agreement with both the EN4 and OFES1 in the 1960s (Fig. 2g). In the
294 Indian Ocean, the OFES1 was much closer to the EN4 than the OFES2. Both the similarities and differences in the
295 OHC came largely from the HV, which dominates the variation of OHC. The notable deviations of the OFES2 relative
296 to others mainly come from the uniquely strong warming in the OFES2 Indian Ocean before around 1980 (Fig. 2d).

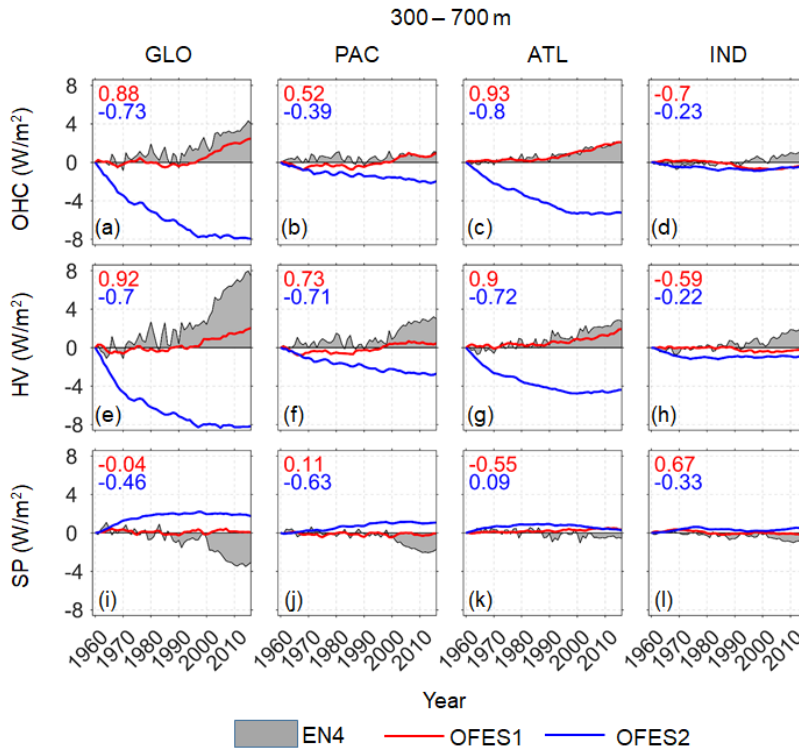
297 A potential issue of the OFES2 is the spin-up, although it started from the calculated the temperature and salinity
298 fields. Without a knowledge about when it is fully spun-up, we here show and compare its simulated results starting
299 from 1960, only excluding the first two years (1958–1959). It seems that the OFES2 has a good agreement with the
300 EN4 since around 1970s in both the Atlantic and Indian Oceans (Fig. 2c, d), which is likely to be related to the better
301 spun-up with time. However, in the Pacific Ocean, the OFES2 was quite similar to the EN4 before 1990, especially
302 in the HV component. This to some extent, may weaken the spin-up argument.

303 304 *Middle layer*

305 In the middle ocean layer (300–700 m) (Fig. 3), there were remarkable differences in the OHC and its HV and SP
306 components between the OFES2 and the other two datasets, most noticeable for the global ocean and the Atlantic
307 Ocean, less so for the Pacific Ocean; there was little difference for the Indian Ocean. The OFES2 showed a moderate
308 Pacific cooling for almost the whole 57-year period and a strong Atlantic cooling trend until around 2000, with a
309 subsequent hiatus in the Atlantic Ocean. There was a minor Indian cooling from the OFES2 in the 1960–70s. In the
310 OFES2, this cooling was mainly due to the decreasing HV, as its spiciness was largely more positive than the other
311 two.

312 In contrast, both the EN4 and OFES1 indicated that this layer was relatively stable before about 1990. Then, the
313 EN4 and the OFES1 both showed the global ocean and the Atlantic Ocean warming (Fig. 3a, c), mostly due to an
314 increase in the HV (Fig. 3e, g). Despite this good agreement between the EN4 and OFES1, there were notable
315 differences in their HV and SP components. Compared to the OFES1, there was a generally stronger positive HV in
316 the EN4 (Fig. 3e–h), and a stronger but negative SP in the EN4, particularly after about 2000 (Fig. 3i, j). A possible
317 reason for this is the fact that there have been much more observations available since the WOCE (World Ocean
318 Circulation Experiment) in the late 1990s and from Argo since the beginning of 2000s. This may have led to a
319 systematic trend in the observational-based dataset EN4. Unlike in the EN4 and OFES2, the SP variations in the
320 OFES1 were almost invisible for almost all the basins. In addition, aforementioned significant warming acceleration
321 from the early 2000s to 2010s in the Indian Ocean (Fig. 2d) can still be seen in the EN4 (Fig. 3d), but this was almost
322 invisible in the two OFES datasets.

323 One major cause of the profound differences between the OFES2 and the EN4 is the spin-up issue. Indeed, even
324 after 2000, clear differences remain in the global ocean. This, on the one hand, is expected because the middle layer
325 takes more time to be well spun-up compared to the upper layer; on the other hand, suggests that special caution is
326 needed when investigating the multi-decadal variations, or even decadal variations in the recent two decades based on
327 the OFES2.



328

329 **Figure 3.** As for Fig.2 but for the middle layer (300–700 m).

330

331 Lower layer

332 In the lower ocean layer (700–2000 m) (Fig. 4), the OFES2 was clearly again the outlier of the three datasets. It showed
 333 that the Atlantic and Indian Oceans experienced cooling from 1960 to the end of 1990s (Fig. 4c, d), then a slight
 334 warming. The Pacific Ocean, however, was shown cooling over the whole 57-year period (Fig. 4b). The better
 335 agreement with the EN4 since the end of 1990s may be related to the spin-up issue of the OFES2, at least to some
 336 extent. However, the agreement between the EN4 and OFES2 was even better than in the middle layer (300–700 m),
 337 particularly in the Atlantic and Indian Oceans. This may weaken the spin-up argument, as it is expected that the
 338 middle layer was more easily spun-up than the lower layer.

339 The OHC variations from the OFES1 and the EN4 were much the same for the global ocean, but this was a result
 340 of the cancelling of the substantial differences in the Pacific and Atlantic Oceans (Fig. 4b, c), and in the HV and SP
 341 (Fig. 4e–l). Specifically, there was a larger OHC increase in the Pacific Ocean from the OFES1 than the EN4, but the
 342 latter showed a larger OHC increase in the Atlantic Ocean. From the perspective of potential temperature
 343 decomposition, the EN4 generally showed a stronger HV increase than the OFES1 in the Atlantic and Indian Oceans
 344 (Fig. 4g, h) but a stronger negative SP or weaker positive SP increase (Fig. 4i–l).

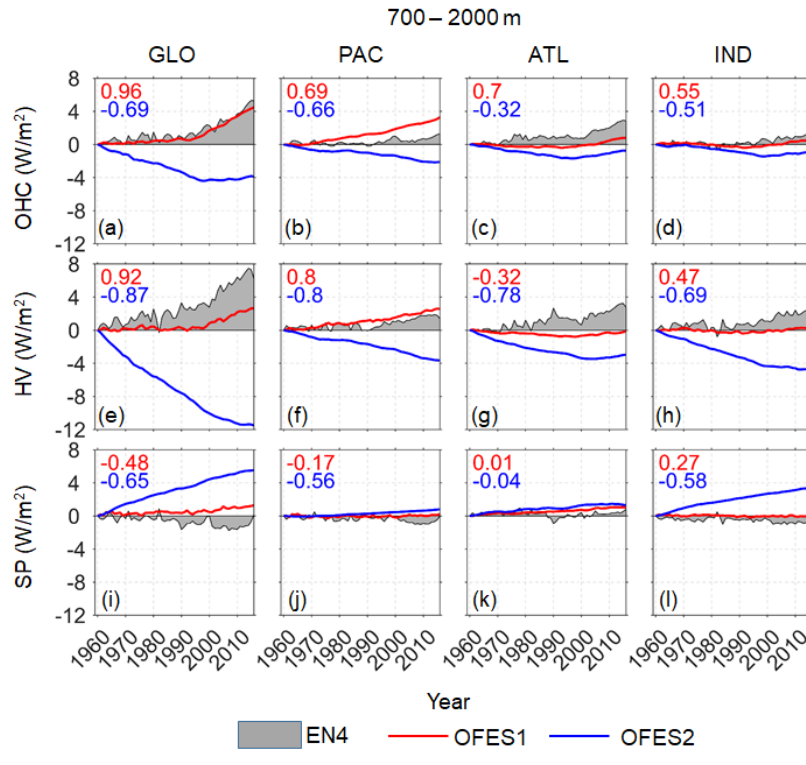
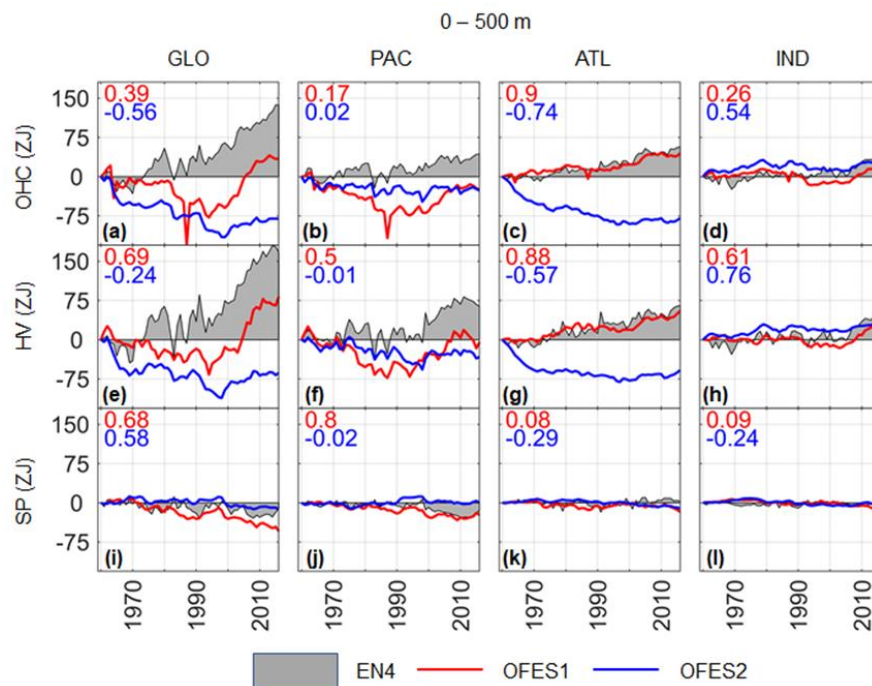


Figure 4. As for Fig.2 but for the lower layer (700–2000 m).

In Fig. 2a, the EN4 shows that the global upper ocean experienced cooling during the 1960s, followed by an approximately linear warming (“linear warming” used here is as a short hand for “warming at a linear rate”) since the 1970s (Achutarao et al., 2007; Zanna et al., 2019). Although this cooling is reproduced in both the OFES datasets, the linear warming appeared started in from around 1994 and 1999 in the OFES1 and OFES2, respectively, more than 20 years later than that in the EN4. In addition, the warming rate in the global upper layer ocean after 1994 was is around $4.30.27 \text{ W-m}^{-2}\text{ZJ/yr}$ from the EN4 and $4.90.34 \text{ W-m}^{-2}\text{ZJ/yr}$ from the OFES1 ($\text{W-m}^{-2}\text{ZJ} = 10^{21}\text{J}$ and yr means yearwatts per meter squared), but only $1.00.07 \text{ W-m}^{-2}\text{ZJ/yr}$ from the OFES2. Unlike in the other datasets, a sharp and remarkable OHC reduction stood out in the OFES1 in 1987 (Fig. 2a).

—In the upper layer of the Pacific Ocean (Fig. 2b), The result from the EN4 shows that the upper layer of the Pacific Ocean was largely warming with some sporadic exceptions (e.g., during the El Chichón eruption around 1982). Conversely, the OFES products indicate an overall cooling before the end of 1980s (OFES1) and the end of 1990s (OFES2) and reversed to warming afterwards, but in different ways. More specifically, the OFES1 indicates cooling before 1987 in the upper Pacific Ocean, with a sudden cooling then occurring. The cooling trend then reversed to warming. In the upper layer of the Atlantic Ocean (Fig. 2c), the OHC time series from the EN4 and the OFES1 are highly correlated (Fig. 2c), with a correlation coefficient of 0.9. In addition, the overall warming rate was is around $1.00.059 \text{ W-m}^{-2}\text{ZJ/yr}$ from the EN4 and $0.8.048 \text{ W-m}^{-2}\text{ZJ/yr}$ from the OFES1. Strikingly, the OFES2 presents a notable cooling of $1.40.12 \text{ W-m}^{-2}\text{ZJ/yr}$ before 2000. Overall, the absolute differences between the three products in the upper layer of the Indian Ocean are the smallest (Fig. 2d), with the OFES2 showing larger largest OHC increase

366 before 2010. A summary of the total warming rate in the upper ocean from 1960–2016 is given in Tab. 2. When
 367 eComparing to the EN4, the OFES data show much weaker warming or even cooling, especially the OFES2.
 368 —The calculated HV and SP can help identify how the ocean water warms or cools (Häkkinen et al., 2016). The HV
 369 dominated the OHC variations (Figs. 2e–h) and evolved substantially different to the SP (Figs. 2i–l). This means
 370 that the OHC variations largely result from the vertical movement of the neutral surfaces over this 57–year period,
 371 as seen in all three products. The HV dominance in OHC variations was has also been examined in Häkkinen et al.
 372 (2016). One interesting point is that the EN4 and OFES1 agrees quite well in the SP of the upper layer of the Pacific
 373 Ocean, although their HV results there are significantly different. In the upper layers of the Atlantic and Indian Oceans,
 374 SP variations are almost negligible. This may result from some consensus of salinity change based on the EN4 and
 375 OFES1.



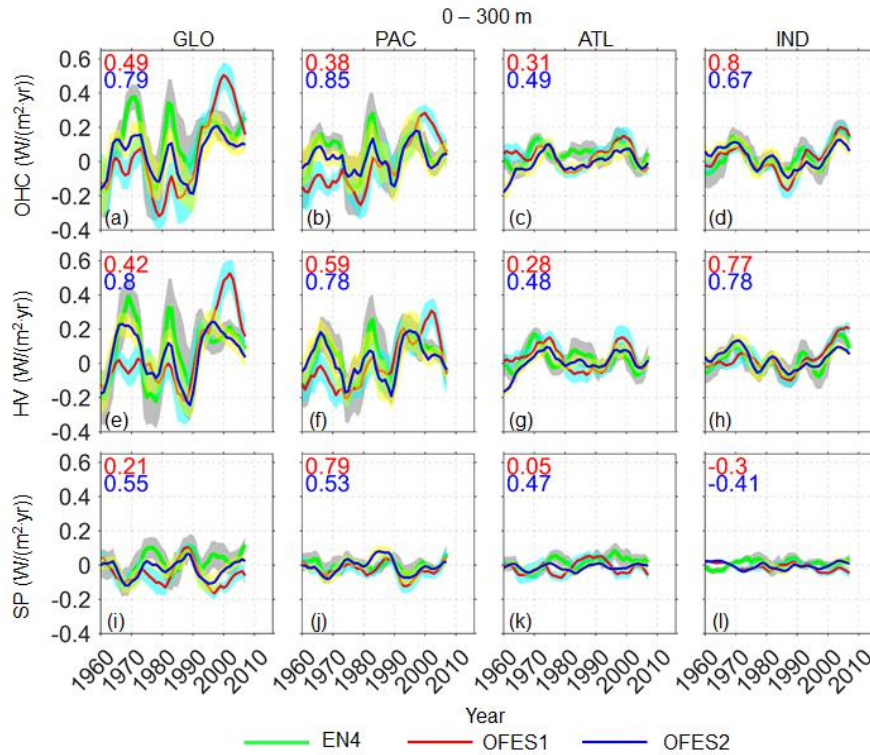
376
 377
 378 **Figure 2.** Time evolution of the global and basin-wide OHC (top), HV (middle) and SP (bottom) in the upper ocean
 379 (0–500 m) based on the three temperature products. The OHC, HV and SP here are converted to the accumulative
 380 heating in $W\cdot m^{-2}$ applied over the entire surface of Earth. Grey shadow: EN4; red solid line: OFES1; blue solid line:
 381 OFES2. Numbers in on the left top-left corners are the correlation coefficients between the OFES1 (red) or OFES2
 382 (blue) and EN4. The OHC hereafter is directly calculated from the potential temperature, rather than the sum of the
 383 HV and SP.
 384
 385

386 **b-3.1.2 The intermediate ocean (500–1400–1500 m) Temporal evolution in the OHC, HV and SP trend**

387 Figs. 2–4 show clearly the similarities and differences between the three datasets in the time series of the OHC, HV
 388 and SP for the period 1960–2016; these vary with time. Therefore, in this section, we calculate the linear trend in the
 389 OHC, HV and SP over a rolling window of 10 years for the three datasets, following (Smith et al. (2015)); the results
 390 for the three layers are shown in Figs. 5–7, respectively. This helps to quantitatively compare the performance of these
 391 data over each temporal window.

392
 393 Upper layer

394 The datasets were similar in the profile of the OHC 10-year rolling trend; they captured most of the peaks and troughs.
 395 There was better agreement in the Indian Ocean (Fig. 5d) than in the other two basins (Fig. 5b, c) but there were still
 396 significant differences even in this shallow layer. The rolling trend for the global ocean from the EN4 was positive
 397 most of the time, except at the beginning of the 1960s and at the ends of the 1970s and 1980s (Fig. 5a). However, the
 398 OFES1 showed a cooling trend in the global ocean before around 1990; it then indicated a larger warming trend than
 399 the other two. The OFES2 generally had a better agreement with the EN4 for the global ocean, but the warming trend
 400 was much smaller than that from the EN4 from the late 1960s to around 1990. Since the beginning of 1990s, the trend
 401 disparity between the OFES2 and the EN4 was much reduced but the OFES2 still showed a consistently weaker
 402 warming trend. This better agreement may be attributed to two causes. Firstly, after around 30-years running, the
 403 OFES2 was believed to have been better spun-up and therefore closer to the actual state. Secondly, it is also possible
 404 that the accuracy of the EN4 data increased as more observational data were included, given that the number of
 405 oceanographic observations has increased significantly since the 1990s (e.g. satellite-based SST measurements).



406

407 **Figure 5.** Temporal evolution of the 10-year rolling trends in the global and basin OHCs (**top row**), HV (**middle row**) and SP
408 (**bottom row**) in the top ocean layer (0–300 m), based on the three datasets. Numbers in the top left corners are the correlation
409 coefficients between the EN4 and the OFES1 (red) or OFES2 (blue). The OHC, HV and SP were converted to accumulative heating
410 ($W m^{-2}$) over the entire surface of the Earth. Thick green line: EN4 (grey shadow: 95% confidence interval); thin red solid line:
411 OFES1 (cyan shadow: 95% confidence interval); thin blue solid line: OFES2 (yellow shadow: 95% confidence interval). The OHC
412 from now on is calculated directly from the potential temperature, rather than as the sum of the HV and SP.
413

414 Among the differences between the three datasets, the three extreme trend peaks at around 1970, 1980 and 2000
415 (Fig. 5a) are particularly prominent, with remarkable differences between the two OFES and EN4, indicating some
416 deficiencies of numerical modelling in the reproducing of strong climate events. Apart from some minor magnitude
417 differences, the three data agreed best in the Indian Ocean (Fig. 5d). The OFES1 was close to the EN4 in showing
418 significant warming in the Indian Ocean in the 2000s, whereas the OFES2 showed a relatively weaker warming. A
419 second better agreement between the three datasets was reached in the Atlantic Ocean.

420 The HV clearly dominated the 10-year rolling trend in all basins (Fig. 5e–h), and the major differences between
421 the three datasets resulted from differences in the HV component. In addition, there was an apparent out-of-phase
422 relationship between the HV and SP trends in the global ocean and Pacific Ocean. This correspondence between the
423 HV and SP is expected for typical stratification associated with subtropical gyres (Hakkinen et al. 2016), with warm
424 and salty water over the cold and fresh water. The OFES1 and OFES2 were quite close in the simulation of spiciness,
425 particularly in the individual basins (Fig. 5i–l).

426 *Middle layer*

427 The variation in the 10-year rolling trend from the OFES1 and the EN4 was much the same for the global, Pacific and
428 Atlantic Oceans, but the latter dataset having a much large uncertainty. The OFES2 showed significantly different and
429 generally cooling trend, especially concentrated in the Atlantic Ocean, consistent with Fig. 3; the reasons why notable
430 cooling trend from the OFES2 in the Atlantic Ocean weakened with time needs a further detailed study. It was found
431 that the cooling trend in the OHC from the OFES2 came largely from the HV. In the Pacific Ocean (Fig. 6b), the
432 OFES2 consistently show a weak cooling trend, but in the middle and late 1960s and after around 1980, both the EN4
433 and OFES1 showed a warming trend of similar magnitudes. The OFES1 also agreed well with the EN4 in the Atlantic
434 Ocean, both indicating weak warming for most of the period but also sporadic cooling trend. However, these good
435 agreements are the compensation results of the significantly different HV and SP components from the OFES1 and
436 EN4. For example, the EN4 showed much stronger HV warming trend than the OFES1 in the Pacific Ocean since the
437 early 1990s, but in the meantime, the EN4 also indicated strong SP cooling trend. In the Indian Ocean, the EN4
438 presented warming trend over much of the 57-year period, whereas the two OFES datasets showed weak variations
439 and reversals between warming and cooling.
440

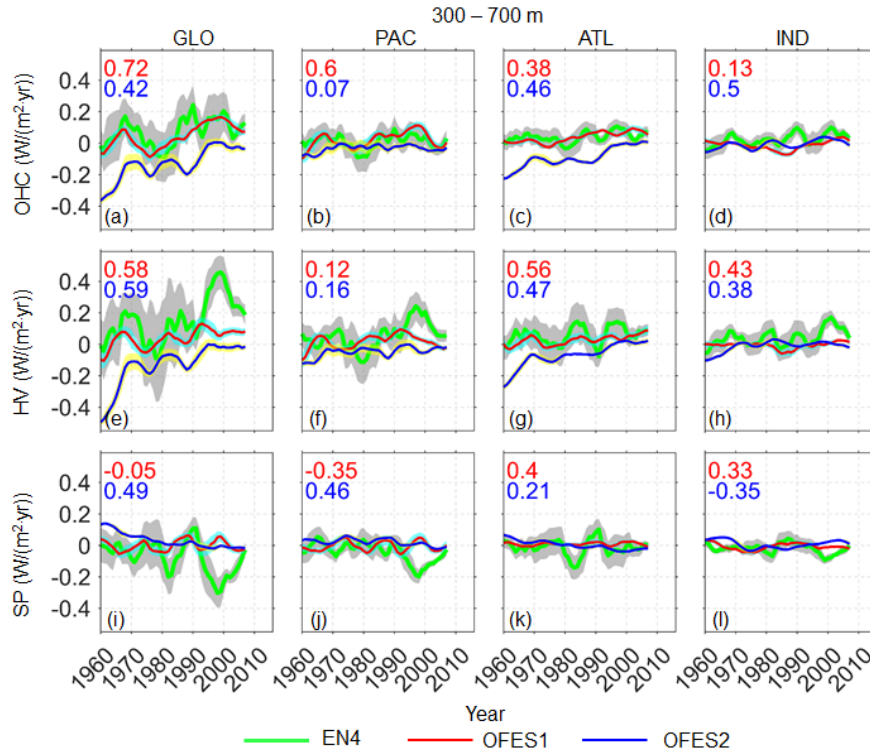


Figure 6. As for Fig. 5 but for middle layer (300–700 m).

Lower layer

As in the middle layer, the OFES2 differed significantly from other two datasets by showing a cooling trend in the global ocean until about 2000 (Fig. 7a). Although a warming trend appeared in the global ocean in the OFES2, the intensity was much lower than that of the EN4 and OFES1. The major differences between the two OFES datasets occurred in the Pacific Ocean (Fig. 7b), and was mostly HV-associated. Despite of the good agreements in the OHC trend between the OFES1 and OFES2 in the Atlantic and Indian Oceans (Fig. 7c, d), their HV and SP components were markedly different, especially in the Indian Ocean (Fig. 7h, l). The OFES1 and the EN4 showed much the same global OHC trend (Fig. 7a), but again this was the result of the significant HV and SP components cancelling each other. The excellent agreement between the EN4 and OFES1 in each basin (Fig. 7b–d) was also the result of cancellations of notable basin-wide differences, especially in the Pacific and Atlantic Oceans (Fig. 7b, c).

To summarize, the OFES2 showed some improvement (better agreement with the EN4) over the OFES1 in the upper layer (above 300 m), but was more of an outlier in the other two layers. It is essential to examine the HV and SP when investigating the OHC trends, as different data products may show much the same OHC evolution, but substantially different HV and SP.

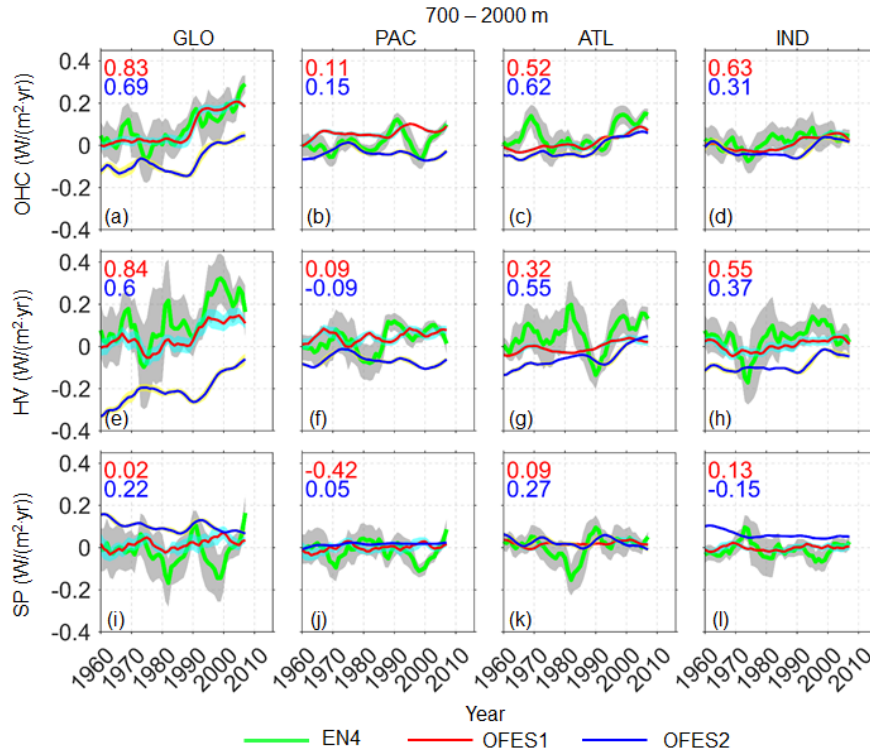
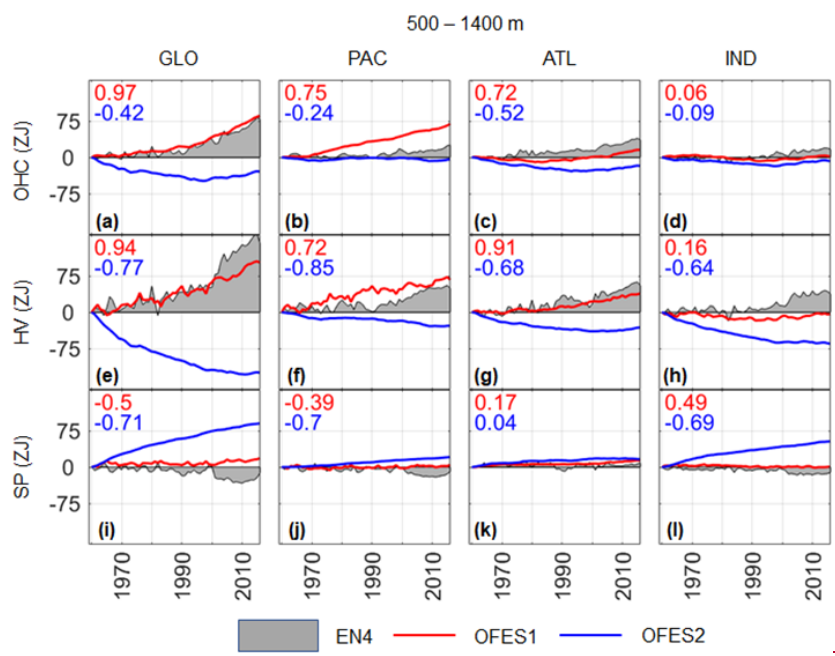


Figure 7. As for Fig. 6 but for the lower layer (700–2000 m).

$2.50.18 \text{ W}\cdot\text{m}^{-2}\text{ZJ}/\text{yr}$ from the EN4 and $2.50.18 \text{ W}\cdot\text{m}^{-2}\text{ZJ}/\text{yr}$ from the OFES1. This temporal evolution profile agrees well with the trend based on NOAA/NODC (shown in (Cheng et al., 2016)), but the depth is between 700–2000 m in that paper. The OFES2 indicates a cooling of $1.30.13 \text{ W}\cdot\text{m}^{-2}\text{ZJ}/\text{yr}$ before 1998, then warming at a rate of $1.0.058 \text{ W}\cdot\text{m}^{-2}\text{ZJ}/\text{yr}$. In the intermediate layer of the Pacific Ocean (Fig. 3b), the EN4 OHC were is closer to the OFES2, both of which shows slight or even negligible OHC variations. On the contrary, The OFES1 indicates a distinct overall warming rate of $1.20.11 \text{ W}\cdot\text{m}^{-2}\text{ZJ}/\text{yr}$ over 1960–2016. In the intermediate layer of the Atlantic Ocean (Fig. 3c), the OHC profile from the OFES1 is similar to that of the EN4, with both of them indicating a relatively stable OHC before the 2000s, and a subsequent approximately linear weak warming. Although the results from the OFES2 show that the intermediate layer of the Atlantic Ocean was cooling before the middle of the 1990s, the two OFES products are similar from around 2000, with a warming of $1.00.073 \text{ W}\cdot\text{m}^{-2}\text{ZJ}/\text{yr}$ from the OFES1 and $0.6.039 \text{ W}\cdot\text{m}^{-2}\text{ZJ}/\text{yr}$ from the OFES2. The warming rate over the same period was is larger in the EN4, reaching $1.40.11 \text{ W}\cdot\text{m}^{-2}\text{ZJ}/\text{yr}$. The OHC variation in the intermediate layer of the Indian Ocean is rather weak except from the EN4 (Fig. 3d), which displays a moderate warming from around the middle of the 1990s. Despite the similarity in the OHC in the global intermediate ocean between the EN4 and OFES1 (Fig. 3a), one can immediately see that the differences in the basin OHC estimates were are notable. Interestingly, these basin differences together contribute to the similarity in the global OHC in the intermediate ocean between the EN4 and OFES1. This may result from the simulation of the heat redistribution between the basins in the OFES1. Tab. 3 summarizes the total warming rate in the intermediate ocean over 1960–2016. On the one hand, although the OFES1 shows the global ocean and basins warmswarmed, as shown in the EN4,

479 the intensity is quite different for each basin. On the other hand, a general weak or moderate cooling was presented
 480 by the OFES2.

481 —Similar to the upper ocean, the HV accounts for much more of the OHC variations than the SP in the intermediate
 482 ocean. Indeed, only the OFES2 shows moderate SP-related warming components in each of the three major basins
 483 (especially in the intermediate layer of the Indian Ocean), and thus significant SP-related warming variations in
 484 the global intermediate ocean. This may indicate the differences in the simulation of salinity between the OFES1 and
 485 OFES2, similar to the bias comparison of sea surface salinity (SSS) in Sasaki et al. (2020). Despite the magnitude
 486 differences, both the EN4 and OFES1 show increases in the warming associated with HV in the intermediate layers of
 487 the Pacific and Atlantic Oceans, whereas the HV estimates from the OFES2 largely decreased with time.



488
 489
 490 **Figure 3. As for Fig. 2 but for the intermediate ocean (500 – 1400/1500 m).**

492 **3.2 Meridional distribution of the zonal-integrated OHC, HV and SP**
 493 **Temporal evolution of the zonal-averaged potential temperature trend**

494 Section 3.1 focused on the temporal characteristics of the global and basin-wide OHC, HV and SP from the three
 495 datasets. Although both similarities and differences were demonstrated, this comparison only in the temporal
 496 domain lacked spatial information. Here, we aim at understanding how the differences were distributed in the
 497 meridional direction. As a first step, we calculated the 10-year rolling trends in the zonal-averaged potential
 498 temperature change for all three datasets (Figs. 8–10). We also calculated the HV and SP components
 499 (Supplementary Information, Figs. 1–6).

500 The complex patterns shown in Figs. 8–10 defy easy interpretation, so we focus on the large-scale patterns of the
 501 similarities and differences.

502
503
504
505
506
507
508
509
510
511
512
513
514
515
516
517
518
519
520
521
522
523
524
525
526
527
528
529
530
531
532
533
534
535
536
537
538

Upper layer

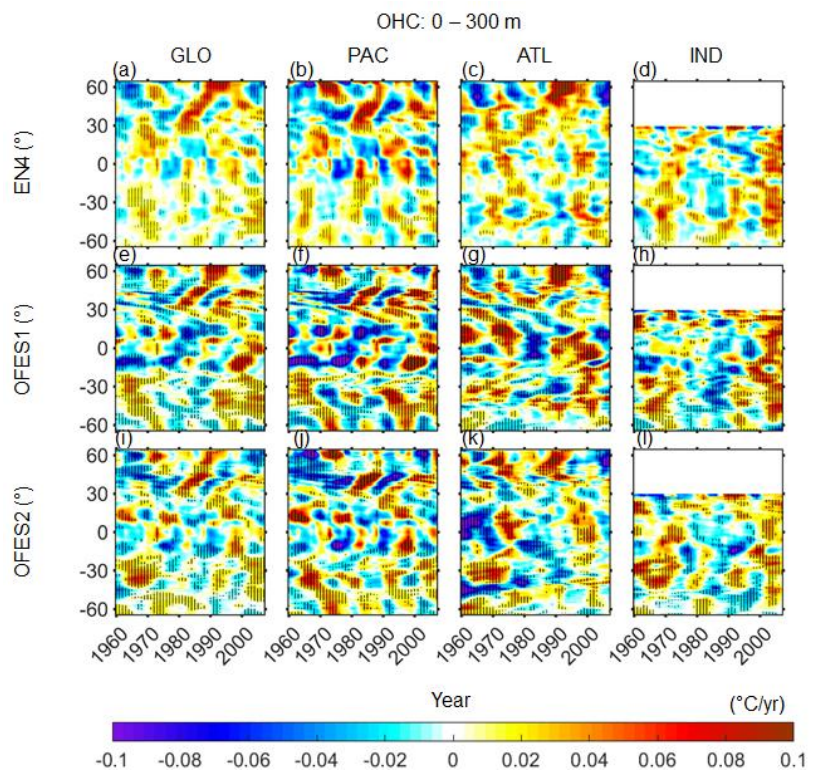
There was a generally reasonable correlation between these datasets at latitudes 30–60° N for both the Pacific and Atlantic Oceans (there is no northern high latitude in the Indian Ocean). More specifically, there was a wave-like cooling trend propagating from around 60° N to 30° N from 1960 to the end of the 1970s in the global ocean; this apparent propagation was especially clear in the EN4 and OFES2. In addition, there was northward propagation of a cooling trend in the 1990s between around 30–45° N. It is reasonable to attribute this cooling to the volcanic eruption of Indonesia’s Mount Agung in 1963, Mexico’s El Chichón in 1982 and the Philippines’ Mount Pinatubo in 1991; the two hindcast simulations were able to reproduce these climate events.

Following these cooling events, there were three subsequent warming trends, as the ocean surface temperature returned back to normal once the aerosols released over several years of volcanic eruptions finally dispersed. Of these warming trends, that following the El Chichón eruption was the most significant; there was a clear northward propagation of the warming from around 30° N to the subpolar areas. Interestingly, the contributions to this large-scale warming and cooling by the SP was comparably to the HV (Supplementary Information, Figs. S1–2), contradicting the general sense that the HV dominates the potential temperature change. In fact, the above-mentioned propagation of the cooling patch from around 60 to 30° N in the 1960–70s was, to a larger extent, associated with the SP.

Equatorward of 30°, large differences emerged in the data. Strong cooling was particularly visible in the OFES1 in the Pacific tropics before around 1990 (Fig. 8f), corresponding to the persistent cooling in the global ocean and Pacific Ocean from the OFES1 in Fig. 2. In the OFES2 Pacific Ocean, clear differences from the EN4 were discerned in the low latitudes before around 1980, then a similar pattern to the EN4 was simulated by the OFES2. In the Atlantic tropics (Fig. 8, 3rd column), there was moderate-to-intense warming in the 1960s in the EN4 and OFES1, but considerable cooling in the OFES2, which may be a result of poor spun-up in the OFES2. All three datasets captured the Atlantic tropical warming in the 1970s, and from the 1990s to the 2000s, but the two OFES datasets estimating a much stronger intensity than the EN4, especially the OFES1. In addition, the OFES1 showed a significant cooling appearing in the Atlantic tropics in the 1980s (Fig. 8g). Although a similar contemporary cooling was shown by the OFES2, its cooling center was shifted several degrees southward. This 1980s Atlantic tropical cooling was comparatively weak in the EN4. Moreover, the OFES2 indicated an approximate 20-year cooling in the vicinity of 45°S in the Atlantic Ocean (Fig. 8k); this cooling in the 1960s existed, but weaker in intensity, in the EN4 and OFES1. In the Indian Ocean, the most significant agreement among the three datasets was the intense warming in the 2000s. In addition, there were some common cooling patterns from the 1980s to the 1990s in all three datasets. Over these latitudes, the HV accounted for more of the potential temperature change than the SP, with the latter in general counteracting the HV (Supplementary Information, Figs. S1–2).

A general property of the similarities and differences between these three datasets is that a better agreement was reached in the poleward of 30° than the latitudes equatorward of 30°. A possible explanation for this latitudinal dependence is that a deeper thermocline at a higher latitudes responded less sensitively to the applied wind stress (Kutsuwada et al., 2019). Kutsuwada et al. (2019) found that the NCEP reanalysis wind stress used as the atmospheric

539 forcing of the OFES1 had some issues, causing much shallower thermocline in the tropical North Pacific Ocean and
 540 therefore large negative temperature differences when comparing to the observations and an OFES version forced by
 541 the wind stress from the satellite measurements (QSCAT). The authors also claimed that the JRA 55 wind stress had
 542 similar problems with the NCEP wind. Indeed, the intense Pacific cooling patches in Fig. 2f was likely to be resulting
 543 from the abnormally shallower thermocline in the tropical Pacific Ocean, consistent with Kutsuwada et al. (2019),
 544 despite different temporal periods were considered.

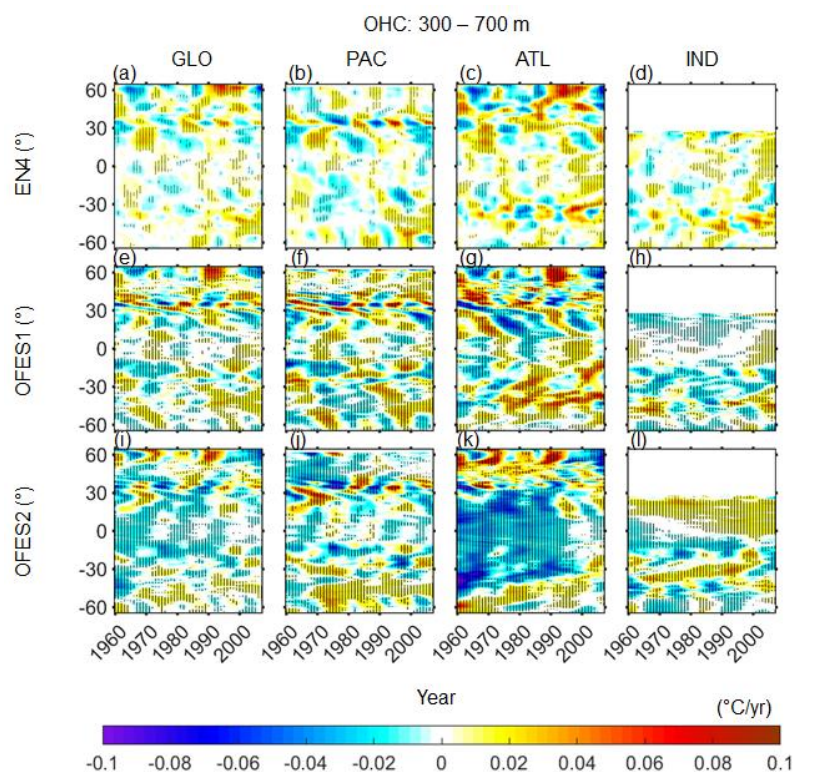


545
 546 **Figure 8.** Temporal evolution of 10-year rolling trend of the zonal averaged potential temperature change in the upper layer of
 547 the ocean (0–300 m). **Left to right:** global, Pacific, Atlantic and Indian Ocean. **Top to bottom:** EN4, OFES1 and OFES2.
 548 Horizontal axis: year; vertical axis: latitude. Stippling indicates the 95% confidence level. The HV and SP counterparts are in the
 549 Supplementary Information, Figs. S1–6.

551 Middle layer

552 In the middle layer between 0–300 m, the three datasets showed relatively poor agreement compared to the upper
 553 layer. The OFES2 differed from the others by showing intense cooling before 2000 in the Atlantic Ocean (Fig. 9k)
 554 and moderate but consistent warming in the northern Indian Ocean over most of the whole period (Fig. 9l). In
 555 addition, there were large-scale cooling patches in the northern Pacific Ocean and along the Indian Equator from the
 556 OFES2, while these cooling were not apparent in the other two datasets. These cooling distributions further showed
 557 where and when the cooling trend from the OFES2 in Figs. 3 occurred and can be at least partially attributed to the
 558 spin-up issue of the OFES2. However, some similarities between the OFES2 and other two datasets emerged in
 559 recent decades. For example, the OFES2 reproduced the marked warming at the high latitudes of the Atlantic Ocean
 560 in the 1980s and 1990s, and a subsequent cooling (Fig. 9k), similar to the EN4 and OFES1.

561 Comparing the OFES1 with the EN4, both similarities and differences can be discerned. The OFES1 generally
 562 agreed with the EN4 north to 30°N, with only a few differences. In the tropics, however, large differences were
 563 found between the OFES1 and EN4. For instance, the OFES1 indicated that the northern Indian Ocean was cooling
 564 consistently (Fig. 9h), but alternate warming and cooling appeared in the EN4 (Fig. 9d). Furthermore, the intense
 565 warming and cooling patches in the southern Atlantic and Indian Oceans, respectively, shown in the OFES1 (Fig.
 566 9g, h), were not clearly visible in the EN4 (Fig. 9c, d). These potential temperature changes mainly resulted from
 567 the vertical displacement of the neutral density surfaces, that is, the HV (Supplementary Information, Fig. S3).
 568 However, the role of the SP cannot be ignored. This was especially clear in the southern hemisphere in the EN4. The
 569 OFES2 also showed that the warming of the northern Indian Ocean was largely SP-related.



570
 571 **Figure 9.** As for Fig. 8 but for the middle layer (300–700 m).
 572

573
 574 Lower layer

575 The northern Atlantic Ocean, especially north to 30°N, dominated the global potential temperature change in the
 576 EN4 (Fig. 10); this was related more to the SP, especially in the intense cooling patch (Supplementary Information,
 577 Fig. S6). Although the OFES1 agreed well with the EN4 in the northern Atlantic Ocean (> 30° N), there were
 578 considerable differences elsewhere between the OFES1 and EN4. More specifically, there was intense HV-
 579 associated warming and cooling in the southern Pacific Ocean in the 1960s and 1970s in the OFES1, but not in the
 580 EN4 (Supplementary Information, Fig. S5). In addition, the warming of the southern Pacific Ocean since about 1990
 581 was much stronger in the OFES1 than in the EN4. The main reason is that there was strong SP cooling in the
 582 southern Pacific Ocean in the EN4 (Supplementary Information, Fig. S6). Moreover, the consistent cooling in the

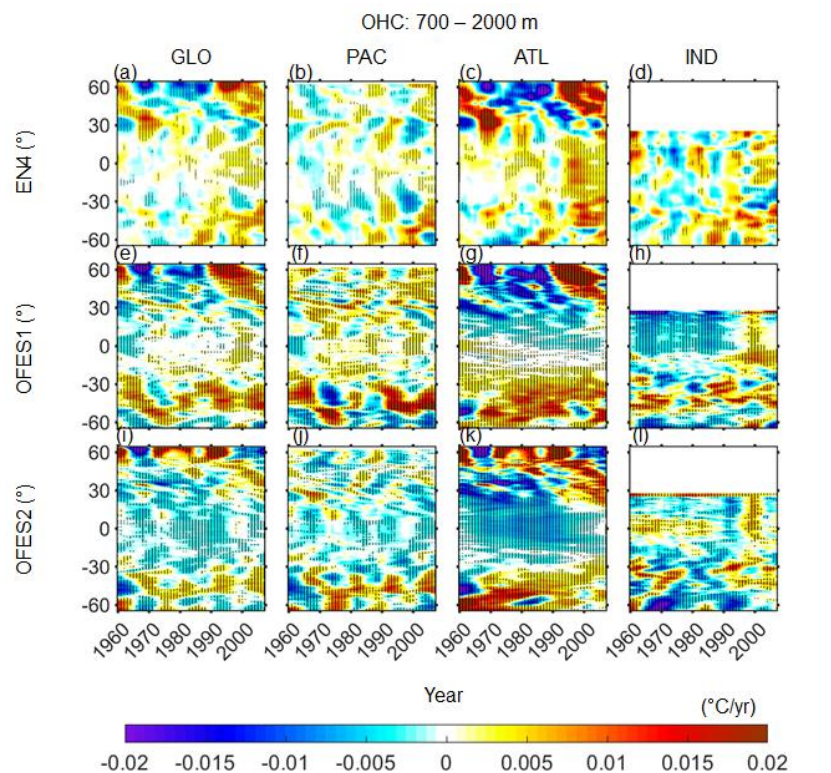
583 Atlantic tropics, the significant warming in the southern Atlantic Ocean and the intense cooling of the northern
584 Indian Ocean before the middle of the 1990s shown by the OFES1 were not evident in the EN4.

585 The OFES2 captured some warming patterns in the southern hemisphere, similar to the OFES; it also agreed
586 with the other two datasets in the intense warming patch in the northern Atlantic Ocean. However, the agreement
587 between the OFES2 and the others was generally poor. Most significantly, cooling was indicated by the OFES2 at
588 the low and middle latitudes in both the Pacific and Atlantic Oceans, especially the latter. Furthermore, both the
589 EN4 and OFES2 showed marked but opposite SP variations in the northern Atlantic Ocean north to 30°N, whereas
590 the OFES1 indicated moderate SP in a similar warming/cooling pattern to the EN4.

591 From Fig. 10, it seems that the spin-up may not be the primary reasons for the differences between the two OFES
592 data and the EN4, as there are no clear improvements in the agreements with the EN4 in the recent decades. Another
593 possible is that the two OFES data have not been fully spun-up even after an integration of more than 50 years for
594 the water in the lower layer.

595 To summarize, the two OFES datasets had come good agreements with the EN4 in the upper ocean layer, but
596 largely confined to the middle-high latitudes. Poor agreements were found in the ocean beneath. Specifically, in the
597 middle ocean layer, the OFES1 had a generally reasonable agreement with the EN4, but large differences exist
598 elsewhere; in the OFES2, intensive cooling patches were simulated, especially in the Atlantic Ocean. Although the
599 spin-up issue may partially explain the notable differences between the OFES data and EN4 for the ocean below 300
600 m, other causes responsible for the examined differences are also possible.

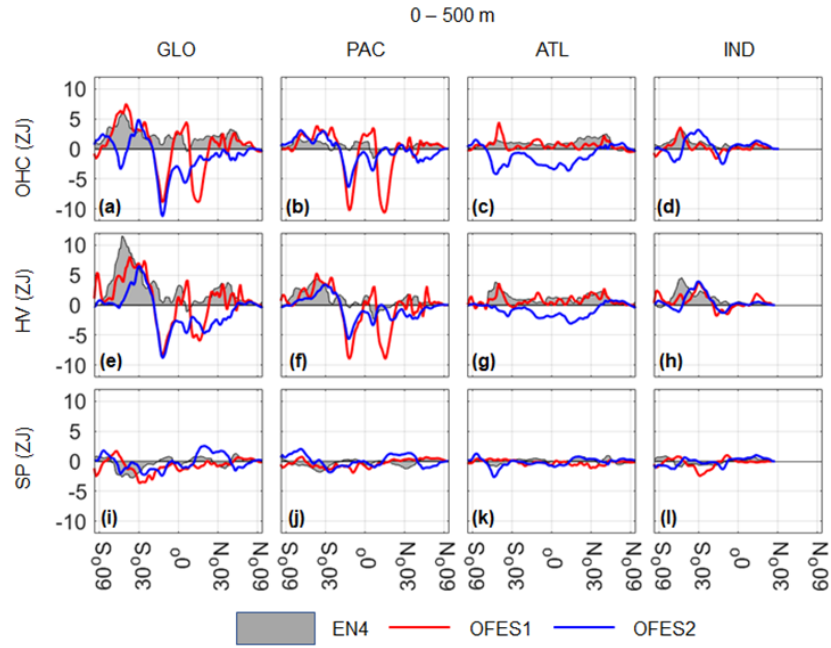
601



602

603 **Figure 10.** As for Fig. 8 but for the lower layer (700–2000 m). Note the different colour scale.

604

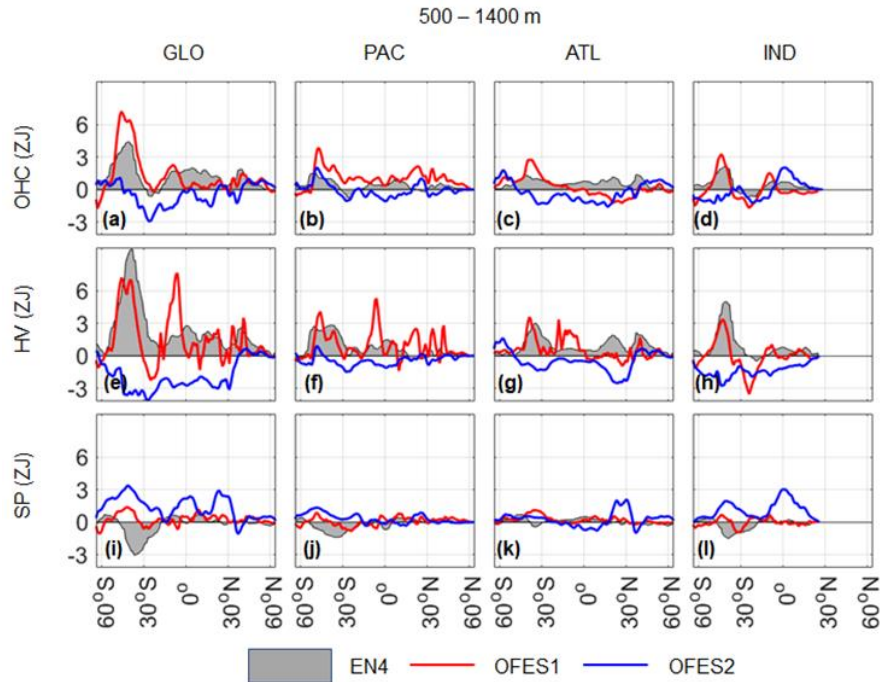


605

606 ~~— mentioned by the other two.~~

607 ~~—As for the meridional OHC distribution in the intermediate layer of the Pacific Ocean (Fig. 5b), the three data~~
 608 ~~shares similar meridional profile of OHC change but differs in the magnitude. More specifically, the OFES2 agrees~~
 609 ~~well with the EN4 between around 64°S and 2517°S. To the nNorth of to 6051°S in the intermediate layer of the~~
 610 ~~Pacific Ocean, the OFES1 consistently indicates a largest consistent OHC increase, whereas the OHC is shown to~~
 611 ~~slightly decrease between north to 3035°S and 20°N in the OFES2, except between 21 30°N. As indicated by the~~
 612 ~~EN4, warming is present found at almost all the latitudes considered in the intermediate layer of the Atlantic Ocean~~
 613 ~~(Fig. 5e). However, cooling can be seen in the OFES data in different latitudal intervalslatitudes. Interestingly,~~
 614 ~~warming is revealed by the OFES1 for the intermediate layer of the southern Atlantic Ocean, where it is akin to the~~
 615 ~~EN4, but cooling dominates in the intermediate layer of the northern Atlantic Ocean as shown by the OFES1. The~~
 616 ~~OFES1 resembles the EN4 in the intermediate layer of the southern Indian Ocean (Fig. 5d) in presenting a significant~~
 617 ~~warming peak slightly north to the north of 5043°S, but this peak is missed by the OFES2. In spite of this distinction,~~
 618 ~~the OFES2 also reveals a large OHC increase near the Equator, just as the other two.~~

619 ~~—The HV component again dominates the OHC variations over almost the whole latitude range. Both the EN4 and~~
 620 ~~OFES2 suggest moderate SP variations, especially the latter. In the EN4, moderate SP variations are located at around~~
 621 ~~40°S in the Pacific and Indian Oceans, but not in the intermediate Atlantic Ocean. However, it is clear that the SP~~
 622 ~~change is mainly related to cooling in the EN4 and warming in the OFES2, signifying notable differences in the~~
 623 ~~variations of salinity.~~



624

625 **Figure 5. As for Fig. 4 but in the intermediate ocean (500–1400–1500 m).**

626

627 **3.3 Depth–time distribution of potential temperature, HV and SP trend**

628 Although we divided the top 2000 m into three layers, some detail was lost in taking layer (vertical) averages. In
 629 this section, we compare vertical trends in the potential temperature change ($\Delta\theta_{OHC}$), and its HV ($\Delta\theta_{HV}$) and SP ($\Delta\theta_{SP}$)
 630 components (Figs. 11–13).

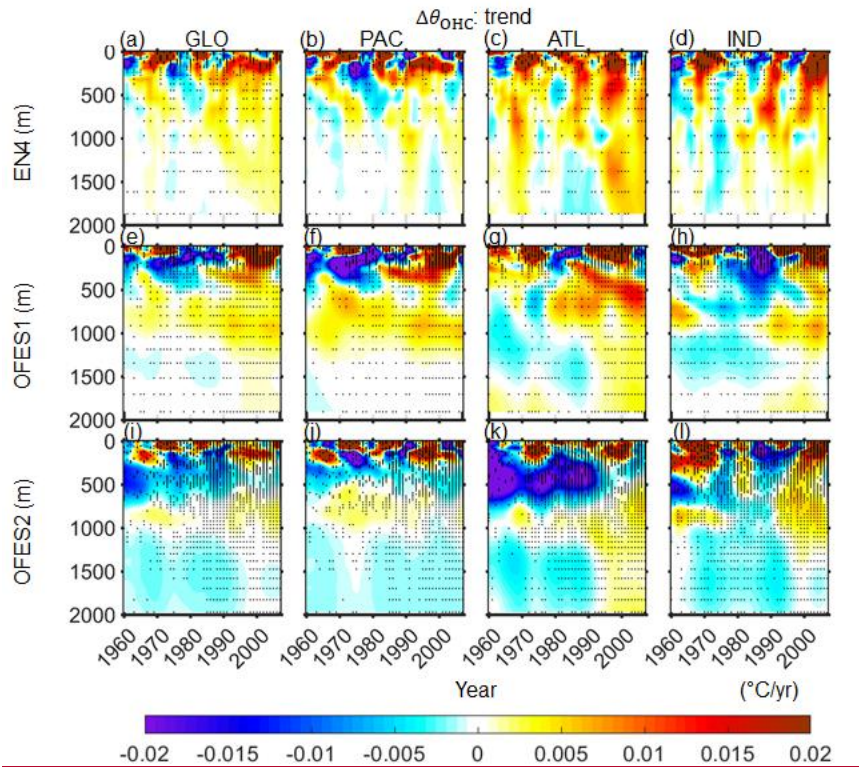
631 For the global ocean, the upper ocean layer above 300 m accounted for most of the warming or cooling (Fig. 11,
 632 left column). The EN4 showed warming over most of the investigated period with a few cooling as a response to the
 633 distinctive climate events. It can be seen that the volcanic eruptions of Mount Agung and El Chichón impacted a
 634 greater depth than the eruption of Pinatubo. The aforementioned strong cooling from the OFES1 in the upper Pacific
 635 layer before 1990 started at a greater depth in the beginning and subsequently ending at a shallower depth (Fig. 11e).
 636 At greater depths, moderate warming or cooling can be found. Specifically, in the EN4, moderate warming can be
 637 seen far deep to around 2000 m since around the early 1990s. The OFES1 showed moderate warming between 500–
 638 1000 m over almost the whole investigated period. Since around the middle of 1990s, a weak warming extended to
 639 the 2000 m based on the OFES1. The differences of the OFES2 from the other two datasets are apparent in the global
 640 ocean below around 200 m, where cooling is the dominant pattern except some weak warming patches between 500–
 641 1000 m (Fig. 11i).

642 In the Pacific Ocean, the OFES2 had a generally reasonable agreement with the EN4 above around 200 m, whereas
 643 the agreement between the OFES1 and the EN4 was poor, despite of some similar warming or cooling patches. Further
 644 below, the EN4 showed periodic warming and cooling. The OFES1 showed consistent warming between around 500–
 645 1200 m, whereas the OFES2 estimated consistent cooling with some exceptions between 500–1000 m. Although

646 beyond the scope of this work, the question on why both the OFES1 and OFES2 showed relatively consistent warming
647 between 500–1000 m, around the depth of the permanent thermocline, necessitate a further work.

648 In the Atlantic Ocean, intense warming or cooling extended deeper when compared to the Pacific Ocean.
649 Specifically, the strong warming in the 1980–90s from the EN4 appeared as deep as around 750 m and moderate
650 warming extended to 2000 m since the middle of 1990s. The OFES1 well captured the warming in the 1970s and
651 1990s, and a subsequent cooling in the 2000s, in the upper layer of the Atlantic Ocean when compared to the EN4.
652 However, the OFES1 estimated a strong cooling in the 1980s in the upper layer of the Atlantic Ocean, which was
653 invisible in the EN4. Interestingly, the OFES1 showed a downward propagation of a strong warming from around 200
654 m to around 800 m since the early 1980s; a downward propagation of cooling from around 600 m to 1800 m can also
655 be seen in the OFES1 Atlantic Ocean (Fig. 11g). Similar to the EN4, moderate warming extended to 2000 m since
656 around the middle of 1990s. As for the OFES2, the most prominent pattern distinguishing it from the others are the
657 extensive cooling patch before around 1990. In addition, it showed moderate cooling below 1000 m before around
658 1990. These two extensive cooling patterns in the upper-middle and deep layers of the Atlantic Ocean by the OFES2
659 raised questions: what are the main causes of these two cooling patches in the OFES2 and why they suddenly stopped
660 at around 1990. One possible reason is that improvement of the reanalysis product of the atmospheric forcing since
661 1990, especially the surface heat flux and wind stress, the latter of which has been shown to be essential to the
662 subsurface temperature simulations (Kutsuwada et al. 2019).

663 In the Indian Ocean, both the OFES1 and OFES2 captured the warming in the 1960–70s and in the 2000s. However,
664 the OFES1 presented an intense cooling in the upper layer in the 1980s; a similar but less extensive cooling can also
665 be seen in the OFES2. Below the upper layer, the EN4 showed largely warming with a major exception of cooling in
666 the 1970s. The two OFES presented notably different patterns. Specifically, between 500–1000 m, there were
667 moderate warming with an intermittent in both the OFES datasets. The intermittent appeared later in the OFES2
668 compared to the OFES1. Below 1000 m, moderate cooling dominated before the middle of 1990s, as shown in both
669 the OFES datasets.

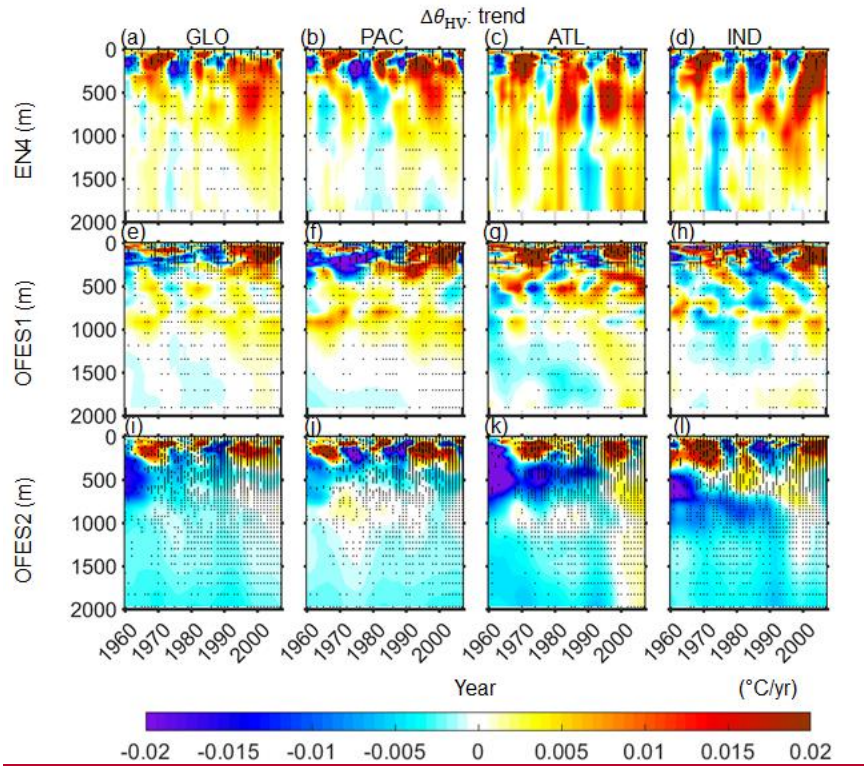


670

671 **Figure 11.** Depth-time patterns of the horizontally averaged potential temperature change $\Delta\theta_{\text{OHC}}$ for (left to right) the global,
 672 Pacific, Atlantic and Indian Oceans. **Top to bottom:** EN4, OFES1 and OFES2. Horizontal axis: year; vertical axis: depth in m.

673

674 To a great extent, the HV components dominated the OHC variations by comparing the Fig. 12 with Fig. 11. For
 675 instance, the profound warming and cooling patterns in Fig. 11 were mostly associated with the HV component. Also,
 676 the moderate cooling below 1000 m in the OFES2 was also mainly related to the HV. Although the SP was generally
 677 weaker and less important than the HV in accounting for the OHC variations, its role cannot be ignored. Indeed,
 678 intense SP-associated warming or cooling were presented in the EN4 in all the major basins. The increased subsurface
 679 SP cooling since 1990s in the Pacific and Indian Oceans were particularly interesting. One speculation is that this may
 680 be related to the great increase of the subsurface salinity observations since 1990s. A possible explanation for the
 681 appearance of the prominent SP cooling in the Pacific and Indian Oceans, but not in the Atlantic Ocean is that the
 682 Atlantic Ocean has been better observed than the Pacific and Indian Oceans before 1990s. Another interesting point
 683 with regards to the SP is the consistent SP warming in the OFES2, but not visible in the other two datasets.



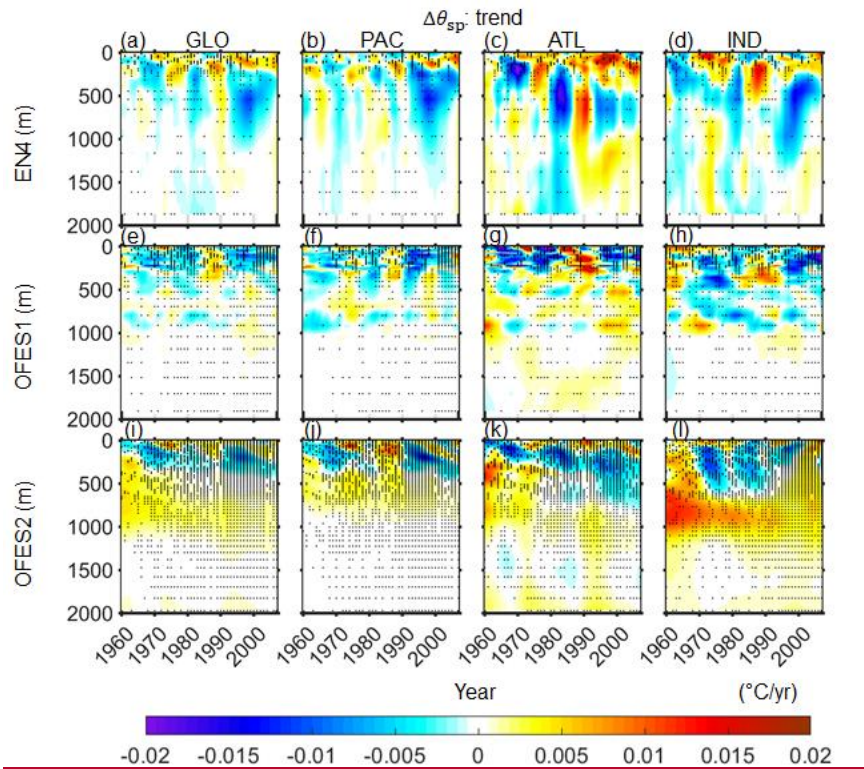
684

685

686

687

Figure 12. Depth-time patterns of the horizontally averaged potential temperature change from the HV component, $\Delta\theta_{HV}$, for (left to right) the global, Pacific, Atlantic and Indian Oceans. **Top to bottom:** EN4, OFES1 and OFES2. Horizontal axis: year; vertical axis: depth in m.



688

689 **Figure 13.** Depth-time pattern of the horizontally averaged potential temperature change from the SP component, $\Delta\theta_{SP}$, for (left
690 to right) the global, Pacific, Atlantic and Indian Oceans. **Top to bottom:** EN4, OFES1 and OFES2. Horizontal axis: year;
691 vertical axis: depth in m.

692 3.3 Spatial patterns of the potential temperature, HV and SP trends-changes

693 To gain a more detailed understanding of the similarities and differences between the potential temperature trends
694 from the three datasets, we presented the spatial distributions of the potential temperature change ($\Delta\theta_{OHC}$), and its HV
695 ($\Delta\theta_{HV}$) and SP ($\Delta\theta_{SP}$) components in the three ocean layers (Figs. 14–16).

697 *Upper layer*

698 Warming was almost ubiquitous in the EN4 (Fig. 14a), particularly strong in the northern Atlantic Ocean and in the
699 Southern Ocean. These two hotspots of warming were expected from both theories and models. Specifically, the
700 shallow ocean ventilation in these two regions could warm faster than the global average (Banks and Gregory 2006;
701 Durack et al. 2014; Fyfe 2006; Talley 2003). Major exceptions of cooling appeared in the Eastern Pacific Equator,
702 along the north Pacific Current, in a meridional band in the southeastern Pacific Ocean, in part of the Argentine Basin
703 and in the southern Indian tropics. All of these cooling regions consists of a small fraction of the global ocean. As
704 with the EN4, both the OFES datasets showed significant warming in the subtropics, high-latitude of the northern
705 Atlantic Ocean and in the Arabian Sea in the Indian Ocean. In addition, the OFES1 was similar to the EN4 in showing
706 cooling along the north Pacific Current. Despite of these similarities, large differences exist between these three
707 datasets. The most significant difference was in the Pacific tropics. Although, as noted earlier, there was a zonal band
708 of cooling in the Pacific tropics in the EN4, this zonal band in the OFES1 and OFES2 was much stronger in intensity
709 and more extensive and mainly related to the HV, especially in the OFES1. These abnormally stronger cooling pattern
710 in the vicinity of Equator were likely to be resulting from the poor qualities of the atmospheric wind stress over some
711 periods. As mentioned earlier, Kutsuwada et al. (2019) demonstrated that the NCEP wind stress used as the forcing
712 of the OFES1 cause much shallower thermocline in the north Pacific tropical area and therefore significant negative
713 differences relative to the observations. In the northeast of the Pacific Ocean, the OFES2 but not the OFES1 and EN4,
714 showed a patch of intense cooling, corresponding to the cooling pattern in the 1960–70s (Fig. 8j). the OFES2 also
715 showed four large cooling areas in the Atlantic Ocean (Fig. 14g). In the Indian Ocean, unlike the EN4, there was a
716 patch of intense cooling along the western coast and in the Indian sector of the Southern Ocean from the OFES1 and
717 OFES2, respectively.

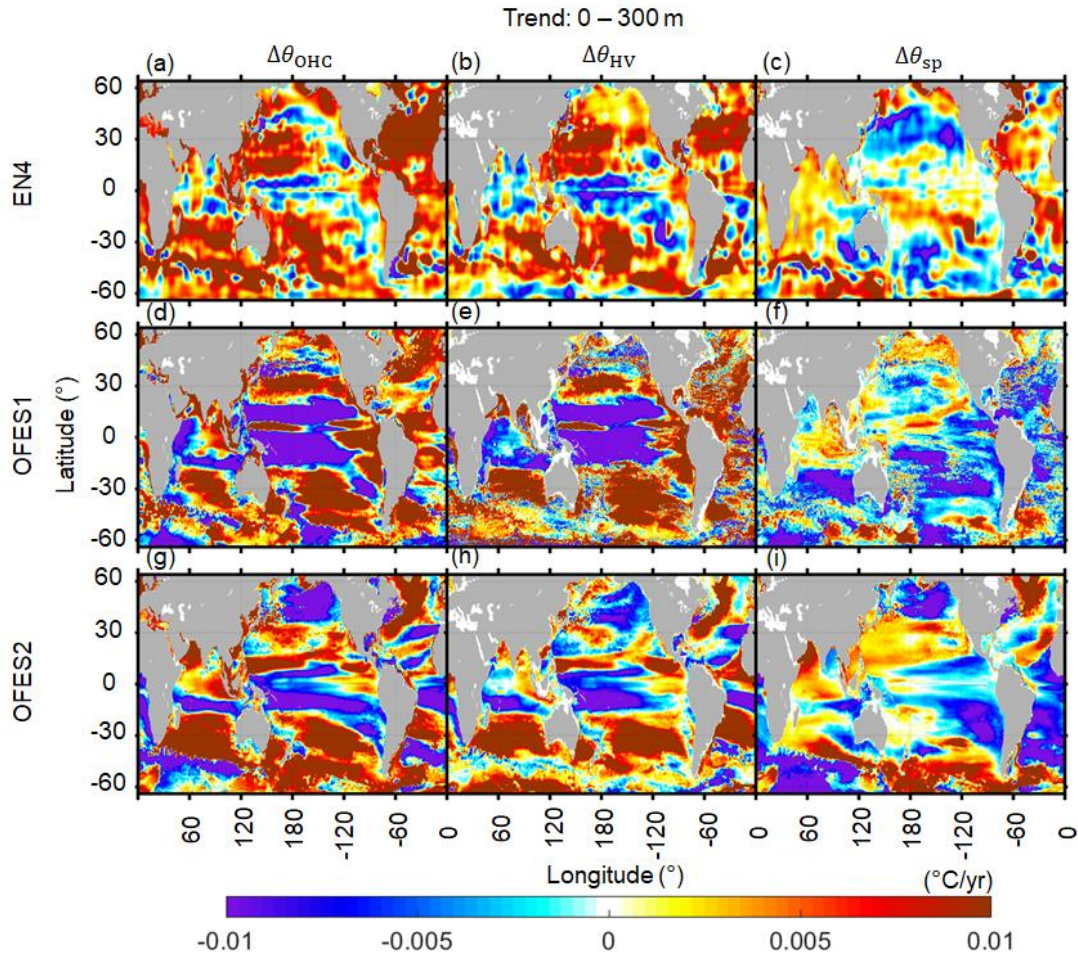
718 The decomposition of the potential temperature changes into HV and SP components showed that the EN4 warming
719 was largely the result of isopycnal deepening (HV) in the subtropics. This is consistent with the finding that the
720 subtropical mode water (STMW) is the primary water mass accounting for global warming (Hakkinen et al., 2016),
721 as we also show later. The SP was generally weaker than the HV, and tended to counteract the HV warming, especially
722 in the subtropics. This dampening effect can be easily understood from Fig. 1 of Hakkinen et al. (2016). For example,
723 in a stratified ocean with warm/salty water above cold/fresh water, typical of the subtropics, a pure warming of one
724 water parcel can be considered as a sum of warming and salination along its original potential-temperature/salinity
725 characteristic (HV part), and a cooling and freshening along the new isopycnal (SP). Two major exceptions were the

726 northern Atlantic subtropics and the Indian Ocean, where SP was mostly warming. The SP warming in the northern
727 Atlantic subtropics results from a large salinity increase through evaporation (Curry et al., 2003; Hakkinen et al.,
728 2016). Similarly, we found that positive SP warming also occurred in most of Indian Ocean, except west to the
729 southwest Australia. Indeed, this SP-related warming in the northern Indian Ocean dominated the potential
730 temperature change, especially in the Arabian Sea. The most significant SP warming, however, was found in the
731 Indian sector of the Southern Ocean (may be related to the freshening of the Southern Ocean), in the southern
732 subtropics of the Atlantic Ocean and in the Labrador Sea (Fig. 14c).

733 Comparing the HV components in the three datasets showed that the two OFES simulations were able to reproduce
734 the subtropical HV warming pattern, although less accurately in the northern Pacific subtropics. The strong and
735 extensive equatorial cooling in the Pacific and Indian Oceans was largely associated with the HV in the two OFES
736 datasets.

737 The SP in the OFES1 was similar to the EN4 in the northern subpolar region of the Pacific Ocean, in part of the
738 northern Pacific subtropics, in the Labrador Sea and in part of the northern Indian Ocean. The OFES2 SP was similar
739 to the EN4 in the Labrador Sea and the western Indian Ocean. In general, however, there were no common patterns
740 in most of the global ocean. In particular, neither of the OFES datasets captured the SP warming in the northern
741 Atlantic subtropics, and the OFES2 indicated moderate SP warming in the north Pacific subtropics and intense SP
742 warming in the Pacific sector of the Southern Ocean, respectively. The improvements of SP from the OFES1 over that
743 from the OFES1 in the Arabian and Indonesian Seas but not in the Bengal Bay was consistent with the S2020, to some
744 extent. The authors demonstrated smaller bias in the water properties in the Arabian and Indonesian Seas, but large
745 salty bias remained in the Bengal Bay in the OFES2.

746 In Fig. 3, we showed that the SP was highly similar between the EN4 and OFES2 in the upper layer of the Pacific
747 Ocean. However, the spatial distributions of the SP component in the Pacific Ocean were seldomly similar between
748 the EN4 and OFES2. That is, the time series of a basin-wide quantity hides many details.



749

750 **Figure 14.** Spatial distributions of $\Delta\theta_{\text{OHC}}$ (top row), $\Delta\theta_{\text{HV}}$ (middle row) and $\Delta\theta_{\text{SP}}$ (bottom row), 1960–2016, in the top ocean
 751 layer (0–300 m). Left to right: EN4, OFES1 and OFES2. Standard deviations of $\Delta\theta_{\text{OHC}}$, $\Delta\theta_{\text{HV}}$ and $\Delta\theta_{\text{SP}}$ are given in the
 752 [Supplementary Information](#).

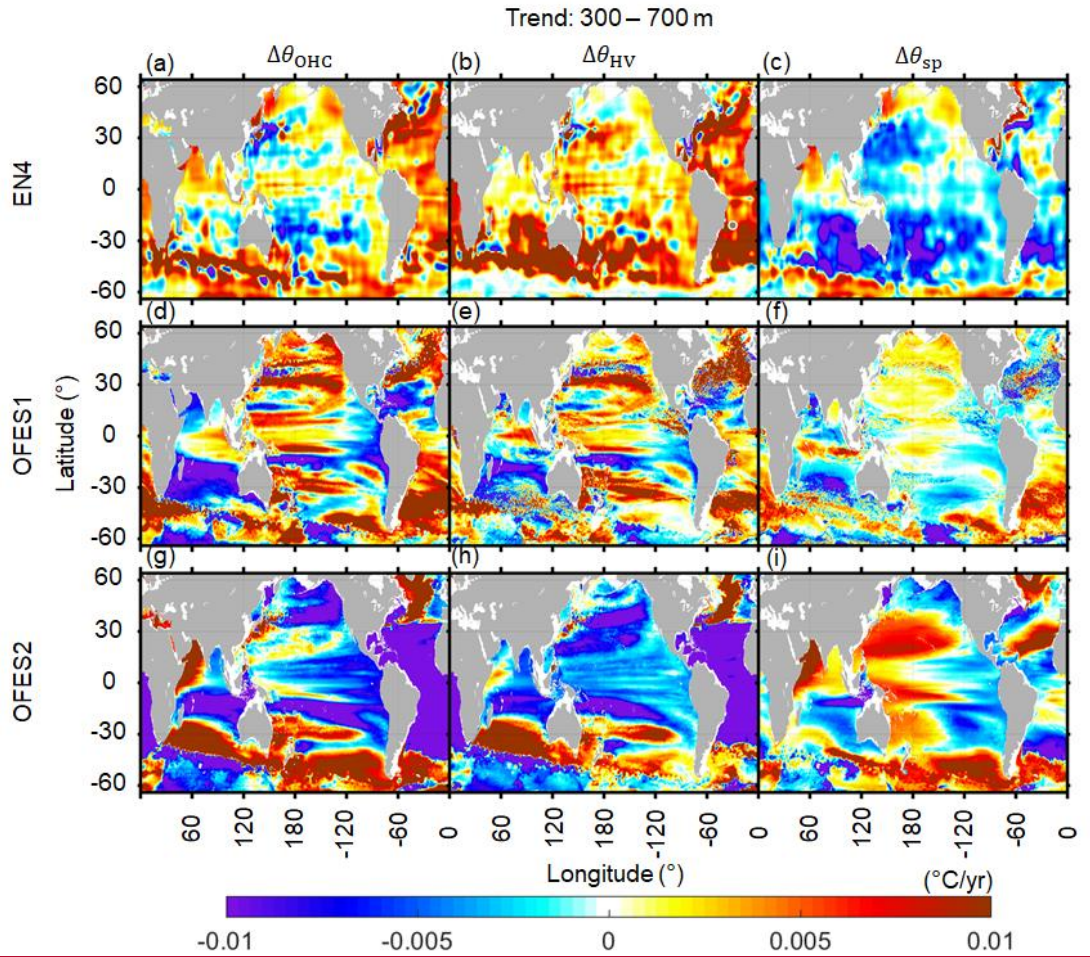
753

754 *Middle layer*

755 The EN4 showed cooling in the ocean, concentrated in the southern Pacific subtropics and in the region associated
 756 with the Kuroshio (Fig. 15a). For the rest of the global ocean, especially over the bulk of the Atlantic Ocean, in the
 757 northern Indian Ocean and along the ACC path in the Southern Ocean, clear warming was presented, accompanied by
 758 sporadic cooling patches. The OFES1 could reproduce some warming patterns in the northern Pacific Ocean, the bulk
 759 of the Atlantic Ocean, in the eastern part of the northern Indian Ocean and parts of the ACC path. However, notable
 760 differences can be found between the OFES1 and EN4. Among these differences, the most prominent is the intense
 761 cooling in the southern Indian Ocean from the OFES1, which was found to occur in the 1990s from Fig. 3(d). In
 762 addition, strong cooling patches were also found in the southern Pacific tropics, west to the central-south America in
 763 the northern Atlantic subtropics, in the Arabian Sea and along the part of southern edge of the ACC. The pattern in
 764 the OFES1 Pacific Ocean clearly appears as zonal bands, but this zonality property was obscure in the EN4. Consistent
 765 with Fig. 3, intense cooling was simulated in all the major basins, with most prominent in the Atlantic Ocean. Besides
 766 these notable cooling patches, large-scale strong warming patterns were found in the Kuroshio region, in the southern

767 Pacific and Indian subtropics, in the northern Atlantic Ocean (north to 35° N), in the western part of the northern
768 Indian Ocean and in the Pacific and Atlantic sectors of the Southern Ocean. In general, over the bulk of the global
769 ocean, there were apparent differences between these three datasets. The above 700 m was relatively well observed,
770 especially in the Atlantic Ocean (even back to 1950–60s, Hakkinen et al., 2016). Therefore, it is likely that the OFES2
771 was the outlier at this multi-decadal scale and there were some potential problems in the OFES1, for example, in the
772 southern Indian Ocean.

773 Interestingly, the HV warming was almost ubiquitous in the middle layer from the EN4, especially in the Southern
774 Hemisphere, consistent with the warming shift towards to the Southern Hemisphere found in Hakkinen et al. (2016).
775 Correspondingly, the SP cooling also occupies most of the global ocean, with a similar southern shift, most prominent
776 to the east and west of the Australia. The major SP warming patches were found in the Sea of Okhotsk, north to the
777 Gulf Stream, in the Arabian Sea and along the southern edge of the ACC. These regions are generally associated with
778 strong salinity variations. Comparing the HV and SP between the EN4 and OFES1 showed that the OFES1 captured
779 some warming patterns in the Pacific and Atlantic, but not the Indian, subtropics. The HV agreement in the southern
780 Pacific and Indian tropics and in the Southern Ocean were mostly poor. As for the SP, the OFES1 reproduced the
781 intense SP cooling west to the Australia and in the southern Pacific subtropics, despite of smaller coverage compared
782 to the EN4. However, the OFES1 showed almost opposite SP trends over most of the global ocean. In the OFES2,
783 both the HV and SP were strong, but the basin-wide cooling was mainly the result of HV. Overall, the OFES2 had a
784 reasonable agreement with the EN4 in the southern subtropics in terms of HV. It also had a common HV warming
785 patch in the northern Atlantic Ocean (north to 35° N) as the EN4. With regards to the SP, the OFES2 was similar to
786 the EN4 in showing SP warming in the Arabian Sea and parts of the southern edge of the ACC. Also, it captured the
787 SP cooling in the eastern Pacific Ocean, along the Gulf Stream path, west to the Australia. Except of these similarities,
788 however, the OFES2 was generally opposite to the EN4.



789

790 **Figure 15.** As for Fig. 14 but for the middle layer (300–700 m).

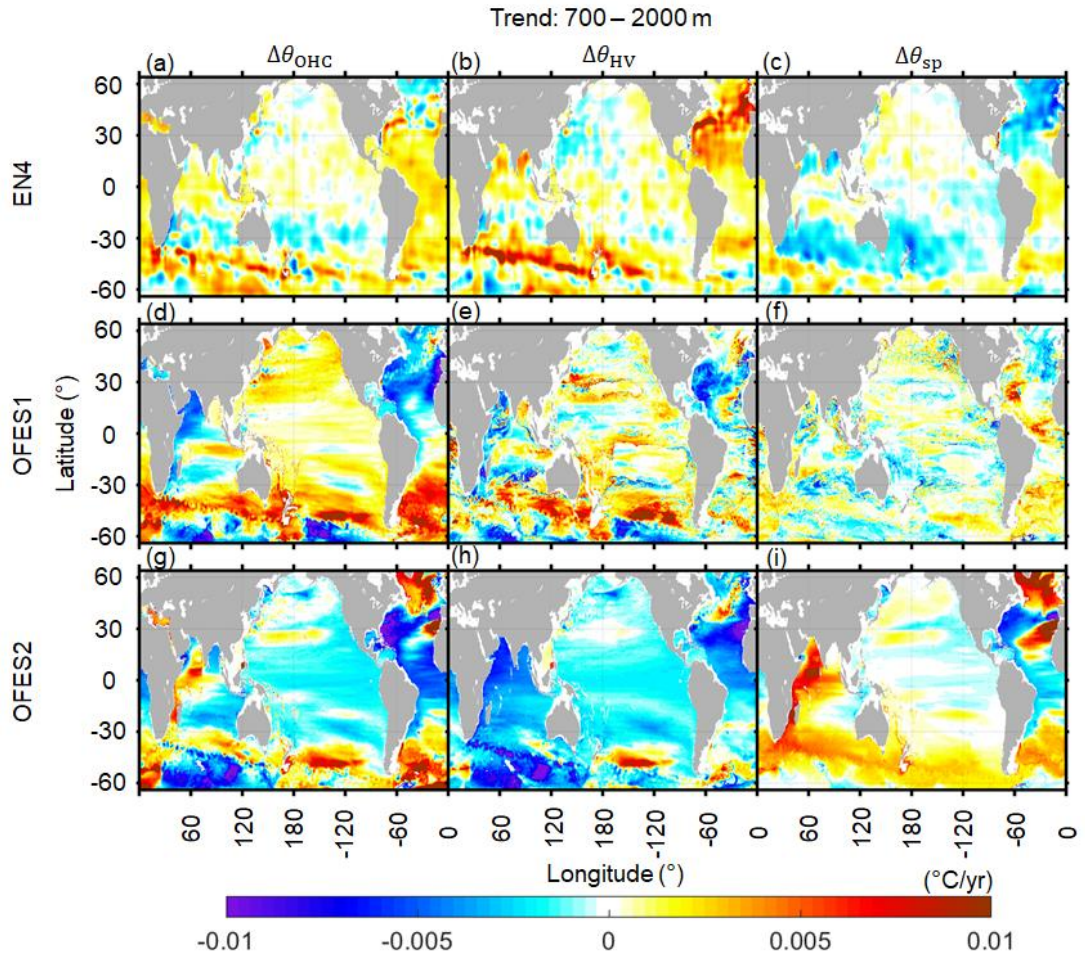
791

792 Lower layer

793 The warming and cooling intensities were generally much weaker than in the top two layers, consistent with many
 794 previous findings that more ocean heating occurs in the upper 700 m than at greater depths (Hakkinen et al., 2016;
 795 Levitus et al., 2012; Wang et al., 2018; Zanna et al., 2019). The EN4 showed widespread warming patches in the
 796 Southern and Atlantic Oceans, as well as three large zonal bands of cooling in the southern subtropics of the Pacific
 797 and Indian Oceans, and in the northern subpolar region of the Atlantic Ocean (Fig. 16a). Similar to the EN4, warming
 798 was seen along the northern edge of the ACC and in the southern Atlantic Ocean in the OFES1, but with much stronger
 799 intensity than the EN4 (Figs. 16a, d). There was also moderate warming over almost the whole Pacific Ocean in the
 800 OFES1. Significant differences between the OFES1 and EN4 were found in the northern Atlantic Ocean, where the
 801 OFES1 showed extensive cooling compared to the moderate warming in the EN4. There was also strong cooling in
 802 the OFES1 Arabian Sea, in contrast to the quite weak warming in the EN4 Arabian Sea. To some extent, the OFES2
 803 was similar to the other two in showing warming along the northern edge of the ACC and in the southern Atlantic
 804 Ocean south to 30°S (Fig. 15g), despite of the intensity differences. It also showed cooling in the low and middle
 805 latitudes of the Atlantic Ocean, as did the OFES1 but opposite to the EN4. However, the bulk of the Pacific Ocean

806 was shown to be cooling in the OFES2, which was almost opposite to the OFES1 (Fig. 15d) and only similar to the
807 EN4 in part of the southern Pacific subtropics (Fig. 15a). Moreover, intense and widespread cooling appeared in the
808 Indian sector of the Southern Ocean in the OFES2. The warming of the northern ACC was captured by the OFES2.
809 In the NE4, there was intense HV warming along the northern edge of the ACC in the Indian and Pacific Oceans,
810 and in the northern Atlantic Ocean (Fig. 16b), which largely accounted for the total potential temperature variations
811 and were generally accompanied by SP cooling (Fig. 16c). In the northern Atlantic tropics and southern Atlantic
812 Ocean, moderate HV and SP warming coexist. We found that the OFES2 captured the HV warming pattern along the
813 northern edge of the ACC, being consistent with the EN4. However, there were remarkable differences from the EN4,
814 particularly in the northern Atlantic and Indian Oceans. As for the SP, there were some similarities between the OFES1
815 and EN4, for example, they both had SP cooling and warming in the northern and southern Atlantic Ocean,
816 respectively. Among the three datasets, the OFES2 showed the most extensive and strong but generally cooling in the
817 HV component, except a patch of HV warming in the Pacific sector of the Southern Ocean, and such a warming patch
818 was also seen in the EN4. In contrast, intense SP warming was estimated in the OFES2 in the Southern Ocean, in the
819 western Indian Ocean, in the northern Atlantic subpolar regions and a large-scale patch of abnormally strong SP
820 warming associated with the Mediterranean Overflow Water (MOW). This very strong SP warming related to the
821 MOW is likely the result of the unrealistic spreading of salty Mediterranean overflow found in S2020.
822 Besides the above-discussed multi-decadal linear trend, we have demonstrated that (not shown here) the significant
823 differences between the two OFES datasets and the EN4 were much reduced if we considered only the period between
824 2005–2016, which was argued to be well spun-up by S2020. In addition, over this 12-year period, the spatial pattern
825 of the OFES2 did show some improvements over the OFES1 for upper and middle layers, but not necessarily for the
826 lower layer, when taking the EN4 as a reference. Does this better agreement come from a better spun-up or come from
827 the improvements of the reanalysis product of the atmospheric forcing for these two OFES data? This interesting
828 question would require a further detailed exploration in the future.

829



830

831 **Figure 16.** As for Fig. 14 but for the lower layer (700–2000 m).

832

833 The two previous sections described the global and basin-wide OHC distributions in the temporal domain and the
 834 longitudinal direction quantitatively. To further investigate the detailed agreements consensus and discrepancies in
 835 the warming or cooling from these three datasets, we calculated the volume-averaged potential temperature θ_{OHC} . This
 836 was calculated by dividing the total OHC variations in the water column of each ocean layer (upper or intermediate)
 837 by the corresponding total water volume and the product of seawater density and specific heat capacity ($\rho \times C_p =$
 838 $4.1 \times 10^6 \text{ kg} \cdot \text{J} \cdot \text{m}^{-3} \cdot \text{K}^{-1}$). We then compared the change in the volume-averaged potential temperature, $\Delta\theta_{\text{OHC}}$ (P2
 839 average (2014–2016) minus P1 average (1960–1962)) from the different datasets, as shown in Fig. 6. We also
 840 calculated $\Delta\theta_{\text{HV}}$ and $\Delta\theta_{\text{SP}}$, derived from the HV and SP, respectively, in a similar way to the $\Delta\theta_{\text{OHC}}$. The reason for
 841 using $\Delta\theta$ rather than the OHC is that the latter is an extensive quantity (grid cell area or volume dependent), but its
 842 variation at each grid is can be directly related to the $\Delta\theta$. To facilitate interpreting the results, we defined major water
 843 masses for both the upper (supplementary Tab. S1) and intermediate (supplementary Tab. S2) oceans in each basin,
 844 following Emery (2001), as shown in Tabs. 4 and 5. Readers are referred to Emery (2001) for more details. The
 845 geographical distribution of the major water masses analysed here can be found in Emery (2001).

846

847

Table 5. Same with Tab. 4, but for the intermediate ocean (500–1400 m).

	Pacific Ocean	Atlantic Ocean	Indian Ocean
	1. Pacific Subarctic Intermediate Water (PSIW), 5–12, 33.8–34.3.	1. Western Atlantic Subarctic Intermediate Water (WASIW), 3–9, 34.0–35.1.	1. Antarctic Intermediate Water (AAIW), 2–10, 33.8–34.8.
	2. California Intermediate Water (CIW), 10–12, 33.9–34.4.	2. Eastern Atlantic Subarctic Intermediate Water (EASIW), 3–9, 34.4–35.3.	2. Indonesian Intermediate Water (IIW), 3.5–5.5, 34.6–34.7.
Water mass (500–1400 m)	3. Eastern South Pacific Intermediate Water (ESPIW), 10–12, 34.0–34.4.	3. Antarctic Intermediate Water (AAIW), 2–6, 33.8–34.8.	3. Red Sea Persian Gulf Intermediate Water (RSPGIW), 5–14, 34.8–35.4.
	4. Antarctic Intermediate Water (AAIW), 2–10, 33.8–34.5.	4. Mediterranean Water (MW), 2.6–11.0, 35.0–36.2.	
		5. Arctic Intermediate Water (AIW), 1.5–3.0, 34.7–34.9.	

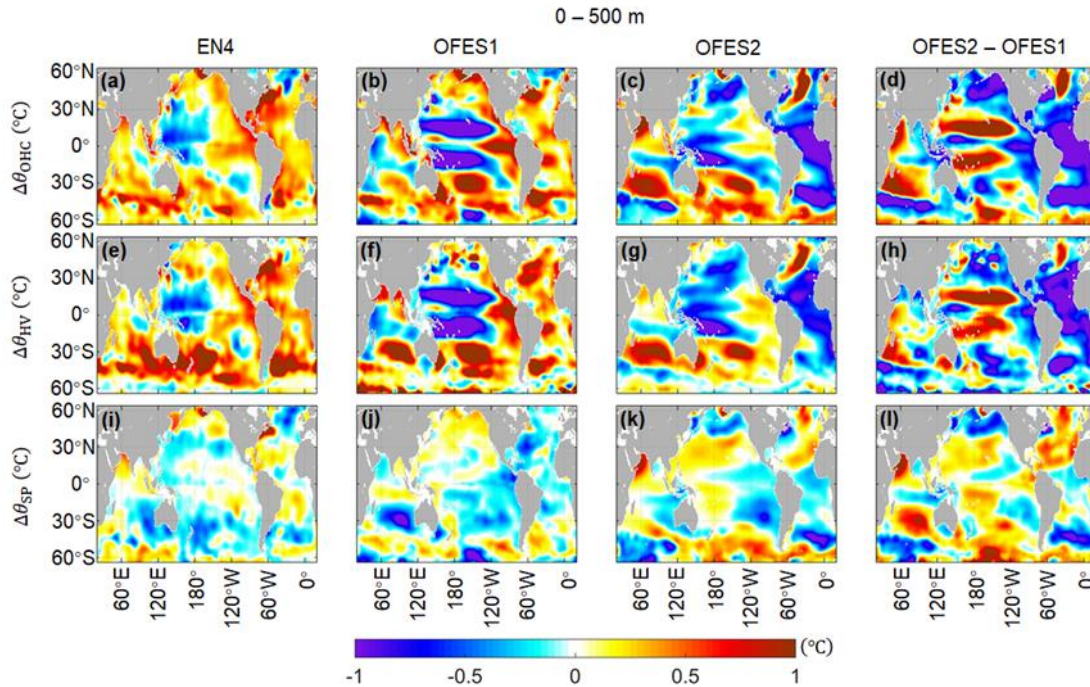
848 ***a* The upper ocean (0–500 m)**

849 Both the EN4 and OFES1 suggest that the Pacific Subarctic Upper Water (PSUW, see Tab. 4 S1 for definition) largely
850 warmed (Fig. 6 a, b), whereas the bulk of the PSUW cooled in the OFES2 (Fig. 6c), except the eastern and northern
851 shelves of the Bering Sea. Interestingly, this PSUW warming (cooling in the OFES2) is largely determined by the
852 spiciness but heave also contributes to the warming. This may indicate a local salinization as a density compensation
853 along the neutral density surface. The OFES1 indicated indicates the strongest heave related cooling pattern band in
854 on the southern flanks of the West North Pacific Central Water (WNPCW) and East North Pacific Central Water
855 (ENPCW), extending eastward to around 120°W (Fig. 6b), whereas the other two presented present only moderate
856 cooling in the center and on the southern side of WNPCW. In the EN4, both the HV and SP contribute to the WNPCW
857 cooling, but SP related warming dampens the WNPCW cooling in the OFES2. It is worthy to be ascertained whether
858 these two remarkable cooling pools in the OFES1 can be related to the cool bias of the SST compared to the WOA13
859 (World Ocean Atlas 2013) over 2005–2012 as shown in Sasaki et al. (2020), although the two time periods are
860 different.

861 —The eastern part of the Pacific Equatorial Water (PEW) is shown to be a heave dominated warming pool hotspot
862 by the OFES1 (Fig. 6b), but and the warming intensity in the EN4 and OFES2 are significantly weaker, especially the
863 OFES2 (Figs. 6a,e). The local SP related cooling weakens this warming in the two OFES data. In the West South
864 Pacific Central Water (WSPCW), a cooling tendency is presented in a small region to the southeast of to the Indonesia
865 in the EN4 (Fig. 6a). This cooling pattern was shown to beis much more extensive in both the OFES1 and OFES2,
866 extending to the East South Pacific Central Water (ESPCW) (Figs. 6b,e). Again, the spiciness enhances the WSPCW

867 cooling in the OFES1 but oppositely weakens the cooling in the OFES2. In the south Pacific Ocean east to 180°, there
868 exists a vast region of warming south to around 20°S in both the OFES1 and OFES2. Between 180°E and 120°W in
869 the southern Pacific Ocean, the warming intensity and coverage are both reduced in the EN4. This warming pattern is
870 largely associated with the ESPCW and the Subantarctic Surface Water (SASW). there exists a region with
871 easily note there is an intense spiciness cooling pattern related to the Antarctic Surface Water (AASW) in the
872 southernmost basin of the Pacific Ocean as shown in the OFES1 (Fig. 6b), but not captured by both either the EN4
873 and or OFES2. Given the local heave warming, we can infer that this is caused by a processes of freshening.
874 —In the upper layer of the Atlantic Ocean, the EN4 and OFES1 indicate that there is a spiciness related cooling
875 tendency associated with the Atlantic Subarctic Upper Water (ASUW) (Fig. 6a, b). In the OFES2, however, there is
876 an intense warming tongue extending from around 30°N to the subarctic (Fig. 6c); a part of the ASUW is shown to
877 have a cooling tendency. This remarkable warming in the OFES2 has both contributions from the heave and spiciness.
878 To some extent, it seems to be consistent with the large warm bias of SST compared to WOA13 over 2005–2012 in
879 Sasaki et al. (2020). As this warming tongue resides in the Gulf Stream and North Atlantic Current, we infer that it
880 may be caused by the problematic pathway of these currents similar to Sasaki et al. (2020). The Western North Atlantic
881 Central Water (WNACW) was widely warming in the EN4 and the OFES1, but this did not occur the bulk of the
882 WNACW cooled in the OFES2. In addition, both the heave and spiciness are found to be responsible for the WNACW
883 warming in the EN4 but spiciness is related to cooling in the OFES1. Clearly, there is large residual between the total
884 OHC derived warming and the sum of heave and spiciness contributions in the WNACW in the OFES1. This residual
885 may be resulting from the air-sea interactions and strong vertical temperature gradient, as stated in Desbruyères et al.
886 (2017). Another striking difference between the OFES2 and others is located in the Gulf of Mexico, which is shown
887 to be cooling (warming) in the OFES2 (EN4 and OFES1). The differences in the Eastern North Atlantic Central Water
888 (ENACW) are also remarkable, with the EN4 indicating moderate warming, the OFES1 minor variations and the
889 OFES2 strong cooling (Figs. 6a–c). Both the EN4 and OFES1 show moderate heave warming in the Atlantic Equatorial
890 Water (AEW), the OFES2 significant cooling. Warming occurred in the bulk of the South Atlantic Central Water
891 (SACW) in both the EN4 and OFES1 (Fig. 6a, b), whereas the OFES2 suggests cooling (by both heave and spiciness),
892 except a local region to the east of South America (Fig. 6c). Furthermore, the OFES2 presents a much stronger
893 warming pattern in the ACC Atlantic sector section of the Atlantic Southern Ocean compared to the other two data.
894 and this warming is found to be attributed to spiciness.
895 —Warming is found in the Arabian Sea Water (ASW), especially in the OFES2 (Fig. 6c), in which the intense
896 warming mainly results from SP, same with the EN4 but opposite to the OFES1. Presumably, there is significant
897 salinity differences between the OFES1 and others, consistent with improvements of SSS in the Arabian Sea and the
898 Red Sea in the OFES2 by well representing the salty overflow. $\Delta\theta$ in the Bengal Bay Water (BBW) is relatively small,
899 except in the OFES1 (Fig. 6b). The weak warming pattern in the Indian Equatorial Water (IEW) in the EN4 is not
900 shown in the other datasets. On the contrary, both the OFES data indicate that the IEW is associated with the heave
901 cooling, with spiciness warming damping and spiciness cooling enhancement in the OFES1 and OFES2, respectively.
902 In the central south Indian Ocean, we note a robust widespread heave-dominant warming in the three data, particularly
903 in the OFES2. Consistently, all the three data reveal a corresponding cooling by way of spiciness, with the one in the

904 OFES1 most significant. Large discrepancies occurred in the Indian Ocean section sector of the ACC, with significant
 905 warming in the EN4 and OFES1, but cooling in the OFES2.
 906 —In summary, the major patterns are similar in the EN4 and OFES1, but differs in strength and span. Secondly, the
 907 discrepancies between the two OFES datasets are marked and comparable to their respective $\Delta\theta$ magnitude, despite
 908 some similarities between the OFES1 and OFES2.



909
910

911 3.4 Temperature-salinity Trends in the HV and SP in the neutral density domain diagrams

912 To analyse the warming and cooling from the perspective of water mass, it is useful to show the HV and SP
 913 components in neutral density coordinates, as suggested by one reviewer. Following Hakkinen et al. (2016), we
 914 calculated the linear trend (over 1960–2016) in the zonal-averaged sinking of the neutral density surfaces in each
 915 major basin (Fig. 17) and the SP-related warming or cooling along the neutral density surfaces (Fig. 18).

916 Our results based on the EN4 were similar to those of Hakkinen et al. (2016), using the EN4, although they used
 917 an earlier EN4 version (EN4.0.2) and considered the period over 1957–2011. Specifically, our EN4 results similarly
 918 showed that the bulk of HV warming (deepening of neutral density surfaces) was associated with a water mass of over
 919 26 kg/m³, and mainly concentrated south to 30° S, to wit, from the ventilation region at high latitudes to the subtropics.
 920 There was one exception in the Atlantic Ocean, where warming also occurred at the low-middle latitudes and in the
 921 northern Atlantic Ocean. The concentrated warming in the northern Atlantic Ocean was attributed to the phase change
 922 of North Atlantic Oscillation (NAO) from negative in the 1950–60s to positive in the 1990s (Hakkinen et al. 2016;
 923 Williams et al. 2014). As explained in Hakkinen et al. (2016), these significant deepening of neutral density surfaces
 924 were associated with the Subtropical Mode Water (STMW, 26.0 < σ_0 (kg/m³) < 27.0) and the Subantarctic Mode
 925 Water (SAMW, 26.0 < σ_0 (kg/m³) < 27.1). These vertical displacements of neutral density surfaces may have resulted

926 from heat uptake via subduction, which then spread from these high-latitude ventilation regions. The large vertical
927 deepening of the STMW and SAMW would then push the Subpolar Mode Water (SPMW, $27.0 < \sigma_0$ (kg/m³) < 27.6)
928 and Antarctic Intermediate Waters (AAIW, $27.1 < \sigma_0$ (kg/m³) < 27.6) down. However, as the vertical displacement of
929 the STMW/SAMW was larger, its volume would have therefore increased and the volume of the underlying
930 SPMW/AAIW decreased (Hakkinen et al., 2016). Besides these significant sinking of neutral density surfaces, there
931 was generally a shoaling pattern of lower density (σ_0 (kg/m³) ranging from 24–26), and mainly concentrated between
932 the Equator and 30° S. To a large extent, this shoaling occurred in the central water, for example, the South Pacific
933 Central Water (SPCW).

934 Here, our focus is not on the detailed mechanisms of warming from the perspective of water mass, as it was in
935 previous studies. Instead, we focus on the differences between the datasets in the trends of the HV and SP.

936 It can be seen that along the surfaces of the Pacific and Indian Oceans, there was generally an appearance of HV
937 warming in almost all the three datasets. In the Atlantic Ocean, however, the EN4 estimated a sea surface cooling
938 south to 30° S and in the northern tropics; the OFES2 also estimated a cooling trend in the Atlantic tropics. Different
939 from both the EN4 and OFES2, the OFES1 showed an intense cooling pattern along the Atlantic surface between
940 around 30–50° N.

941 South to 30° S, large downward movements associated with the STMW, SAMW and AAIW were found in all the
942 three basins in the EN4; in the OFES1, the dominant pattern in the three basins was sinking but was surrounded by
943 shoaling patches; larger differences from the EN4 were found in the OFES2, which showed significant and extensive
944 shoaling patterns, especially in the Indian Ocean. The almost opposite trend in the vertical displacements of the neutral
945 density surfaces between the OFES2 and the observational-based EN4 may indicate that the water mass properties
946 simulated in the OFES2 were unrealistic, at least at this multi-decadal scale.

947 In the ocean interior between 30°S and 30° N, the OFES1 presented shoaling patterns in the northern and southern
948 Pacific and Indian Oceans, but not prominent in the Atlantic Ocean. Although these shoaling patterns in the Pacific
949 and Indian Oceans were also seen in the EN4, as noted earlier, the magnitude in the EN4 was generally much smaller.
950 The OFES2 had a better agreement with the EN4 in the shoaling pattern in the southern Pacific subtropics. It also
951 captured the shoaling in the EN4 Indian Ocean, with a similar coverage but generally stronger. The shoaling in the
952 southern Atlantic subtropics was not typical in the OFES2, similar to the OFES1 but different from the EN4.

953 North to 30° N, sinking was widespread in the EN4, particularly strong in the northern Atlantic Ocean. This very
954 strong sinking in the northern Atlantic Ocean came mainly from the SPMW and STMW. In the EN4 Pacific Ocean,
955 there was some shoaling patches, which was related to the North Pacific Intermediate Water (NPIW), and to a large
956 extent, corresponded to the HV cooling in Fig. 16(b). In the OFES1, the pattern was filled with both sinking and
957 shoaling patches and defies easy interpretation. However, an apparent outlier is the intense shoaling in the OFES1
958 northern Atlantic Ocean (mainly below 700 m from Figs. 14–16), just opposite to the EN4. The shoaling of neutral
959 density surfaces in the OFES2 Pacific Ocean north to 30° N was even more prominent than in the OFES1. The OFES2
960 had a better agreement with the EN4 in the sinking patterns in the Atlantic Ocean north to 30° N.

961

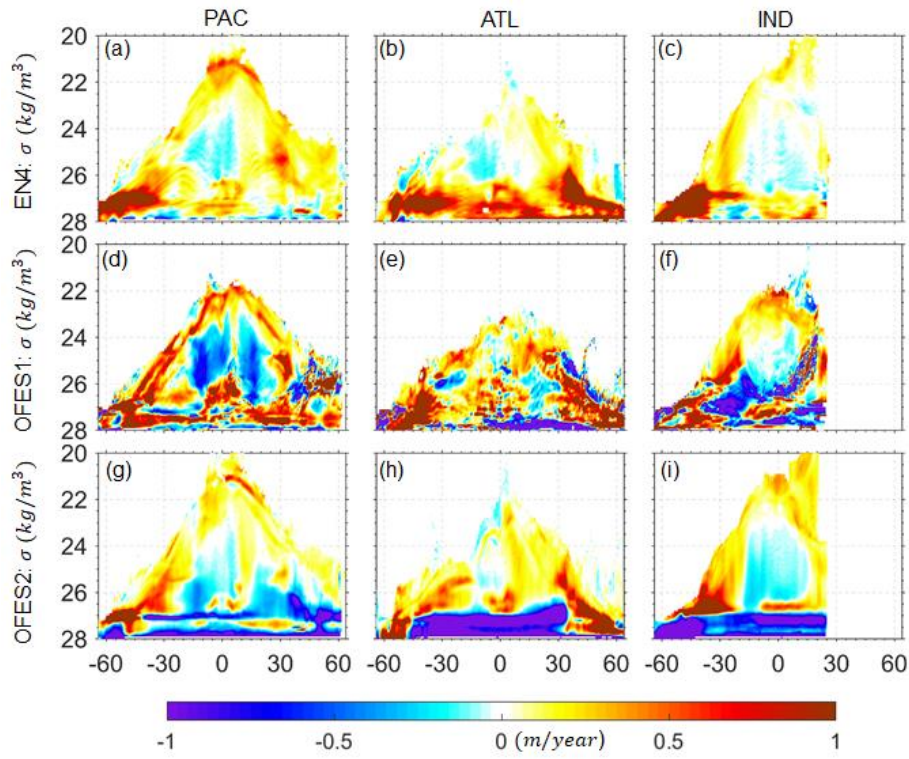
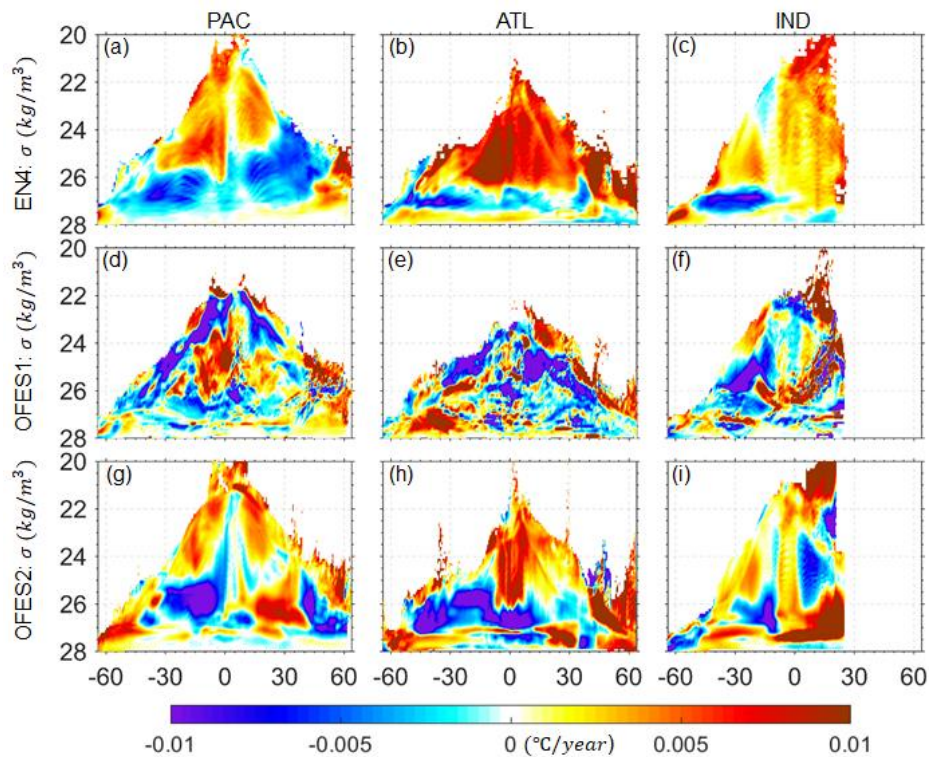


Figure 17. Linear trends in the zonal-averaged sinking of the neutral density surfaces in the Pacific (left column), Atlantic (middle column) and Indian (right column) Oceans. Top to bottom: EN4, OFES1, OFES2. Positive values mean deepening of the neutral density surfaces. The calculation was for the water above 2000 m.

The major SP warming in the EN4 Pacific Ocean was associated with the STUW and Pacific Central Water in the low and middle latitudes, with a shift towards to the southern hemisphere. The northern high-latitude SP warming was mainly related to the Pacific Subarctic Intermediate Water (PSIW). The two SP cooling came from the STMW, corresponding to the sinking pattern in Fig. 17(a). This HV warming / SP cooling was particularly typical in the subtropical regions and the HV warming / SP warming was typical in the subpolar regions, as noted above and more details were presented in Hakkinen et al. (2016). Very strong SP warming occurred in the Atlantic Ocean, resulting from salination via the evaporation process. In the southern Atlantic Ocean, pattern of SP cooling is mostly associated with the sinking of STMW.

The SP pattern from the OFES1 was quite noisy and had generally poor agreements between the OFES1 and the EN4 in terms of SP warming, which is likely to be resulting from some issues of salinity simulation in the OFES1. As shown in S2020, the OFES1 was not capable of simulating salty outflows, for example, the outflow through the Persian Gulf into the Indian Ocean. There were notable improvements in the salinity field in the OFES2 over OFES1, mainly attributed to the inclusion of river runoff and a sea-ice model, but some issues still remained, e.g., poor performance in the simulation the Mediterranean outflow. Overall, the SP warming pattern in the density coordinate was significantly improved in the OFES2 when compared to the OFES1. When combing Figs. 14–16, however, one can see that the similarities in the SP estimation between the OFES2 and the EN4 was confined to small fraction of the global ocean, mainly in the upper and middle layers of the Labrador Sea and the northern Indian Ocean in the Southern

984 Ocean. In addition, the OFES2 was also similar to the EN4 in showing a patch of SP cooling in the western part of the
 985 northern Atlantic subtropics.

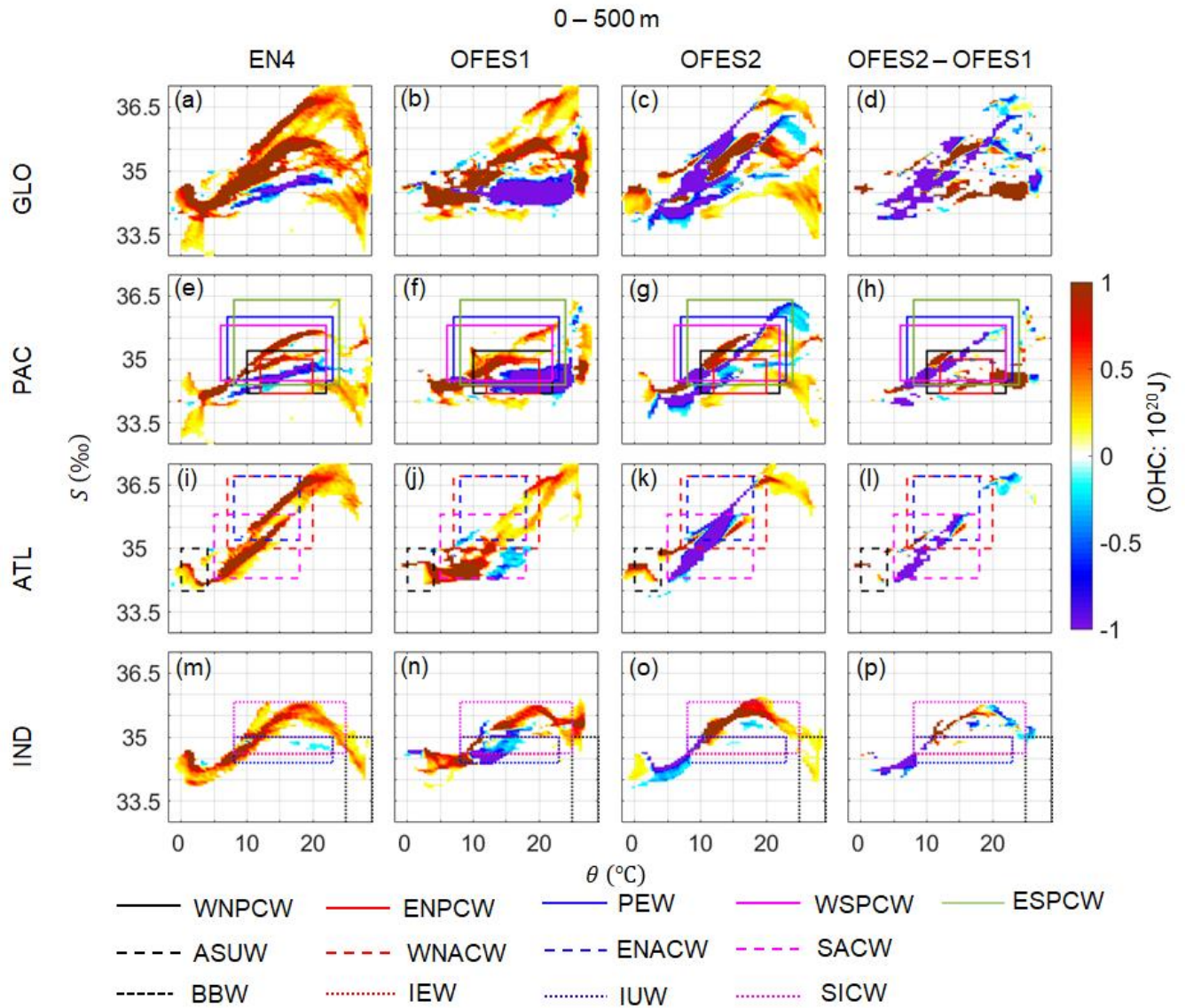


986 **Figure 18.** Linear trends in the zonal-averaged warming or cooling along the neutral density surfaces in the Pacific (left column),
 987 Atlantic (middle column) and Indian (right column) Oceans. Top to bottom: EN4, OFES1, OFES2.
 988 (Hakkinen et al. 2016)(Hakkinen et al. 2016)(Levitus et al. 2012)(Hakkinen et al. 2016)(Ernst and Ernst 2000)(Liu
 989 and Tanhua 2021)(O'Connor et al. 2005)(Emery 2001)(Emery 2001)Figures Figs. 6, and 7 8 in Section section 3.3
 990 demonstrated the similarities and differences in the patterns of $\Delta\theta$ by analysing the warming/cooling tendencies in the
 991 major water masses (a body of water with specific temperature–salinity characteristics; Tables 2, 3S1–S2). To further
 992 understand the contributions of the different water masses to the OHC variations quantitatively, we constructed a
 993 variant of the canonical temperature salinity ($T-S$) diagram. In this special $T-S$ diagram, we display the total OHC
 994 variations in the different temperature and salinity intervals (Figs. 8, 910–11). Note that for a better visualization, we
 995 only present the dominant temperature and salinity domains, and have bounded the major water masses by different
 996 line styles and colours. As the differences in temperature and/or salinity in different water masses can be quite minor,
 997 there are many overlaps in the $T-S$ diagrams. Therefore, Figs. 8 and 910–11 need to be combined with Figs. 6 and 7 8
 998 for a clearer interpretation.

1000 **α The upper ocean (0–500 m)**

1001 The temperature–salinity characteristics are generally similar in the three datasets, especially between the EN4 and
 1002 OFES2. The $T-S$ diagrams from the EN4 and OFES1 for the Pacific Ocean are similar (Figs. 8e10e,f); the major
 1003 discrepancy is associated with the WNPCW, with the EN4 indicating a much smaller OHC decrease, similar to the
 1004 OFES2 (Fig. 8g10g). In addition, the PEW is associated with an OHC increase in all the data. In the Atlantic Ocean,

005 the ASUW contributes to the OHC increase in all the datasets, especially the EN4 and OFES2 (Figs. 8i10,k). However,
 006 the spatial distribution of $\Delta\theta$ in Fig. 6c indicates that the ASUW in the EN4 and OFES1 cooled. Therefore, the cooling
 007 associated with the ASUW may be compensated by warming of water with similar temperature-salinity characteristics
 008 elsewhere. In the WNACW, both the EN4 and OFES1 suggest a notable OHC increase (Figs. 8i10i,j), whereas there
 009 is a large OHC decrease in the OFES2 (Fig. 8k10k). The ENACW accounts for large and moderate OHC increase in
 010 the EN4 and OFES1, respectively, but marked OHC decrease in the OFES2 (Fig. 8k10k). The IEW leads to large
 011 OHC decrease in the OFES1 and OFES2 (Figs. 8n10n,o), but not in the EN4 (Fig. 8m10m). The three datasets all
 012 indicate significant cooling in the SICW. It is found that a large fraction of OHC increase by water cooler than 8°C
 013 in the upper layer of Indian Ocean but not resides represented by in any water masses defined in Tab. 4S1. Moreover,
 014 strong OHC variations (mostly positive) are also associated with the water warmer than the major water masses,
 015 especially in the upper layers of the Pacific and Atlantic Oceans, which are related to the near-surface warming.



016
 017 **Figure 17.**

018 **3.5 A basin-wide heat budget analysis**

019 The fundamental mechanisms controlling the oceanic thermal state include the net surface heat flux, the zonal and
020 meridional heat advection in the horizontal direction and the vertical heat advection and diffusion (Fig. 1b). Lateral
021 heat diffusion was not considered here, as it was found to play a minor role from our analysis (not shown). Since our
022 focus is on the global and basin-wide OHC in the three vertical layers, we calculate and compare the inter-basin heat
023 exchange, and the vertical heat advection and diffusion, integrated over each basin from 1960–2016. No vertical heat
024 diffusivity data were available from the OFES1, and the vertical heat diffusivity from the OFES2 was temporarily
025 unavailable due to a security incident. This prevented us from calculating the vertical heat diffusion directly. As an
026 alternative, we calculated the residual of the OHC change and all the related heat transport into each basin, and took
027 it as a proxy for the vertical diffusion. This indirect method may suffer from some errors, for instance, it includes the
028 impacts of river runoff in the OFES2, but can still provide us with important information. Our calculations are listed
029 in Tables 2–4.

031 Upper layer

032 In the Pacific Ocean, the changing rate of the time-averaged OHC was rather low, and similar in the OFES1 and
033 OFES2. However, the averaged surface heat flux in the OFES1 was twice that in the OFES2, indicating that more heat
034 was injected to the OFES1 Pacific Ocean. Vertically, both indicated a net downward flux of heat in the Pacific Ocean
035 at 300 m, but much stronger intensity in the OFES1 (different by around 0.7 W/m^2); this may be related to their
036 different wind-forcing sources, as the downward heat advection in the upper ocean was mainly from the wind-driven
037 Ekman pumping in the subtropical gyres. Indeed, Kutsuwada et al. (2019) claimed that the NCEP wind stress curl was
038 too strong and caused overly strong Ekman pumping. There was 0.150 W/m^2 more eastward heat advection through
039 the water passage between the Australian mainland and 64° S (P3 in Fig. 1a) in the OFES2. Although the MHA from
040 the Southern Ocean to the Pacific Oceans (P4) was of opposite sign in the two OFES datasets, the relatively small
041 absolute value indicated that this difference was slight. The Drake Passage (P5) is the major water passage through
042 which heat is exchanged between the Pacific and Atlantic Oceans. There was 0.108 W/m^2 more heat loss through the
043 P5 into the Atlantic Ocean in the OFES1. P7 and P8 connect the Pacific and the Indian Oceans; the Indonesian
044 Throughflow (ITF) flows through the P7. The MHA through the P7 was almost two times stronger in the OFES2 than
045 in the OFES1, with a difference of 0.637 W/m^2 . This indicated an enhancement of the IFT simulated by the OFES2,
046 which agreed well with Sasaki et al. (2018), who showed that the inclusion of a tidal-mixing scheme resulted in an
047 intensification of the ITF, remembering that the a tidal-mixing scheme was implemented in the OFES2 but not OFES1.
048 In addition, the OFES1 showed more heat transported westward into the Indian Ocean between Papua New Guinea
049 and Australia (P8) but the small absolute heat advection indicated that it was not the major cause of the OHC
050 discrepancy between the OFES1 and OFES2. The net heat advection through the Bering Strait (P9) was rather weak
051 in both datasets. The indirect calculation of the VHD showed that there was net downward heat diffusion at a depth
052 of 300 m in the Pacific Ocean in both the two OFES datasets but with a much stronger intensity (different by 0.747
053 W/m^2) in the OFES1.

054 In the Atlantic Ocean, the OHC increased at an average rate of 0.032 W/m² in the OFES1 but decreased by 0.014
 055 W/m² in the OFES2. There was net surface heating in the OFES1 Atlantic Ocean but minor cooling in the OFES2.
 056 The two OFES datasets were also profoundly different in the VHA at 300 m. Specifically, the OFES1 showed a net
 057 downward heat advection, the OFES2 an upward and much weaker heat advection. Again, this difference in the VHA
 058 was likely the result of different wind stress datasets in the two OFES, as discussed above. The OFES1 showed 0.158
 059 W/m² more heat transported from the Atlantic Ocean to the Indian Ocean through the P1 between South Africa and
 060 64° S. As mentioned above, more heat was advected into the Atlantic Ocean through the Drake Passage (P5) in the
 061 OFES1. Additionally, there was more heat advected southward from the Atlantic Ocean to the Southern Ocean in the
 062 OFES1 (P6). The wide passage connecting the north Atlantic Ocean to the Arctic Ocean (P10) also served as the major
 063 channel through which the Atlantic Ocean exchanged heat; the two OFES datasets gave similar heat loss. All these
 064 differences combined led us to conclude that the respective values for the vertical heat diffusion at 300 m differed by
 065 0.411 W/m² (more upward heat diffusion in the OFES1).

066 In the Indian Ocean, the averaged OHC increasing rate was 0.009 W/m² higher in the OFES2 than in the OFES1.
 067 The time-averaged surface heat flux in the OFES2 was 0.729 W/m² less than that in the OFES1. Both datasets showed
 068 a net downward heat advection but that in the OFES2 was around three times stronger. The small difference in the
 069 southward heat advection across the 64° S (the P2) only affected the OHC in the upper Indian Ocean to a small extent.
 070 In contrast, the differences in the HF, VHA and the MHA associated with the ITF contributed to the difference and
 071 led us to calculate a remarkable discrepancy of 1.898 W/m² in the VHD at a depth of 300 m in the Indian Ocean. The
 072 enhanced ITF is one of the main contributors to the larger OHC increase in the upper layer of the OFES2 Indian Ocean
 073 (Fig. 2).

074 To summarize, there was generally more surface heat flux into the major basins in the OFES1. The vertical heat
 075 advection was generally downward, indicating the essential role of the subtropical Ekman pumping in the heat uptake
 076 in the upper ocean layer. The differences of these two (HF and VHA) were mainly from the different atmospheric
 077 forcing used in the two OFES datasets, emphasizing the importance of reliable atmospheric in the numerical ocean
 078 modelling. Although the different wind stress could also produce different lateral advectons through the P1–P10, the
 079 local-integrated differences were generally smaller than the basin-integrated differences. The most prominent
 080 difference in the lateral heat advection is associated with the ITF, mainly as a result of the adoption of a tidal-mixing
 081 scheme. This ITF-related difference and the indirectly inferred VHD suggested the significance of vertical mixing in
 082 producing the examined differences of OHC.

083
 084 **Table 2.** Time-averaged OHC, surface heat flux (HF) and advection of heat through the major water passages for the
 085 upper layer of each basin (0–300 m). VHA is at a depth of 300 m. Residual: difference between the OHC increase and
 086 all the heat flux into a basin, approximately the vertical diffusion of heat. All quantities converted to W/m² applied
 087 over the entire surface of the Earth. Values smaller than 0.001 are set to 0.

PACIFIC OCEAN (0–300 m)										
	OHC	HF	VHA	P3	P4	P5	P7	P8	P9	Residual
OFES1	-0.025	2.135	-0.814	1.233	0.011	-0.891	-0.728	-0.162	-0.003	-0.808

<u>OFES2</u>	<u>0.007</u>	<u>1.066</u>	<u>-0.113</u>	<u>1.383</u>	=	<u>-0.783</u>	<u>-1.365</u>	<u>-0.100</u>	<u>0</u>	<u>-0.061</u>
<u>0.020</u>										
<u>ATLANTIC OCEAN (0–300 m)</u>										
	<u>OHC</u>	<u>HF</u>	<u>VHA</u>	<u>P1</u>	<u>P5</u>	<u>P6</u>	<u>P10</u>	<u>Residual</u>		
<u>OFES1</u>	<u>0.032</u>	<u>0.184</u>	<u>-0.445</u>	=	<u>0.891</u>	<u>-0.085</u>	<u>-0.440</u>	<u>0.749</u>		
<u>0.823</u>										
<u>OFES2</u>	<u>-0.014</u>	<u>-0.036</u>	<u>0.005</u>	=	<u>0.783</u>	<u>-0.051</u>	<u>-0.388</u>	<u>0.338</u>		
<u>0.665</u>										
<u>INDIAN OCEAN (0–300 m)</u>										
	<u>OHC</u>	<u>HF</u>	<u>VHA</u>	<u>P1</u>	<u>P2</u>	<u>P3</u>	<u>P7</u>	<u>P8</u>	<u>Residual</u>	
<u>OFES1</u>	<u>0.026</u>	<u>0.195</u>	<u>-0.639</u>	<u>0.823</u>	=	<u>-1.233</u>	<u>0.728</u>	<u>0.162</u>	<u>0.028</u>	
<u>0.038</u>										
<u>OFES2</u>	<u>0.035</u>	<u>-0.534</u>	<u>-2.091</u>	<u>0.665</u>	=	<u>-1.383</u>	<u>1.365</u>	<u>0.100</u>	<u>1.926</u>	
<u>0.012</u>										

088

089

090 *Middle layer*

091 There were no significant differences between the OFES1 and OFES2 in the horizontal and vertical heat transports in
092 the middle layer (300–700 m) of the Pacific Ocean (Tab. 3). It can be seen that the IFT was weak for this depth layer
093 and its differences between the OFES1 and OFES2 was small (0.084 W/m²). However, heat was advected or diffused
094 from the upper layer (at 300 m, the top face of the middle ocean layer). There was a difference of around 0.747 W/m²
095 in the VHD at a depth of 300 m in the Pacific Ocean and a difference of 0.701 W/m² in the VHA. All these together
096 led us to infer a VHD difference of 1.295 W/m² at a depth of 700 m in the Pacific Ocean, with more heat was diffused
097 downward in the OFES1.

098 In the Atlantic Ocean, the averaged OHC trend was positive in the OFES1 but negative in the OFES2, different by
099 0.129 W/m². A VHA of -1.585 W/m² was calculated for the OFES2, 32% stronger than that for the OFES1.
100 Additionally, more heat was lost through the P1 into the Indian Ocean and more heat was advected into the Atlantic
101 Ocean through the Drake Passage in the OFES1. Small differences also occurred in the heat advection between the
102 Atlantic Ocean, and the Southern (P6) and the Arctic (P10) Oceans. The vertical heat transport (VHA + VHD) at the
103 300 m of the Atlantic Ocean (Tab. 2) was close from the two OFES data. The resulting inferred VHD through the
104 depth of 700 m in the Atlantic Ocean was upward in both datasets but 0.393 W/m² stronger in the OFES2.

105 The averaged OHC trend in the Indian Ocean was weakly negative in both the OFES1 and OFES2. 0.142 W/m²
106 more heat was advected downward at a depth of 700 m in the OFES2. Horizontally, 0.121 W/m² more heat was
107 acquired from the Atlantic Ocean (through the P1) in the OFES1 but there were neglectable differences in the lateral
108 heat transport through the others passages connecting the Indian Ocean with the other basins. The time-averaged VHD
109 at 700 m in the Indian Ocean was 0.423 W/m² in the OFES1 and 1.083 W/m² in the OFES2.

110 To summarize, the notable cooling trend in the Pacific and Atlantic Ocean (Fig.3) from the OFES2 came mainly
111 from the vertical heat transport (VHA + VHD) processes. For example, there was a net upward heat advection at 300

m in the OFES2 Atlantic Ocean and a stronger downward heat advection at 700 m, as a result, more heat was lost vertically in the middle layer of the OFES2 Atlantic Ocean compared to the OFES1 Atlantic Ocean.

Table 3. As for Tab. 2 but for the middle layer (300–700 m). VHA is at a depth of 700 m.

PACIFIC OCEAN (300–700 m)									
	<u>OHC</u>	<u>VHA</u>	<u>P3</u>	<u>P4</u>	<u>P5</u>	<u>P7</u>	<u>P8</u>	<u>P9</u>	<u>Residual</u>
OFES1	0.017	-0.096	1.208	-0.026	-1.056	0.044	0	0	-1.679
OFES2	-0.034	-0.084	1.247	-0.030	-0.917	-0.040	0	0	-0.384
ATLANTIC OCEAN (300–700 m)									
	<u>OHC</u>	<u>VHA</u>	<u>P1</u>	<u>P5</u>	<u>P6</u>	<u>P10</u>	<u>Residual</u>		
OFES1	0.037	-1.203	-0.770	1.056	0.056	-0.057	1.260		
OFES2	-0.092	-1.585	-0.649	0.917	0.017	-0.102	1.653		
INDIAN OCEAN (300–700 m)									
	<u>OHC</u>	<u>VHA</u>	<u>P1</u>	<u>P2</u>	<u>P3</u>	<u>P7</u>	<u>P8</u>	<u>Residual</u>	
OFES1	-0.010	-0.519	0.770	-0.043	-1.208	-0.044	0	0.423	
OFES2	-0.013	-0.661	0.649	-0.043	-1.247	0.040	0	1.083	

Lower layer

Consistent with Fig. 4, the OFES2 showed cooling in the bottom (700–2000m) layer of each basin, but the OFES1 an overall warming (Tab. 4). In the Pacific Ocean, the VHA at 2000 m was downward and of similar magnitude in the two OFES datasets. Due to the vertical coherence of the ACC, there was intense eastward heat advection through the P3 and P5, even below 700 m, with the OFES2 showing greater advection. The horizontal heat advection through the P4 and P7 was relatively weak but again larger in the OFES2. For example, the MHA through the P7 was more than two times larger in the OFES2. In fact, more heat advected southward into the Indian Ocean through the ITF was found in all the ocean layers (the OFES1 showed a weakly northward heat advection in the middle layer). As a result of these differences, and the VHA and VHD at a depth of 700 m, we calculated a significant difference in the VHD between the two OFES datasets at a depth of 2000 m in the Pacific Ocean of around 1.252 W/m² in the downward direction.

Unlike at 2000 m in the Pacific Ocean, there was much stronger downward heat advection at 2000 m in the OFES2 Atlantic Ocean. The dominant horizontal heat advections were through the P1 and P5, with the OFES2 showing stronger heat advection at both the two passages. We calculated a downward heat diffusion at a depth of 2000 m of 0.216 W/m² in the OFES1 Atlantic Ocean and an upward VHD of 0.383 W/m² in the OFES2 Atlantic Ocean.

In the Indian Ocean, the calculated downward heat advection was two times stronger in the OFES1; there were also some moderate differences in the horizontal heat advection. The resulting VHD at 2000 m was upward in both the OFES1 and OFES2, but much greater (by 0.455 W/m²) in the latter.

To summarize, differences in the lateral heat advection through the major passages P1–P10 in the lower layer was small, and the major drivers of the examined OHC differences between the OFES1 and OFES2 came largely from the vertical heat transport (VHA + VHD), similar to the situation in the middle layer.

Table 4. As for Tab. 2 but for the lower layer (700–2000 m). VHA is at a depth of 2000 m.

PACIFIC OCEAN (700–2000 m)									
	OHC	VHA	P3	P4	P5	P7	P8	P9	Residual
OFES1	0.058	-0.126	0.951	$\frac{-0.04}{7}$	$\frac{-1.12}{0}$	-0.035	0	0	-1.341
OFES2	-0.037	-0.105	1.146	$\frac{-0.08}{0}$	$\frac{-1.29}{4}$	-0.082	0	0	-0.089
ATLANTIC OCEAN (700–2000 m)									
	OHC	VHA	P1	P5	P6	P10	Residual		
OFES1	0.014	-0.029	$\frac{-0.97}{4}$	1.120	0.066	0.105	-0.216		
OFES2	-0.013	-0.536	$\frac{-1.05}{9}$	1.294	0.003	-0.031	0.383		
INDIAN OCEAN (700–2000 m)									
	OHC	VHA	P1	P2	P3	P7	P8	Residual	
OFES1	0.007	-0.241	0.974	$\frac{-0.03}{3}$	$\frac{-0.95}{1}$	0.035	0	0.126	
OFES2	-0.018	-0.120	1.059	$\frac{-0.05}{2}$	$\frac{-1.14}{6}$	0.082	0	0.581	

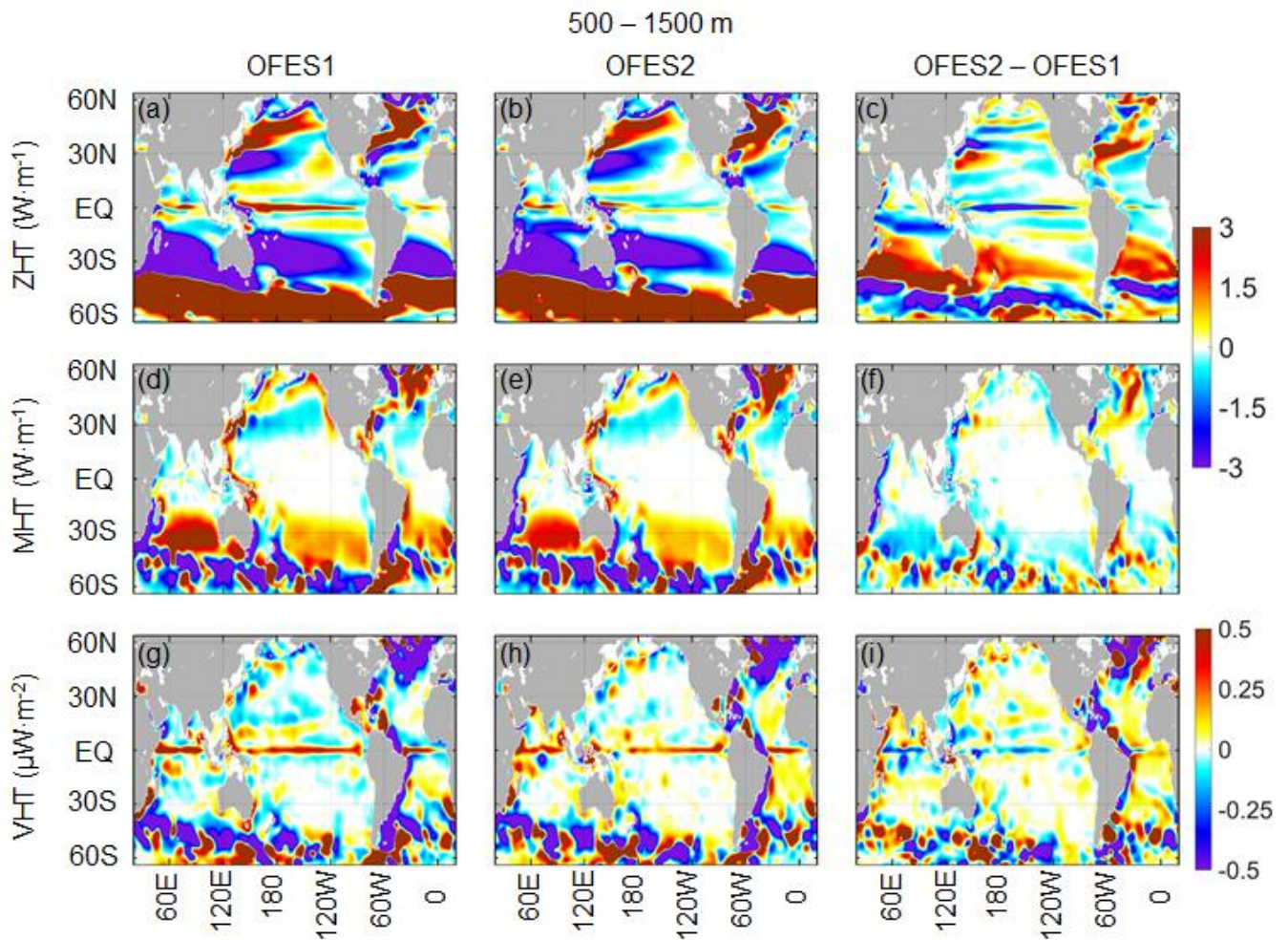
For a quantitative comparison of heat transport, we calculated the horizontal heat transport through the major water passages connecting each basin (Fig. 1a) for the upper and intermediate oceans and basin integrated vertical heat transport at the depth of 500 m (Tab. 4) and 1500 m (Tab. 5). Note that these heat transport are time-averaged quantities from 1960 to 2016 and converted to $W \cdot m^{-2}$ showing the heating rate it accounts for.

— In the upper layer of the Pacific Ocean, the total OHC change is close between the OFES1 and OFES2. However, the total surface heat flux in the OFES1 is two times of that in the OFES2, indicating that more heat is injected to the Pacific Ocean. Vertically, . Through the water passage between the Australian mainland and the 64°S (P3), there are more eastward heat advection in the OFES2. Although the MHT from the Southern Ocean to the Pacific Oceans (P4) differs significantly, the relatively small absolute value indicates that this difference can only produce minor impacts. Drake Passage (P5) is the major water passage exchanging heat between the Pacific Ocean and the Atlantic Ocean. There are more heat flowing through the P5 into the Atlantic Ocean in the OFES1. P7 and P8 connects the Pacific and the Indian Ocean, and the Indonesian Throughflow (ITF) flows across the P7. It is found that the through the P7 is two times stronger in the OFES2 compared to the OFES1, possibly indicating an enhancement of the IFT simulated by the OFES2. This agrees well with the finding of Sasaki et al. (2018), in which the inclusion of a tidal mixing scheme results in an intensification of ITF. In addition, the OFES1 presents more heat transported westward into the Indian Ocean between the Papua New Guinea and the Australia (P8). The net heat advection through the Bering Strait is rather weak (P9) in both data. Comparatively, there is net downward heat diffusion at the depth of 500 m in the Pacific Ocean by the OFES1 but net upward heat diffusion in the OFES2.

— For the Atlantic Ocean, the OHC increases $0.048 W \cdot m^{-2}$ in the OFES1 but decreases by $0.073 W \cdot m^{-2}$ in the OFES2. Despite the similarity in the spatial pattern (Fig. 12), there are net heating for the Atlantic Ocean in the OFES1 but cooling in the OFES2, and this large surface heat flux discrepancy mainly occurs at the high latitudes of the north Atlantic Ocean. There are remarkable differences in the VHT at the depth of 500 m in the Atlantic Ocean between the two OFES data. More specifically, the OFES1 shows a net downward heat advection but the OFES2 indicates a much

162 stronger and upward heat advection. Through the P1 from the South Africa to the 64°S, the OFES1 shows more heat
 163 transported out from the Atlantic Ocean to the Indian Ocean. As mentioned above, more heat was advected into the
 164 Atlantic Ocean through the Drake Passage in the OFES1. , there are more heat transported southward from the Atlantic
 165 Ocean to the Southern Ocean in the OFES1 (P6). The wide passage connecting the north Atlantic Ocean to the Arctic
 166 Ocean also serves as a dominant region where the Atlantic Ocean loses the heat (P10), through which these two OFES
 167 data simulates approximately the same heat loss into the Arctic through. These notable VHT discrepancy and the
 168 approximately similar horizontal heat transport leads us to infer that their vertical heat diffusion may differ from each
 169 other as high as $1.64 \text{ W} \cdot \text{m}^{-2}$.

170 — For the upper layer of the Indian Ocean, the total OHC increase is higher in the OFES2 than the OFES1. It can
 171 be seen that the time averaged surface heat flux for the Indian Ocean in the OFES2 is $0.73 \text{ W} \cdot \text{m}^{-2}$ less than that of the
 172 OFES1. Both these two data reveal a net downward heat advection but the OFES2 is around two times stronger. The
 173 subtle difference of southward heat advection across the 64°S can only impact the OHC in the upper Indian Ocean to
 174 a less extent. On the contrary, the differences in the HF, VHT, ZHT through the P3 and MHT associated with the ITF
 175 lead us to infer large discrepancy in the VHD at the depth of 500 m in the Indian Ocean.



177

178 **Figure 1214. As for Fig. 11 13 but in the intermediate ocean (500–1400/1500 m). ZHT and MHT are vertically**
179 **integrated between 500 m and 1400/1500 m per unit width; VHT is the vertical heat flux through the depth of**
180 **1400/1500 m per unit area.**

181 —As shown in Fig. 7, the OFES2, unlike the OFES1, shows cooling in the low and middle latitudes of the
182 intermediate layer of the Southern Atlantic Ocean, which cannot be well explained by the heat transport distribution
183 in Fig. 12. But it may be related to the lesser downward heat transport at the depth of 500 m (Figs. 11g-i), as less heat
184 was vertically added into the intermediate ocean via its upper boundary. In the intermediate layer of the Atlantic
185 Ocean, the stronger ZHT associated with the Gulf Stream can account for the local larger negative $\Delta\theta$ in the OFES2.
186 In addition, the more intense MHT north of 30°N in the Atlantic Ocean contributes to the warming tongue there in the
187 OFES2. The notable warming in the RSPGIW in the OFES2 largely results from greater upward heat transport at the
188 depth of 1400 m. Lesser MHT in the central south Indian Ocean may be related to the strong cooling central and
189 eastern parts of the intermediate layer of the Indian Ocean. In the vertical direction, the OFES2 shows upward heat
190 transport consistently between around 30°S – 30°N in the Atlantic Ocean, but this cannot explain the cooling of the
191 intermediate layer of the Atlantic Ocean in the same horizontal coverage. Again, the large-scale pattern of both the
192 horizontal and vertical heat fluxes are largely similar between the OFES1 and OFES2. However, clear discrepancies
193 exist. In the zonal direction, the major differences are found to be related to the westward heat advection in the southern
194 subtropics, with the OFES2 has generally weaker heat flux. The eastward heat advection associated with the ACC is
195 also generally weaker in the OFES2. In the northern hemisphere, the dominant ZHT is by the Kuroshio and Gulf
196 Stream. The OFES2 shows a weaker Kuroshio related ZHT and larger ZHT by the Gulf Stream. In the meridional
197 direction, weaker equatorward heat flux is seen in the OFES2, the pattern of differences is complex in the Southern
198 Ocean. In the northern Atlantic Ocean, there is a stronger widespread MHT in the middle from around 30°N northward
199 to the subpolar. The VHT pattern is highly noisy and defies easy verbal description. However, in the bulk of the tropics
200 and subtropics of the Atlantic Ocean, there is more heat advected upward in the OFES2. Also, the downward heat flux
201 in the northern north Atlantic Ocean is stronger in the OFES2.

202 —A quantitative analysis of the heat transport for the intermediate layer of the Pacific Ocean shows that there are no
203 significant differences in the horizontal heat transport (Tab. 5). However, heat can be advected or diffused from the
204 upper layer to the intermediate layer of the Pacific Ocean, that is, at the depth of 500 m. As it is inferred that there is
205 a difference of around $1.36\text{ W}\cdot\text{m}^{-2}$ in the VHD at the depth of 500 m in the Pacific Ocean, a VHD difference of around
206 $0.35\text{ W}\cdot\text{m}^{-2}$ is therefore calculated at the depth of 1500 m in the Pacific Ocean.

207 —For the intermediate layer of the Atlantic Ocean, there are some moderate differences in the VHT, MHT through
208 the P6 and P10 between the OFES1 and OFES2. The resulting inferred equivalent vertical heat diffusion through the
209 depth of 1500 m in the Atlantic Ocean is slightly in the OFES2.

210 —There is more heat vertically advected downward at the depth of 00 m in the Indian ocean in the OFES1. Through
211 all the passages connecting the Indian Ocean to others, more heat is found to be advected horizontally in the OFES2.
212 e infer that the time-averaged VHD at the depth of 1500 m in the Indian Ocean is $0.16\text{ W}\cdot\text{m}^{-2}$ over this 57 years period
213 in the OFES1 and $1.91\text{ W}\cdot\text{m}^{-2}$ in the OFES2.

1214 4 Conclusions and Discussion

215 In this paper, we estimated the OHC from two ~~high~~eddy-resolution hindcast simulations, OFES1 and OFES2, with
216 a major focus on their differences. The global observation-based dataset EN4 ~~acts~~acted as a reference, ~~and~~†The
217 ~~following principal points~~main findings were ~~found~~as follows.

218 1. Multi-decadal ~~W~~warming was clearly seen in most of the global ocean (0–~~1400~~2000 m), especially ~~by~~in the
219 EN4 and OFES1. The warming was mainly ~~manifested by the result of the vertical displacements~~deepening of the
220 neutral density surfaces (HV component), with a lesser contributions from changes along the neutral surfaces (SP
221 component) of regional importance.

222 2. Significant differences in the OHC (or potential temperature) were found between the OFES1 and OFES2. ~~The~~
223 ~~similarly distributed surface heat fluxes could not account for the differences in the warming/cooling distributions.~~
224 ~~Differences in the horizontal and vertical heat transports were found to be only partially responsible for the revealed~~
225 ~~OHC differences between the two OFES~~†the major causes for these ~~discrepancies are found to be~~were fourfold.
226 Firstly, there ~~are~~was generally more net surface heat flux in the OFES1. Secondly, ~~we found that~~ the ITF ~~is~~was
227 almost two times stronger in the OFES2, especially ~~for~~in the top 300 m. Thirdly, the ~~intensity~~ differences in the
228 intensity of the vertical heat advection ~~were~~can be large, particularly at ~~the~~ 300 m ~~depth of~~in the Indian Ocean. Finally,
229 ~~it was inferred that there exist~~ remarkable differences in the vertical heat diffusion were inferred.

230 Although we have detailed the OHC differences between the OFES1 and OFES2, and also analysed the horizontal
231 and vertical heat transports in an attempt to understand the causes of these differences, more work is needed to
232 improve. Firstly, a direct calculation of the vertical heat diffusion was desirable to have a more reliable and accurate
233 comparison between the two datasets. In addition, decomposing the vertical heat diffusion into tidal mixing and mixed-
234 layer vertical mixing is also an interesting topic and may help to isolate the effects of tidal mixing on the ocean state.
235 Besides, we expect to see a detailed comparison of the wind stress from these two datasets over this 57-year period.
236 This is inspired by the work of Kutsuwada et al. (2019) and our detection of the large vertical heat advection.
237 Considering the apparent differences of the SP between the OFES2 and the other two datasets, a comprehensive
238 comparison of salinity between both the OFES1 and OFES2 with observations were required. This helped the
239 community to determine their choice of datasets for their own research purposes.

240 One may argue that being not well spun-up may be also a major cause for the disparities between the OFES2 with
241 others, since that the OFES1 follows a 50-year climatological simulation. This is likely to be a cause. However, large
242 differences remain in the temporal evolution of the global and basin OHCs, even during the last two decades. In
243 addition, for example, S2020 found that the Azores Current was simulated in the OFES2 in the initial two decades but
244 disappeared after 1970. This, to some extent, weaken the spin-up argument, but does not rule out the possibility. The
245 OFES2 was not expected to be highly sensitive to the spin-up issue, as it started with conditions from the OFES1
246 rather than from scratch. That said, there were indeed some improvements in the OFES2 for the recent decades, for
247 example, over 2005-2016. Two potential explanations are: firstly, the model was full spun-up after a couple of decades
248 of integration; secondly, improvements of the reanalysis atmospheric forcing data contributed to the simulation
249 improvements.

250 Finally, the OFES products, especially the OFES1, did replicate some of the warming and cooling trends shown
251 by the EN4 and in the literature, despite their having no observational-based constraints. However, the clear
252 differences between the two OFES datasets and the EN4 suggest the importance of observational data in improving
253 the hindcast performance. The significant differences in the vertical heat diffusion between the two OFES datasets
254 also suggest that special attention should be given to validation of the vertical mixing scheme in future ocean
255 modelling.

256 ~~Although we have detailed the OHC differences between the OFES1 and OFES2, and also analysed the horizontal~~
257 ~~and vertical heat transports in an attempt to understand the causes behind the differences, more work is needed to~~
258 ~~further understand the causes. Of the various possible causes, we speculate that and being not fully spun up of the~~
259 ~~OFES2 and vertical mixing could be vital to the subsurface OHC evolution and distribution, given that lateral heat~~
260 ~~diffusion is likely to be similar in pattern due to the same horizontal mixing scheme applied. However, large~~
261 ~~discrepancies remain in the temporal evolution of the global and basin OHC even during the recent two decades. Also,~~
262 ~~the OFES2 is expected to be less sensitive to the spin up issue as it starts from the simulated condition from the OFES1~~
263 ~~rather than from the rest. Although we indirectly infer the vertical heat diffusion in this paper, it is desirable to directly~~
264 ~~calculate and compare the vertical heat diffusion. The importance of vertical diffusion was justified in Bryan (1987),~~
265 ~~where the vertical diffusivity was found to play a vital role in the simulations of OGCMs, e.g., the meridional heat~~
266 ~~transport. In addition, the vertical diffusion of heat itself is directly related to the heat budget according to the primitive~~
267 ~~equation of temperature. The vertical diffusivity is only available for the OFES2, a limit hampering our further dig~~
268 ~~into the discrepancies of vertical heat diffusion between the two OFES datasets. Furthermore, decomposing the vertical~~
269 ~~heat diffusion into tidal mixing and mixed layer vertical mixing could also help to isolate the effects of the inclusion~~
270 ~~of tidal mixing on the ocean state.~~

271 ~~—In spite of no observational based constraints, we found that the OFES products, especially the OFES1, did present~~
272 ~~some of the warming or cooling trend shown by the EN4 and in the literature. However, the clear differences between~~
273 ~~the two OFES data and the EN4 may suggest the importance of data assimilation in improve the hindcast performance,~~
274 ~~if the vertical mixing was found to be significant in causing the examined differences between the OFES2 and the~~
275 ~~others. Based on the significant difference of our infer of the vertical heat diffusion between the two OFES data, it~~
276 ~~suggests special attention will be called on the vertical mixing scheme validation for the future ocean modelling.~~

277
278 **Author contributions:** F.L conceived the study. All authors contributed to the details of study design. F.L conducted
279 the calculations and analysis. F.L drafted the manuscript; Z.L and X.H.W improved the writing.

280
281 **Acknowledgements:** This is publication No. 87 of the Sino-Australian Research Consortium for Coastal
282 Management (previously the Sino-Australian Research Centre for Coastal Management). This work was supported by
283 the Key Special Project for Introduced Talents Team of the Southern Marine Science and Engineering Guangdong
284 Laboratory (Guangzhou; GML2019ZD0210). The authors thank Dr Peter McIntyre for improving the manuscript. The
285 authors acknowledge public access to the data used in this paper from the UK Meteorological Office and the
286 JAMSTEC.

287 ~~This is publication No. 87 of the Sino-Australian Research Consortium for Coastal Management (previously the Sino-~~
288 ~~Australian Research Centre for Coastal Management). This work was supported by the Key Special Project for~~
289 ~~Introduced Talents Team of the Southern Marine Science and Engineering Guangdong Laboratory (Guangzhou;~~
290 ~~GML2019ZD0210). The authors thank Dr. Peter McIntyre for improving the manuscript. The authors acknowledge~~
291 ~~public access to the data used in this paper from the UK Meteorological Office and the JAMSTEC.~~

293 ~~—Code and data availability: OFES1 and OFES2 are based on the MOM3, available at [https://github.com/mom-](https://github.com/mom-ocean/MOM3)~~
294 ~~[ocean/MOM3](https://github.com/mom-ocean/MOM3).~~

295 ~~Code for decomposing the potential temperature: <http://www.teos-10.org/software.htm>.~~

296 ~~Original EN4 data: <https://www.metoffice.gov.uk/hadobs/en4/download-en4-2-1.html>.~~

297 ~~Original OFES1 temperature and salinity data:~~
298 ~~http://apdrc.soest.hawaii.edu/dods/public_ofes/OFES/ncep_0.1_global_mmean.~~

299 ~~Due to a data security incident, access to the OFES2 data has been temporarily suspended.~~

300 ~~The data and codes (including the publically available scripts for completion) needed to reproduce the results of this~~
301 ~~paper are archived on Zenodo (<https://doi.org/10.5281/zenodo.5205444>). The archived data are annual mean values~~

302 ~~calculated from the original data. Both the OFES1 and OFES2 are based on the MOM3, available at~~

303 ~~<https://github.com/mom-ocean/MOM3>. The outputs of these two OFES data are kindly provided to the public by the~~

304 ~~JAMSTEC. The Code used to decompose the potential temperature can be found at [http://www.teos-](http://www.teos-10.org/software.htm)~~

305 ~~[10.org/software.htm](http://www.teos-10.org/software.htm). The original EN4 data (kindly provided by the United Kingdom's Met Office Hadley Centre) is~~

306 ~~at <https://www.metoffice.gov.uk/hadobs/en4/download-en4-2-1.html>. The original OFES1 temperature and salinity~~

307 ~~data are available can be accessed at~~

308 ~~http://apdrc.soest.hawaii.edu/dods/public_ofes/OFES/ncep_0.1_global_mmean/temp.info and~~

309 ~~http://apdrc.soest.hawaii.edu/dods/public_ofes/OFES/ncep_0.1_global_mmean/salt.info; . Due to data security~~

310 ~~incident, the OFES2 data is temporally suspended at presents. All the data and codes (including the publically available~~

311 ~~scripts for completion) needed to reproduce the results of this paper is archived on Zenodo ([10.5281/zenodo.5055697](https://doi.org/10.5281/zenodo.5055697)).~~

312 ~~These archived data are calculated annual mean values from the downloaded original data. the OFES2 temperature~~

313 ~~and salinity data were downloaded from <http://www.jamstec.go.jp/esc/fes/dods/OFES2/Monthly/temp.info> and~~

314 ~~<http://www.jamstec.go.jp/esc/fes/dods/OFES2/Monthly/salt.info>; the EN4 temperature data at~~

315 ~~<https://www.metoffice.gov.uk/hadobs/en4/download-en4-2-1.html>.~~

1316 **References**

1317 Abraham, J. P., Reseghetti, F., Baringer, M., Boyer, T., Cheng, L., Church, J., Domingues, C., Fasullo, J. T., Gilson,
1318 J., Goni, G., Good, S., Gorman, J. M., Gouretski, V., Ishii, M., Johnson, G. C., Kizu, S., Lyman, J., MacDonald, A.,
1319 Minkowycz, W. J., Moffitt, S. E., Palmer, M., Piola, A., Trenberth, K. E., Velicogna, I., Wijffels, S., and Willis, J.: A
1320 review of global ocean temperature observations: implications for ocean heat content estimates and climate change,
1321 *Rev. Geophys.*, 51, 450-483, doi.org/10.1002/rog.20022, 2013.

1323 AchutaRao, K. M., Ishii, M., Santer, B. D., Gleckler, P. J., Taylor, K. E., Barnett, T. P., Pierce, D. W., Stouffer, R. J.,
1324 and Wigley, T. M. L.: Simulated and observed variability in ocean temperature and heat content, *Proc. Natl. Acad.*
1325 *Sci.*, 104,10768-10773, doi.org/10.1073/pnas.0611375104, 2007.

1326

1327 Allison, L. C., Roberts, C. D., Palmer, M. D., Hermanson, L., Killick, R. E., Rayner, N. A., Smith, D. M., and Andrews,
1328 M. B.: Towards quantifying uncertainty in ocean heat content changes using synthetic profiles, *Environ. Res. Lett.*,
1329 14, 084037, doi.org/10.1088/1748-9326/ab2b0b, 2019.

1330

1331 Balmaseda, M. A., Trenberth, K. E., and Källén, E.: Distinctive climate signals in reanalysis of global ocean heat
1332 content, *Geophys. Res. Lett.*, *Geophys Res Lett.*, 40, 1754-1759, doi.org/10.1002/grl.50382, 2013.

1333

1334 Bindoff, N. L., and McDougall, T. J.: Diagnosing climate change and ocean ventilation using hydrographic data, *J.*
1335 *Phy. Oceanogr.*, 24, 1137-1152, doi.org/10.1175/1520-0485(1994)024<1137:DCCAOV>2.0.CO;2, 1994.

1336 Carton, J. A., Chepurin, G. A. and Chen, L.: SODA3: A New Ocean Climate Reanalysis, *J. Climate*, *Journal of*
1337 *Climate*, 31, 6967-6983, https://doi.org/10.1175/JCLI-D-18-0149.1, 2018.

1338

1339 Banks, H. T., and Gregory, J. M.: Mechanisms of ocean heat uptake in a coupled climate model and the implications
1340 for tracer based predictions of ocean heat uptake, *Geophys. Res. Lett.*, 33, L07608,
1341 https://doi.org/10.1029/2005GL025352, 2006.

1342

1343 Carton, J. A., Chepurin, G., A. and Chen, L.: SODA3: A New Ocean Climate Reanalysis, *J. Climate.*, 31, 6967-6983,
1344 https://doi.org/10.1175/JCLI-D-18-0149.1, 2018.

1345

1346 Carton, J. A., Penny, S. G., and Kalnay, E.: Temperature and salinity variability in the SODA3, ECCO4r3, and ORAS5
1347 ocean reanalyses, 1993–2015, *J. Climate.*, 32, 2277-2293, doi.org/10.1175/JCLI-D-18-0605.1, 2019.

1348

1349 Chen, X., Yan, Y., Cheng, X., and Qi, Y.: Performances of seven datasets in presenting the upper ocean heat content
1350 in the South China Sea, *Adv. Atmos. Sci.*, 30, 1331-1342, doi.org/10.1007/s00376-013-2132-1, 2013.

1351

1352 Cheng, L., Trenberth, K. E., Palmer, M. D., Zhu, J., and Abraham, J.: Observed and simulated full-depth ocean heat
1353 content changes for 1970–2005, *Ocean Sci.*, 12, 925-935, doi.org/10.5194/os-12-925-2016, 2016.

1354

1355 Cheng, L., and Zhu, J.: Artifacts in variations of ocean heat content induced by the observation system changes.
1356 *Geophys. Res. Lett.*, *Geophysical Research Letters*, 41, 7276-7283, https://doi.org/10.1002/2014GL061881, 2014.

1357

1358 Church, J. A., White, N. J., and Arblaster, J. M.: Significant decadal-scale impact of volcanic eruptions on sea level
1359 and ocean heat content, *Nature.*, 438, 74-77, doi.org/10.1038/nature04237, 2005.

1360
1361 Curry, R., Dickson, B. and Yashayaev, I.: A change in the freshwater balance of the Atlantic Ocean over the past four
1362 decades. *Nature*, 426, 826-829, <https://doi.org/10.1038/nature02206>, 2003.
1363
1364 Desbruyères, D., McDonagh, E. L., King, B. A., and Thierry, V.: Global and Full-Depth Ocean Temperature Trends
1365 during the Early Twenty-First Century from Argo and Repeat Hydrography. *J. Climate*. ~~*Journal of Climate*~~, 30, 1985-
1366 1997, doi.org/10.1175/JCLI-D-16-0396.1, 2017.
1367
1368 Desbruyeres, D., Purkey, S. G., Mcdonagh, E. L., Johnson, G. C. and King, B. A.: Deep and abyssal ocean warming
1369 from 35 years of repeat hydrography. *Geophys. Res. Lett.*, 43, 10356-10365, doi.org/10.1002/2016GL070413, 2016
1370 Dong, S., Garzoli, S., and Baringer, M.: The role of interocean exchanges on decadal variations of the meridional heat
1371 transport in the South Atlantic, *J. Phys. Oceanogr.*, 41, 1498-1511, doi.org/10.1175/2011JPO4549.1, 2011.
1372
1373 [Durack, P. J., Gleckler, P. J., Landerer, F. W., and Taylor, K. E.: Quantifying underestimates of long-term upper-](#)
1374 [ocean warming, *Nat. Climate Change.*, 4, 999-1005, <https://doi.org/10.1038/nclimate2389>, 2014.](#)
1375
1376 Du, Y., Qu, T., Meyers, G., Masumoto, Y., and Sasaki, H.: Seasonal heat budget in the mixed layer of the southeastern
1377 tropical Indian Ocean in a high-resolution ocean general circulation model, *J. Geophys. Res. Oceans.*, 110, C04012,
1378 doi.org/10.1029/2004JC002845, 2005.
1379
1380 Emery, W.: Water Types and Water Masses, *Encyclopedia of Ocean Sciences*, doi.org/10.1006/rwos.2001.0108, 4,
1381 3179-3187, 2001.
1382
1383 Ernst, W. G.: *Earth systems: processes and issues*. Cambridge University Press, 2000.
1384
1385 Forget, G., Campin, J.-M., Heimbach, P., Hill, C. N., Ponte, R. M., and Wunsch, C.: ECCO version 4: an integrated
1386 framework for non-linear inverse modeling and global ocean state estimation. *Geosci. Model Dev.*, ~~*Geoscientific*~~
1387 ~~*Model Development*~~, 8 (10), 3071–3104, [doi:10.5194/gmd-8-3071-2015](https://doi.org/10.5194/gmd-8-3071-2015), 2015.
1388
1389 [Fyfe, J.: Southern Ocean warming due to human influence, *Geophys. Res. Lett.*, 33, L19701, \[10.1029/2006GL027247\]\(https://doi.org/10.1029/2006GL027247\),](#)
1390 [2006](#)
1391
1392 Gleckler, P. J., Santer, B. D., Domingues, C. M., Pierce, D. W., Barnett, T. P., Church, J. A., Taylor, K. E., Achutarao,
1393 K., Boyer, T. P., and Ishii, M.: Human-induced global ocean warming on multidecadal timescales, *Nat. Climate*
1394 *Change.*, 2, 524-529, doi.org/10.1038/nclimate1553, 2012.
1395

1396 Good, S. A., Martin, M., and Rayner, N. A.: EN4: Quality controlled ocean temperature and salinity profiles and
1397 monthly objective analyses with uncertainty estimates, *J. Geophys. Res. Oceans.*, 118, 6704-6716,
1398 doi.org/10.1002/2013JC009067, 2013.
1399

1400 Häkkinen, S., Rhines, P. B. and Worthen, D. L.: Heat content variability in the North Atlantic Ocean in ocean
1401 reanalyses, *Geophys. Res. Lett.*, ~~*Geophysical Research Letters*~~, 42, doi.org/10.1002/2015GL063299, 2901-2909,
1402 2015.
1403

1404 Häkkinen, S., Rhines, P. B., and Worthen, D.: Warming of the global ocean: Spatial structure and water-mass trends,
1405 *J. Climate.*, 29, 4949-4963, doi.org/10.1175/JCLI-D-15-0607.1, 2016.
1406

1407 IPCC.: Climate Change 2013: The Physical Science Basis. Cambridge University Press, 1535pp.,
1408 doi:10.1017/CBO9781107415324, 2013.
1409

1410 Jackett, D. R., and McDougall, T. J.: A neutral density variable for the world's oceans, *J. Phys. Oceanogr.*, 27, 237-
1411 263, doi.org/10.1175/1520-0485(1997)027<0237:ANDVFT>2.0.CO;2, 1997.
1412

1413 Jayne, S. R., and Laurent, L. C. St.: Parameterizing tidal dissipation over rough topography, *Geophys. Res. Lett.*, 28,
1414 811-814, doi.org/10.1029/2000GL012044, 2001.
1415

1416 Kalnay, E., Kanamitsu, M., Kistler, R., Collins, W., Deaven, D., Gandin, L., Iredell, M., Saha, S., White, G., Woollen,
1417 J., Zhu, Y., Chelliah, M., Ebisuzaki, W., Higgins, W., Janowiak, J., Mo, K. C., Ropelewski, C., Wang, J., Leetmaa,
1418 A., Reynolds, R., Jenne, R., and Joseph, D.: The NCEP/NCAR 40-year reanalysis project, *B. Am. Meteorol. Soc.*,
1419 77, 437-472, doi.org/10.1175/1520-0477(1996)077<0437:TNYRP>2.0.CO;2, 1996.
1420

1421 [Kutsuwada, K., Kakiuchi, A., Sasai, Y., Sasaki, H., Uehara, K., and Tajima, R.: Wind-driven North Pacific Tropical](#)
1422 [Gyre using high-resolution simulation outputs, *J. Oceanogr.*, 75, 81-93, 10.1007/s10872-018-0487-8, 2019.](#)

1423 Large, W. G., McWilliams, J. C., and Doney, S. C.: Oceanic vertical mixing: A review and a model with a nonlocal
1424 boundary layer parameterization, *Rev. Geophys.*, 32, 363-403, doi.org/10.1029/94RG01872, 1994.
1425

1426 Lee, S., Park, W., Baringer, M. O. A., Gordon, L., Huber, B. A., and Liu, Y.: Pacific origin of the abrupt increase in
1427 Indian Ocean heat content during the warming hiatus, *Nature Geosci.*, 8, 445-449, doi.org/10.1038/ngeo2438, 2015.
1428

1429 Levitus, S., Antonov, J. I., Boyer, T. P., Baranova, O., Garcia, H. E., Locarnini, R. A., Mishonov, A. V., Reagan, J.
1430 R., Seidov, D., and Yarosh, E. S.: World ocean heat content and thermocline sea level change (0–2000 m), *Geophys.*
1431 *Res. Lett.*, 39, 1955-2010, doi.org/10.1029/2012GL051106, 2012.
1432

1433 Liang, X., Piecuch, C. G., Ponte, R. M., Forget, G., Wunsch, C., and Heimbach, P.: Change of the global ocean vertical
1434 heat transport over 1993–2010, *J. Climate.*, 30, 5319-5327, doi.org/10.1175/JCLI-D-16-0569.1, 2017.
1435

1436 Liang, X., Liu, C. R., Ponte, M. and Chambers, D. P.: A Comparison of the Variability and Changes in Global Ocean
1437 Heat Content from Multiple Objective Analysis Products During the Argo Period. *J. Climate., Journal of Climate*, 1-
1438 47, doi.org/10.1175/JCLI-D-20-0794.1, 2021.
1439

1440 Liu, C., X. Liang, D. P. Chambers, and R. M. Ponte, 2020: Global Patterns of Spatial and Temporal Variability in
1441 Salinity from Multiple Gridded Argo Products. *J. Climate. Journal of Climate*, 33, 8751-8766.
1442

1443 Liu, M., and T. Tanhua.: Water masses in the Atlantic Ocean: characteristics and distributions. *Ocean Sci.*, 17, 463-
1444 486, doi.org/10.5194/os-17-463-2021, 2021.
1445

1446 Noh, Y., and Kim, H. J.: Simulations of temperature and turbulence structure of the oceanic boundary layer with the
1447 improved near-surface process, *J. Geophys. Res. Oceans.*, 104, 15621-15634, doi.org/10.1029/1999JC900068, 1999.
1448

1449 O'Connor, B. M., Fine, R. A. and Olson, D. B.: A global comparison of subtropical underwater formation rates. *Deep*
1450 *Sea Research Part I: Oceanographic Research Papers*, 52, 1569-1590, doi.org/10.1016/J.DSR.2005.01.011, 2005.
1451

1452 Palmer, M. D., Mcneall, D. J., and Dunstone, N. J.: Importance of the deep ocean for estimating decadal changes in
1453 Earth's radiation balance, *Geophys. Res. Lett.*, 38, L13707, doi.org/10.1029/2011GL047835, 2011.
1454

1455 Pierce, D. W., Barnett, T. P., Achutarao, K., Gleckler, P. J., Gregory, J. M., and Washington, W. M.: Anthropogenic
1456 warming of the oceans: Observations and model results, *J. Climate J. Clim.*, 19, 1873-1900,
1457 doi.org/10.1175/JCLI3723.1, 2006.
1458

1459 Sasaki, H., Sasai, Y., Kawahara, S., Furuichi, M., Araki, F., Ishida, A., Yamanaka, Y., Masumoto, Y., and Sakuma,
1460 H.: A series of eddy-resolving ocean simulations in the world ocean-OFES (OGCM for the Earth Simulator) project,
1461 *Oceans '04 MTS/IEEE Techno-Ocean '04 (IEEE Cat. No. 04CH37600) 3*, 1535-1541, 2004.
1462

1463 Sasaki, H., Kida, S., Furue, R., Aiki, H., Komori, N., Masumoto, Y., Miyama, T., Nonaka, M., Sasai, Y., and Taguchi,
1464 B.: A global eddying hindcast ocean simulation with OFES2, *Geosci. Model Dev.*, 13, 3319-3336,
1465 doi.org/10.5194/gmd-13-3319-2020, 2020.
1466

1467 Smith, D. M., Allan, R.P., Coward, A.C., Eade, R., Hyder, P., Liu, C., Loeb, N.G., Palmer, M.D., Roberts, C.D. and
1468 Scaife, A.A.: Earth's energy imbalance since 1960 in observations and CMIP5 models. *Geophys. Res.*
1469 *Lett., Geophysical Research Letters*, 42, 1205-1213, doi.org/10.1002/2014GL062669, 2015.

1470
1471 Spence, P., Saenko, O. A., Sijp, W., and England, M.: The role of bottom pressure torques on the interior pathways of
1472 North Atlantic deep water, *J. Phys. Oceanogr.*, 42, 110-125, doi.org/10.1175/2011JPO4584.1, 2012.
1473
1474 St. Laurent, L. C., Simmons, H. L., and Jayne, S. R.: Estimating tidally driven mixing in the deep ocean, *Geophys.*
1475 *Res. Lett.*, 29, 21-21–21-24, doi.org/10.1029/2002GL015633, 2002.
1476
1477 Talley, L. D.: Shallow, Intermediate, and Deep Overturning Components of the Global Heat Budget, *J. Phys.*
1478 *Oceanogr.*, 33, 530-560, [https://doi.org/10.1175/1520-0485\(2003\)033<0530:SIADOC>2.0.CO;2](https://doi.org/10.1175/1520-0485(2003)033<0530:SIADOC>2.0.CO;2), 2003.
1479
1480 Trenberth, K. E., Fasullo, J. T., Von Schuckmann, K., and Cheng, L.: Insights into Earth's energy imbalance from
1481 multiple sources, *J. Climate.*, 29, 7495-7505, doi.org/10.1175/JCLI-D-16-0339.1, 2016.
1482
1483 Tsujino, H., Urakawa, S., Nakano, H., Small, R. J., Kim, W. M., Yeager, S. G., Danabasoglu, G., Suzuki, T., Bamber,
1484 J. L., Bentsen, M., Böning, C. W., Bozec, A., Chassignet, E. P., Curchitser, E., Boeira Dias, F., Durack, P. J., Griffies,
1485 S. M., Harada, Y., Ilicak, M., Josey, S. A., Kobayashi, C., Kobayashi, S., Komuro, Y., Large, W. G., Le Sommer, J.,
1486 Marsland, S. J., Masina, S., Scheinert, M., Tomita, H., Valdivieso, M., and Yamazaki, D.: JRA-55 based surface
1487 dataset for driving ocean-sea-ice models (JRA55-do), *Ocean Model.*, 130, 79-139,
1488 doi.org/10.1016/j.ocemod.2018.07.002, 2018.
1489
1490 Von Schuckmann, K., Palmer, M. D., Trenberth, K. E., Cazenave, A., Chambers, D. P., Champollion, N., Hansen, J.,
1491 Josey, S. A., Loeb, N. G., and Mathieu, P. P.: An imperative to monitor Earth's energy imbalance, *Nat. Climate*
1492 *Change.*, 6, 138-144, doi.org/10.1038/nclimate2876, 2016.
1493
1494 Wang, G., Cheng, L., Abraham, J., and Li, C.: Consensuses and discrepancies of basin-scale ocean heat content
1495 changes in different ocean analyses, *Clim. Dyn.*, 50, 2471-2487, doi.org/10.1007/s00382-017-3751-5, 2018.
1496
1497 Wang, X. H., Bhatt, V., and Sun, Y.-J.: Study of seasonal variability and heat budget of the East Australian Current
1498 using two eddy-resolving ocean circulation models, *Ocean. Dyn.*, 63, 549-563, doi.org/10.1007/s10236-013-0605-5,
1499 2013.
1500
1501 Wunsch, C.: The decadal mean ocean circulation and Sverdrup balance, *J. Mar. Res.*, 69, 417-434, doi.org/
1502 10.1357/002224011798765303, 2011.
1503
1504 Zanna, L., Khatiwala, S., Gregory, J. M., Ison, J., and Heimbach, P.: Global reconstruction of historical ocean heat
1505 storage and transport, *Proc. Natl. Acad. Sci.*, 116, 1126-1131, doi.org/10.1073/pnas.1808838115, 2019.
1506

1507 Zhang, Y., Feng, M., Du, Y. H., Phillips, E., Bindoff, N. L., and McPhaden, M. J.: Strengthened Indonesian
1508 Throughflow Drives Decadal Warming in the Southern Indian Ocean, *Geophys. Res. Lett.*, 45, 6167-6175, 2018,
1509 doi.org/10.1029/2018GL078265.